



Université du Québec  
à Rimouski



## **ACQUISITION DE L'AIMANTATION REMANENTE DANS LES SÉDIMENTS**

Thèse présentée

dans le cadre du programme de doctorat en océanographie et du doctorat en sciences de la

Terre et environnement

en vue de l'obtention du grade de Philosophiae Doctor

PAR

© ÉDOUARD PHILIPPE

**Juillet 2019**



**Composition du jury:**

**Jean-Carlos Montero-Serrano, président du jury, ISMER-UQAR**

**Jean-Pierre Valet, directeur de recherche, IPGP**

**Guillaume St-Onge, directeur de recherche, ISMER-UQAR**

**Pierre Francus, codirecteur de recherche, INRS-ETE**

**Simo Spassov, examinateur externe, rapporteur, Royal Meteorological Institute of Belgium**

**Julie Carlut, rapporteure, IPGP**

Dépôt initial le 2 avril 2019

Dépôt final le 8 juillet 2019



UNIVERSITÉ DU QUÉBEC À RIMOUSKI  
Service de la bibliothèque

Avertissement

La diffusion de ce mémoire ou de cette thèse se fait dans le respect des droits de son auteur, qui a signé le formulaire « *Autorisation de reproduire et de diffuser un rapport, un mémoire ou une thèse* ». En signant ce formulaire, l'auteur concède à l'Université du Québec à Rimouski une licence non exclusive d'utilisation et de publication de la totalité ou d'une partie importante de son travail de recherche pour des fins pédagogiques et non commerciales. Plus précisément, l'auteur autorise l'Université du Québec à Rimouski à reproduire, diffuser, prêter, distribuer ou vendre des copies de son travail de recherche à des fins non commerciales sur quelque support que ce soit, y compris l'Internet. Cette licence et cette autorisation n'entraînent pas une renonciation de la part de l'auteur à ses droits moraux ni à ses droits de propriété intellectuelle. Sauf entente contraire, l'auteur conserve la liberté de diffuser et de commercialiser ou non ce travail dont il possède un exemplaire.



« On doit exiger de moi que je  
cherche la vérité, mais non que je la  
trouve. » Denis Diderot, 1713-1784.



## **REMERCIEMENTS**

Pour commencer, je tiens à rappeler qu'une thèse est le fruit de nombreuses collaborations scientifiques qui permettent de faire de nouvelles découvertes. Cette thèse fut une longue aventure. Elle aura duré cinq ans. Cinq années réparties entre deux laboratoires, dans deux pays différents, deux continents différents. Mes deux maisons sont le laboratoire de paléomagnétisme de l'Institut de Physique du Globe de Paris et le laboratoire de paléomagnétisme et de géologie marine de l'Institut des Sciences de la Mer de Rimouski. J'ai donc une très longue liste de personnes à remercier, j'oublierai sûrement des noms, je ne pourrai pas tous les citer, et je m'en excuse.

En tout premier lieu, je tiens à remercier mes deux directeurs de thèse qui m'ont offert l'opportunité d'une vie, celle d'effectuer cette thèse. Un grand merci à Jean-Pierre Valet pour m'avoir fait découvrir le paléomagnétisme depuis mon premier stage de master et d'avoir cru en moi jusqu'au bout. Un autre grand merci à Guillaume St-Onge pour m'avoir fait découvrir la sédimentologie et d'avoir toujours été d'un optimisme à toute épreuve. Je remercie aussi mon codirecteur Pierre Francus pour son partage de connaissances sur les varves. Un très grand merci également à Marie-Pier St-Onge d'avoir proposé mon nom comme étudiant sur le nouveau projet de thèse qu'avait Guillaume. Ce projet de thèse a beaucoup évolué. La confiance et la liberté que l'on m'a données, ainsi que les instruments de mesures mis à ma disposition à l'IPGP, m'ont permis de faire de grandes choses. Je tiens ensuite à remercier les nombreuses personnes avec qui j'ai pu collaborer scientifiquement durant cette thèse. Un très grand merci à Antoine Gagnon-Poiré, Obinna Nzekwe, Pierre-Marc Godbout et Ramon Egli pour leur collaboration.

Un grand merci à l'ensemble de l'équipe du laboratoire de l'ISMER: Arthur Bieber, Charles-Édouard Deschamps, Julie Heggdal Velle, Myriam Caron, Naïs Sirdeys, Omain

Kurtos, Pierre-Arnaud Desiage, Quentin Beauvais, Quentin Duboc, Sarah Letaïef et Yan Lévesque.

Un autre gros merci à l'ensemble de l'équipe du laboratoire de paléomagnétisme de l'IPGP. Je tiens à faire un remerciement spécial à Anojh Thevarasan, Aude Isambert, Cyrielle Tanty, Fernando Lopes, Frédéric Fluteau, Guillaume Le Hir, Jean Besse, Jean-Pascal Cogné, Julia Ricci, Kévin Jourde, Lena Lecourt, Marianne Greff et Sylvie Larousse, pour les nombreux repas du midi et pauses-café passés à discuter de sujets plus ou moins scientifiques. Je tiens aussi à remercier France Lagroix pour les nombreuses discussions dans le train et l'aide apportée pour les analyses magnétiques. Merci aussi à Nabil Garoum pour la formation sur les impressions 3D et les nombreuses impressions 3D qui ont permis de mener à bien de nombreuses expériences. Un grand merci à Fernando Lopes, Jean Besse, Jean-Pascal Cogné, Laure Meynadier et Yves Gallet pour leur soutien moral et leurs conseils dans les moments où j'en avais le plus besoin.

La fin de mon doctorat représente la fin de mes études. Je tiens donc à remercier chaleureusement mes parents pour leur soutien moral et financier durant ces nombreuses années d'études. Je remercie aussi le reste de ma famille élargie pour leur soutien moral et les bons repas.

Le plus grand de mes remerciements va à mon épouse Amel. C'est elle qui m'a soutenu depuis le tout début de mes études. Elle a supporté mes changements d'humeur, mes périodes moins drôles, mon choix de partir pendant plus de 15 mois sans elle à Rimouski, pour finalement me suivre la deuxième fois pour venir s'installer à Rimouski avec moi. Elle m'a également aidé pour les nombreuses relectures et corrections, dont j'ai eu besoin tout au long de mon doctorat. Encore un grand merci à mon épouse si formidable.

Finalement, je remercie le NSERC, le GEOTOP, l'UQAR, l'IPGP, l'ERC, l'INRS, le CNRS, le FRQNT et la chaire de recherche en géologie marine pour avoir contribué au financement de mon doctorat, ainsi que pour les congrès et les missions de terrain.

## RÉSUMÉ

La mesure de l'aimantation rémanente des sédiments permet de reconstituer les variations du champ magnétique terrestre dans le passé. La variabilité du champ géomagnétique nous renseigne sur la dynamique interne de la Terre et son enregistrement sédimentaire peut également servir d'outil stratigraphique. Outre sa relation avec le champ magnétique terrestre, l'aimantation des sédiments est contrainte par l'environnement sédimentaire. Pour parvenir à établir fidèlement l'enregistrement paléomagnétique, il est nécessaire de déterminer les mécanismes mis en cause lors de l'acquisition de l'aimantation. L'objectif de cette thèse est de mieux comprendre les processus responsables de l'acquisition de l'aimantation par les sédiments en étudiant les paramètres sédimentaires et magnétiques impliqués dans le blocage des grains magnétiques au sein du sédiment. Pour cela, des sédiments varvés du lac proglaciaire Ojibway, ainsi que des turbidites, ont été étudiés.

Dans le premier chapitre, il est question de la limite de l'utilisation des U-channels pour l'étude des variations rapides du champ magnétique terrestre, notamment dans le cas des excursions et des inversions. Pour cela, une comparaison entre des mesures ponctuelles et U-channels, de différentes inversions et excursions, ont été faites. Nous avons créé différentes tailles d'excursions et avons constaté que les excursions enregistrées sur moins de 7,5 cm étaient à peine détectées par des mesures U-channels. Pour les inversions, les mesures U-channels lissent le signal des enregistrements et génèrent des artefacts. Nous avons testé la convolution des mesures ponctuelles par différentes fonctions de réponse. Les résultats montrent que même de petits changements dans la fonction de réponse peuvent générer des différences significatives dans les résultats.

Dans le second chapitre, nous nous sommes concentrés sur des sédiments du lac proglaciaire Ojibway (~ 8.5 ka cal BP) et plus particulièrement sur plusieurs lits d'été et d'hiver d'épaisseur centimétrique qui ont été échantillonnés individuellement. Des analyses paléomagnétiques, granulométriques et géochimiques ont été réalisées sur chaque lit. Les déclinaisons magnétiques ne montrent pas de fortes déviations systématiques par rapport à la direction attendue, contrairement aux inclinaisons qui sont beaucoup plus faibles que celles attendues. L'aplanissement de l'inclinaison est systématiquement plus prononcé en hiver ( $25.5^\circ \pm 4.3^\circ$ ) qu'en été ( $12.5^\circ \pm 3.3^\circ$ ). Les lits d'été sont plus épais que les lits d'hiver et sont caractérisés par une susceptibilité magnétique plus forte, un rapport Ca/Fe plus élevé en raison de la dilution du Fe par l'augmentation du contenu en carbonate, et des grains sédimentaires et magnétiques plus grossiers. Ces observations reflètent l'apport de particules détritiques plus grossières pendant l'été, tandis que la fraction plus fine est restée en suspension jusqu'à la déposition en hiver. Une différence de compaction des lits d'hiver

et d'été et une variation de la composition des grains magnétiques pourraient être responsable des différences observées. Ces résultats indiquent que la variation de la lithologie peut jouer un rôle dominant sur les enregistrements magnétiques des sédiments.

Dans le troisième chapitre, une compilation de données magnétiques de 17 couches déposées rapidement (RDL) avec des épaisseurs variables allant de 7,1 cm à 1510 cm a été faite. Cette étude a été menée d'un point de vue statistique pour mettre en avant les mécanismes d'acquisition de l'aimantation, qui jouent un rôle majeur durant ce type de dépôt. Nous avons trouvé une relation logarithmique entre l'amplitude des changements d'inclinaison, ainsi que l'amplitude des tailles de grains magnétiques et l'épaisseur des RDL. L'inclinaison et la taille des grains sont elles-mêmes corrélées les unes aux autres par une loi logarithmique. Comme il n'y a pas de relation entre l'écart d'inclinaison et la profondeur, la compaction ne peut expliquer de tels écarts significatifs. La flocculation varie probablement selon la grosseur du grain, mais, encore une fois, l'amplitude des écarts d'inclinaison est difficile à expliquer. La turbulence inhérente au processus de dépôt de tels événements est probablement le facteur dominant. Cette interprétation est appuyée par des calculs visant à décrire l'impact des courants de fond.

Au final, cette thèse avait pour but principal d'améliorer nos connaissances sur les mécanismes d'acquisition de l'aimantation par les sédiments. Cette étude a permis de mettre en avant deux nouveaux mécanismes, qui ont une influence sur l'enregistrement de l'aimantation dans les sédiments: la turbulence et une faible variation de la composition magnétique.

Mots-clés: paléomagnétisme, U-channel, aimantation naturelle rémanente, aimantation rémanente détritique, varve, turbidite, hyperpycnite.

## ABSTRACT

The natural remanent magnetization (NRM) of sediments can be used to reconstruct variations of Earth's magnetic field in the past. The variability of the geomagnetic field provides information on Earth's internal dynamics and its sedimentary record can also serve as a stratigraphic tool. In addition to its relationship with the Earth's magnetic field, sediment magnetization is constrained by the sedimentary environment. To succeed in faithfully tracking the paleomagnetic variations, it is necessary to determine which processes are involved during the acquisition of the magnetization. The aim of this thesis is to better understand processes responsible for the acquisition of magnetization by sediments by studying sedimentary and magnetic parameters involved in the blocking of magnetic grains within the sediment. For this purpose, varved sediments of the proglacial Lake Ojibway, as well as turbidites, have been studied.

The first chapter is about the limits of the use of U-channels for the study of rapid variations of the Earth's magnetic field, especially for excursions and reversals. For this, a comparison between discrete measurements and U-channels, from different inversions and excursions, was made. We created different excursion sizes and found out that excursions recorded over less than 7.5 cm are barely detected in U-channel measurements. Regarding reversals, U-channel measurements smooth the signal of low-resolution records and generate artifacts. We tested the convolution of discrete samples measurements by different response functions. The results show that even small response function changes can generate significant differences in results.

In the second chapter, we focused on sediments from the proglacial Lake Ojibway ( $\sim 8.5$  ka cal BP) and more particularly on several centimeter-thick summer and winter beds that were sampled individually. Paleomagnetic, granulometric and geochemical analyses were conducted on each bed. Magnetic declinations do not show strong systematic deviations from the expected direction, contrary to inclinations, which are much shallower than expected. Inclination shallowing is systematically more pronounced in winter ( $25.5^\circ \pm 4.3^\circ$ ) than in summer ( $12.5^\circ \pm 3.3^\circ$ ). Summer beds are thicker than winter beds and characterized by stronger magnetic susceptibility, higher Ca/Fe ratio due to Fe dilution by the large increase in carbonate content, and coarser sedimentary and magnetic grains. These observations reflect the input of coarser detrital particles during summer, while the finer fraction remained in suspension until deposition in winter. Differential compaction of the winter and summer beds and variations of magnetic grain composition might be responsible for the observed differences. These results indicate that lithological changes can play a dominant role on magnetic sediment records.

In the third chapter, we have compiled magnetic data of 17 rapid deposit layers (RDL) with varying thicknesses ranging from 7.1 cm to 1510 cm. This study was conducted from a statistical point of view to highlight the mechanisms of acquisition of magnetization, which play a major role during this type of depositions. We found a logarithmic relationship between the amplitude of inclination changes, as well as the amplitude of magnetic grain sizes and the RDL thickness. Inclination and grain sizes are themselves correlated to each other by a logarithmic law. As there is no relationship between the deviation and depth, compaction cannot account for such significant deviations. Flocculation likely varies with grain size, but again, the amplitude of the inclination deviations is difficult to explain. Turbulence inherent to the depositional process of such events is most likely the dominant factor. This interpretation is supported by calculations aimed at describing the impact of bottom currents.

In the end, the main aim of this thesis was to improve our knowledge of the mechanisms of magnetization's acquisition by sediments. This study highlighted two new mechanisms, which have an influence on the recording of magnetization in sediments: turbulence and a little variation in magnetic composition.

Keywords: paleomagnetism, U-channel, natural remanent magnetization, detrital remanent magnetization, varve, turbidite, hyperpycnite.

## TABLE DES MATIÈRES

REMERCIEMENTS .....	ix
RÉSUMÉ .....	xi
ABSTRACT .....	xiii
TABLE DES MATIÈRES.....	xv
LISTE DES FIGURES.....	xix
LISTE DES TABLEAUX .....	xxv
LISTE DES ABRÉVIATIONS, DES SIGLES ET DES ACRONYMES .....	xxvii
INTRODUCTION GÉNÉRALE .....	1
LE CHAMP MAGNÉTIQUE TERRESTRE.....	1
L'ENREGISTREMENT DU CHAMP MAGNÉTIQUE TERRESTRE DANS LES SÉDIMENTS.....	4
Les modèles.....	4
Les expériences .....	7
LES VARVES ET LES TURBIDITES .....	10
LIEU D'ÉTUDE.....	10
ÉCHANTILLONNAGE ET MESURE DE L'AIMANTATION DANS LES SÉDIMENTS.....	11
Échantillonnage .....	11
Mesure d'aimantation .....	12
OBJECTIFS DE RECHERCHE .....	14
ORGANISATION DE LA THÈSE.....	17
AUTRES RÉALISATIONS ET COLLABORATIONS .....	18
Articles 18	
Présentations .....	19
Collaborations .....	20

RÉFÉRENCES.....	21
CHAPITRE 1 LES ENREGISTREMENTS PALÉOMAGNÉTIQUES DES U-CHANNELS SONT-ILS APPROPRIÉS POUR L'ÉTUDES DES INVERSIONS ET DES EXCURSIONS?.....	25
1.1    RÉSUMÉ EN FRANÇAIS DU PREMIER ARTICLE .....	25
1.2    ARE PALEOMAGNETIC RECORDS FROM U-CHANNELS APPROPRIATE FOR STUDIES OF REVERSALS AND EXCURSIONS?.....	27
1.3    INTRODUCTION .....	27
1.4    MEASUREMENT RESOLUTION .....	29
1.5    EXPERIMENTAL PROTOCOL .....	31
1.6    SIMULATION OF GEOMAGNETIC EXCURSIONS .....	35
1.6.1    Previous Studies.....	35
1.6.2    Artifacts Induced by U-channel Measurements.....	36
1.7    SIMULATIONS OF POLARITY TRANSITIONS .....	39
1.8    U-CHANNEL MEASUREMENTS AND SIGNAL CONVOLUTION .....	43
1.9    CONCLUSIONS .....	46
1.10    ACKNOWLEDGMENTS.....	48
1.11    REFERENCES.....	49
CHAPITRE 2 INFLUENCE DE LA LITHOLOGIE SUR L'AIMANTATION RÉMANENTE ENREGISTRÉE DANS LES SÉDIMENTS VARVÉS DU LAC GLACIAIRE OJIBWAY (CANADA).....	55
2.1    RÉSUMÉ EN FRANÇAIS DU DEUXIÈME ARTICLE .....	55
2.2    INFLUENCE OF LITHOLOGY ON THE REMANENT MAGNETIZATION AS RECORDED IN VARVED SEDIMENTS FROM THE GLACIAL LAKE OJIBWAY (CANADA) .....	57
2.3    INTRODUCTION .....	57
2.4    ORIGIN OF SAMPLES AND GEOLOGICAL CONTEXT .....	60
2.5    METHODS.....	61
2.5.1    Sedimentary analyses .....	61

2.5.2	Magnetic measurements .....	62
2.6	RESULTS .....	63
2.6.1	Lithological and chemical characteristics .....	63
2.6.2	Magnetics properties .....	66
2.7	DISCUSSION.....	76
2.8	CONCLUSIONS .....	81
2.9	ACKNOWLEDGMENTS .....	82
2.10	REFERENCES.....	82
 CHAPITRE 3 IMPACT DE LA TURBULENCE SUR L'ALIGNEMENT MAGNÉTIQUE DANS LES SÉDIMENTS .....		 91
3.1	RÉSUMÉ EN FRANÇAIS DU TROISIÈME ARTICLE.....	91
3.2	IMPACT OF TURBULENCE ON MAGNETIC ALIGNEMENT IN SEDIMENTS .....	93
3.3	INTRODUCTION.....	93
3.4	METHODOLOGY.....	96
3.4.1	Core MD99-2222 .....	96
3.4.2	Cores from Tanty et al. (2016) .....	97
3.5	COMPARISON OF RDL FROM CORE MD99-2222.....	97
3.5.1	Magnetic characteristics .....	97
3.5.2	Coherent features between RDL.....	100
3.6	DISCUSSION.....	103
3.6.1	Compaction and flocculation.....	103
3.6.2	Effect of turbulence.....	107
3.7	CONCLUSION .....	112
3.8	ACKNOWLEDGMENTS .....	112
3.9	SUPPORTING INFORMATION.....	113
3.10	REFERENCES.....	125
 CONCLUSION GÉNÉRALE.....		 133



## LISTE DES FIGURES

Figure 1: Vue d'artiste du vent solaire et de la magnétosphère terrestre (source: NASA).....	2
Figure 2: Composante du champ magnétique terrestre.....	3
Figure 3: Illustration des filtres du blocage des grains magnétiques lors de l'acquisition de la pDRM (Roberts et Winklhofer, 2004).....	7
Figure 4: Processus d'acquisition de l'aimantation par les sédiments (Roberts et al., 2013).....	9
Figure 5: Localisation des zones d'échantillonnage des carottes G1 à G7 (lac Ojibway, Canada), MD01-2477 (Golfe de Corinthe), MD12-3418 (Golfe du Bengale), MD98-2194 (Mer de Chine) and MD99-2222 (Fjord du Saguenay, Canada).....	11
Figure 6: Échantillonnage de U-channels et de cubes.....	12
Figure 7: Magnétomètre cryogénique 2G Enterprises de l'IPGP.....	13
Figure 8: Response functions of model 755-R (2G Enterprises) magnetometers with different sets of sensing coils. The type and location of the magnetometers are mentioned in each panel. IPGP (Institut de Physique du Globe de Paris), LSCE (Laboratoire des Sciences du Climat et de l'Environnement), and ISMER (Institut des sciences de la mer de Rimouski).....	29
Figure 9: (a) Evolution of the remanent magnetization (intensity, declination, and inclination) of the synthetic samples as a function of time. The maximum duration of the experiments (3 hr) is indicated by the orange zone. (b) Alternating field demagnetization diagrams of the anhysteretic remanent magnetization (ARM) imparted to the synthetic samples. The solid symbols correspond to projections onto the horizontal plane, while the open symbols represent projections onto the vertical plane.....	33

Figure 10: (a) Angular variation (blue squares) and intensity (red squares) changes measured for individual cubes for a 6-cm-long excursion simulated by four reversely magnetized cubes. (b) Same as (a) for the equivalent U-channel. (c) Angular deviation for excursions recorded over increasing length intervals. (d) Same as (c) for magnetization intensity. (e) Maximum angular deviation from the original polarity and minimum moment variation measured in U-channel samples as a function of excursion length. The maximum angular deviation does not reach 180° for events smaller than 20 cm. ....	34
Figure 11: Artificial VGP paths derived from U-channel measurements for (a) 4.5-cm and (b) 12-cm events. ....	38
Figure 12: Simulations of a 2-kyr polarity transition recorded over an 18-cm stratigraphic interval. (a) Angular deviation (blue squares) and magnetization intensity (red squares) of individual cubes as a function of their position in the simulated sequence, and (b) angular deviation (blue dots) and magnetization intensity (red dots) derived from the corresponding U-channel. (c) Initial VGP path derived from the single samples, and (d) VGP path obtained from the U-channel measurements. ....	40
Figure 13: Same as Figure 12 for a 30-cm simulated transitional interval recorded in sediment with 15 cm/kyr deposition rate and a 2-kyr transition. ....	41
Figure 14: Same as Figure 13 for a more complex 2-kyr transition over a 30-cm transitional interval with a 15 cm/kyr deposition rate. ....	42
Figure 15: Convolution of measurements for successive discrete samples recording a 2-kyr polarity transition over 30 cm. (a) Angular deviation (blue dots) and magnetization intensity (red dots) for measurements of individual 1.5-cm samples. (b) Angular deviation (blue dots) and magnetization intensity (red dots) obtained from U-channel measurements. (c) Angular deviation (green) and magnetization intensity (purple) after convolution of discrete sample measurements by the Institut de Physique du Globe de Paris (IPGP) high-resolution (HR) superconducting quantum interference device (SQUID) response functions. (d) Same as (c) with the IPGP direct current SQUIDS. (e) Same as (c) using the Laboratoire des Sciences du Climat et de l'Environnement (LSCE) magnetometer response. (f) Same as (c) using the Institut des sciences de la mer de Rimouski (ISMER) magnetometer response. ....	45

Figure 16: VGP paths shown in Figure 15 for the measurements and calculated convolutions.....	46
Figure 17: (a) Geographic locations of Lake Ojibway (b) and Lake Matagami during deglaciation ~8500 cal BP. Red stars indicate the site location. Blue arrows show glacial flow-lines associated with the residual ice domes. Modified from Roy et al. (2015). .....	59
Figure 18: From left to right as a function of depth within the G7 core: core photograph, HU numbers related to sediment density derived from the CAT-Scan images and composite column that summarizes the succession of winter and summer beds. Downcore evolution of typical magnetic (inclination, declination, magnetic susceptibility) and sedimentary (Ca/Fe ratio, Fe/cps and grain size) parameters within the G7 core. Black (resp. pink dots) on inclination and declination correspond to single samples (resp. U-channels). Red line in the inclination represents the GAD value. Fe profile in peak area is normalized by the counts per second (cps) at the corresponding depth.....	64
Figure 19 : Photography of a thin section from core G7 under normal light (a) and polarized light (b). A bar code is shown on the right, the white and black zones correspond respectively to summer and winter beds. ....	66
Figure 20: Thermomagnetic curves of low-field susceptibility versus temperature of two summer and two winter beds. Heating (resp. cooling) curves are shown in red (resp. in blue). .....	67
Figure 21: Demagnetization diagrams. Typical vector end-point diagrams for two summer and two winter beds. Solid symbols correspond to projections onto the horizontal plane, while open symbols represent projections onto the vertical plane.....	69
Figure 22: Stereoplot of the magnetic directions recorded by the 1-cm thick beds within the G7 interval. Red and blue dots indicate summer and winter beds, respectively. The present day-field direction is shown by an asterisk. The summer bed inclinations are closer to the geocentric axial dipole value at the site than the winter ones.....	70
Figure 23: Magnetic and sedimentary properties for each individual 1-cm thick bed from the G7 core. Red and blue data points correspond to the summer and winter beds, respectively. Red line and green dashed line on inclination represent	

respectively the GAD value and the inclination value at the same latitude around 9000 cal BP.....	72
Figure 24: Day plot obtained for the 1-cm thick beds within the G7 core. Red (resp. blue) directions are for summer (resp. winter) beds. The orange star indicates the direction of the geocentric axial dipole at the site.....	74
Figure 25: FORCs of the summer bed at 39.6 cm (a) and winter bed at 40.9 cm (b) in the G7 core. Backfield, hysteresis and central ridge coercivity distributions derived from the original FORC measurements for summer bed (c) and winter bed (d). FORC zoom of the central ridge isolate from the other contribution for summer bed (e) and winter bed (f). All diagrams have been generated using VARIFORC built-in functions (Egli, 2013).....	75
Figure 26: (a) Stereographic projection of the $k_1$ and $k_3$ axes of the magnetic susceptibility ellipsoid. (b) Flinn diagram, $k_1/k_2$ represents the lineation and $k_2/k_3$ the foliation. (c) T-P' diagram showing the shape factor $T = (2\log k_2 - \log k_1 - \log k_3)/(\log k_1 - \log k_3)$ as a function of the corrected degree of anisotropy $P' = \exp(2\eta_1 - \eta_2 + \eta_2 - \eta_2 + \eta_3 - \eta_2)$ with $\eta_i = \ln k_{ii} = 1,2,3$ and $\eta = (\eta_1 + \eta_2 + \eta_3)/3$ (Jelinek, 1981). Red and blue dots indicate summer and winter beds, respectively.....	77
Figure 27: Inclination deviation relative to the GAD as a function of the thickness of upper bed. A linear regression is plotted in green.....	80
Figure 28: Mean of inclination, declination, NRM/ARM and S-ratio recorded by the 1-cm thick beds within the G7 interval. Red and blue dots indicate summer and winter beds, respectively. Green dashed line on inclination represents the inclination value at the same latitude around 9000 cal BP.....	81
Figure 29: Location of the sampling sites of cores MD01-2477 (Gulf of Corinth), MD12-3418 (Bay of Bengal), MD98-2194 (China Sea) and MD99-2222 (Saguenay Fjord, Canada).....	95
Figure 30: Sedimentological and physical properties of core MD99-2222 (St-Onge et al., 2004).....	98
Figure 31: Sedimentological and physical properties of the RDL 1 event from core MD99-2222 (St-Onge et al., 2004). Red curves were obtained by singular spectrum analysis (SPA). The maximum amplitude changes in inclinations and grain sizes were	

calculated from the SPA results and are shown by blue arrows. Green line in the inclination represents the geocentric axial dipole (GAD) value. The grey zone represents a normal period of sedimentation before the RDL1 deposition.....	99
Figure 32: Amplitude of inclination changes within 16 RDLs as a function of their thickness. Black, red and pink closed circles are for turbidites, hyperpycnites and other RDLs from core MD99-2222, respectively. Green closed circles show the values of the four turbidites studied by Tanty et al. (2016).....	101
Figure 33: Amplitude of grain size changes within 12 RDLs as a function of their thickness. Black, red and pink closed circles are for turbidites, hyperpycnites and other RDLs from core MD99-2222, respectively.....	102
Figure 34: Amplitude of inclination changes as a function of grain sizes changes within 12 RDLs. Same symbols as in Figure 33.....	104
Figure 35: Amplitude of inclination changes within 12 RDLs as a function of their average depth in core MD99-2222. Black, red and pink closed circles are for turbidites, hyperpycnites and other RDLs from core MD99-2222, respectively.....	105
Figure 36: Inclination as a function of sediment mean grain size in 13 RDLs. ....	106
Figure 37: Numerical simulations of DRM acquired by floes containing $100 \times 2 \mu\text{m}$ diameter particles with a magnetic moment $m = 5 \text{ fAm}^2$ in presence of a $100 \mu\text{T}$ magnetic field with $60^\circ$ inclination in an infinite water column for different friction velocities (a) Intensity profiles (after normalization) as a function of flow azimuth. (b) Inclination profiles as a function of flow azimuth. (c) Declination profiles as a function of flow azimuth. ....	111
Figure 38: Sedimentological and physical properties of the RDL 2 event from core MD99-2222 (St-Onge et al., 2004). Red curves were obtained by singular spectrum analysis (SPA). Green line in the inclination represents the geocentric axial dipole (GAD) value. ....	113
Figure 39: Same as Figure 38 for RDL 3 event.....	114
Figure 40: Same as Figure 38 for RDL 4 event.....	115
Figure 41: Same as Figure 38 for RDL 5 event.....	116

Figure 42: Same as Figure 38 for RDL 6 event .....	117
Figure 43: Same as Figure 38 for RDL 7 event .....	118
Figure 44: Same as Figure 38 for RDL 8 event .....	119
Figure 45: Same as Figure 38 for RDL 9 event .....	120
Figure 46: Same as Figure 38 for RDL 10 event .....	121
Figure 47: Same as Figure 38 for RDL 11 event .....	122
Figure 48: Same as Figure 38 for RDL 12 event .....	123
Figure 49: Same as Figure 38 for RDL 13 event .....	124
Figure 50: Processus d'acquisition de l'aimantation par les sédiments mis en avant dans cette étude. Les courbes rouge et bleue représentent la variation de l'inclinaison hypothétique pour deux compositions de grains magnétiques différentes soumises à un champ magnétique avec une inclinaison représentée en vert. La variation de l'inclinaison durant la compaction est en pointillé car son comportement n'est pas encore bien connu (Roberts et Winklhofer, 2004). La courbe en violet représente un cas particulier où la bioturbation jouerait un rôle important de remise en suspension des grains .....	140

## **LISTE DES TABLEAUX**

Tableau 1: Localisation des sédiments étudiés .....	10
---	----



## **LISTE DES ABRÉVIATIONS, DES SIGLES ET DES ACRONYMES**

<b>a.f.</b>	<i>alternating field</i> , champ alternatif
<b>ARM</b>	<i>anhysteretic remanent magnetisation</i> , aimantation rémanente anhystéritique
<b>d.c.</b>	<i>direct current</i> , courant continu
<b>DRM</b>	<i>detrital remanent magnetization</i> , aimantation rémanente détritique
<b>FORC</b>	<i>first-order reversal curve</i> .
<b>GAD</b>	<i>geocentric axial dipole</i> , dipole axial géocentré
<b>Hc</b>	<i>coercive force</i> , coercivité
<b>Hcr</b>	<i>remanent coercive force</i> , coercivité rémanente
<b>INRS-ETE</b>	Institut National de la Recherche Scientifique Eau Terre Environnement
<b>IPGP</b>	Institut de Physique du Globe de Paris
<b>IRM</b>	<i>isothermal remanent magnetization</i> , aimantation rémanente isothermale
<b>ISMER</b>	Institut des Sciences de la Mer à Rimouski
<b>k</b>	<i>magnetic susceptibility</i> , susceptibilité magnétique

<b>k<sub>AARM</sub></b>	<i>susceptibility of the anhysteretic remanent magnetisation</i> , susceptibilité de l'aimantation rémanente anhystérétique
<b>LSCE</b>	Laboratoire des Sciences du Climat et de l'Environnement
<b>MAD</b>	<i>maximum angular deviation</i> , déviation angulaire maximum
<b>MD</b>	<i>multidomain</i> , domaines multiples
<b>Mr</b>	<i>saturation remanence</i> , rémanence à saturation
<b>Ms</b>	<i>saturation magnetisation</i> , aimantation à saturation
<b>MSCL</b>	<i>multi-sensor core logger</i> , banc de mesures
<b>NRM</b>	<i>natural remanent magnetisation</i> , aimantation naturelle rémanente
<b>pDRM</b>	<i>post-detrital remanent magnetization</i> , aimantation rémanente post-déposition
<b>PSD</b>	<i>pseudo-single domain</i> , domaine pseudo-simple
<b>RDL</b>	<i>rapidly deposited layers</i> , couches déposées rapidement
<b>SD</b>	<i>single domain</i> , domaine simple
<b>SIRM</b>	<i>saturation isothermal remanent magnetization</i> , aimantation rémanente isothermale à saturation

<b>SP</b>	<i>superparamagnetic</i> , superparamagnétique
<b>SQUID</b>	<i>superconducting quantum interference device</i>
<b>UQAM</b>	Université du Québec à Montréal
<b>UQAR</b>	Université du Québec à Rimouski
<b>VADM</b>	<i>virtual axial dipole moment</i> , moment dipolaire axial virtuel
<b>VGP</b>	<i>virtual geomagnetic pole</i> , pôle géomagnétique virtuel



## **INTRODUCTION GÉNÉRALE**

La mesure de l'aimantation rémanente des sédiments (NRM) permet de reconstituer les variations du champ magnétique terrestre dans le passé. Il sert d'outil stratigraphique, notamment au niveau du Quaternaire, riche en inversions et excursions géomagnétiques. Il sert aussi pour les études magnétiques environnementales (e.g., Meynadier et al., 1992; Valet & Meynadier, 1993; Roberts et al., 1997; Channell et al., 2000; Channell & Kleiven, 2000; Stoner et al., 2000; Valet, 2003; Barletta et al., 2010; Macrì et al., 2010; Mazaud et al., 2012). Cependant, l'aimantation des sédiments, en plus de dépendre du champ magnétique terrestre, dépend, dans une moindre mesure, de l'environnement sédimentaire.

Cette thèse s'intéresse à l'enregistrement du champ magnétique terrestre dans les sédiments. Il est donc nécessaire, dans un premier temps, de présenter le champ magnétique terrestre et de discuter de sa variation séculaire, des excursions et des inversions. Dans un second temps, nous aborderons l'état des connaissances actuelles sur l'enregistrement du champ magnétique par les sédiments. Pour finir, il sera question de l'échantillonnage et de la mesure de l'aimantation dans les sédiments.

## **LE CHAMP MAGNÉTIQUE TERRESTRE**

Depuis des centaines d'années, le champ magnétique terrestre est utilisé comme outil de navigation. En effet, la boussole permet de s'orienter par rapport aux pôles magnétiques. Mais ce n'est pas la seule fonction du champ magnétique. Il est tout aussi important que l'atmosphère et permet la vie sur Terre. Il protège cette dernière des vents solaires et des rayons cosmiques en agissant comme un bouclier protecteur (Figure 1).

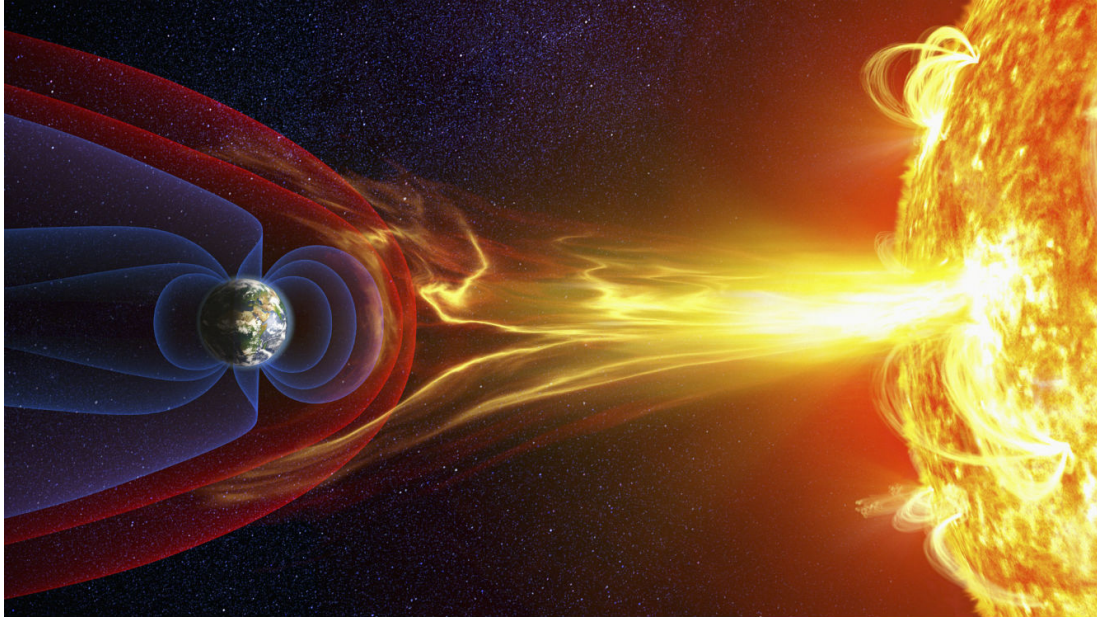


Figure 1: Vue d'artiste du vent solaire et de la magnétosphère terrestre (source: NASA).

Le champ magnétique, qui est à 90% dipolaire (Tauxe, 2010; Dubois et al., 2016), est dû principalement au mouvement du fer liquide dans le noyau externe de la Terre. Ainsi, une représentation simplifiée de celui-ci serait le champ magnétique d'un aimant, c'est à dire d'un dipôle axial (GAD) aligné avec l'axe de la Terre. Le champ magnétique terrestre  $\vec{B}$  est défini par sa déclinaison D, son inclinaison I et sa norme B (Figure 2). La déclinaison représente l'angle entre les pôles Nord géographique et magnétique. L'inclinaison représente l'angle du champ magnétique par rapport au plan horizontal. Actuellement, celui-ci est positif dans l'hémisphère Nord et négatif dans l'hémisphère Sud. Ce qui n'a pas toujours été le cas.

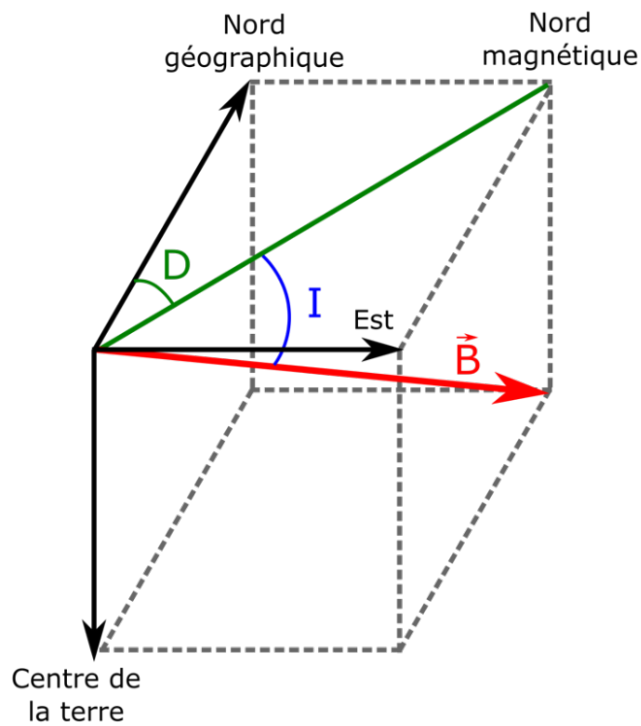


Figure 2: Composante du champ magnétique terrestre.

En effet, le champ magnétique terrestre n'est pas fixe. Il varie au cours du temps. Il possède une variation séculaire, correspondant principalement à des variations de la partie non-dipolaire du champ magnétique terrestre à l'échelle du siècle. Il y a aussi de grandes variations, telles que les excursions et les inversions. Ainsi, pour prévoir l'évolution du champ magnétique terrestre, il est nécessaire de comprendre ses variations à différentes échelles de temps. Pour cela, il est essentiel d'étudier les enregistrements passés de ce dernier. Le champ magnétique terrestre ancien peut s'enregistrer dans différents matériaux, comme dans des poteries, des coulés volcaniques ou encore des sédiments. Cette étude se concentrera sur l'enregistrement du champ magnétique terrestre ancien dans les sédiments lacustres ou marins.

## L'ENREGISTREMENT DU CHAMP MAGNÉTIQUE TERRESTRE DANS LES SÉDIMENTS

L'acquisition de l'aimantation des sédiments est un phénomène complexe qui implique de nombreux paramètres. Pour comprendre ce phénomène, de nombreuses expériences et de nombreux modèles ont été proposés ces 60 dernières années (Nagata, 1961; Collinson, 1965; Stacey, 1972; Denham and Chave, 1982; Tauxe, 1993; Quidelleur et al., 1995; Katari et al., 2000; Katari and Bloxham, 2001; Carter-Stiglitz et al., 2006; Heslop et al., 2006; Tauxe et al., 2006; Shcherbakov and Sycheva, 2010; Spassov and Valet, 2012; Roberts et al., 2013). L'hypothèse de base demeure toujours la proportionnalité du champ magnétique à l'aimantation rémanente détritique (DRM). Cette dernière est acquise par le sédiment :  $DRM \approx k \times B_{anc}$ , où  $k$  est la constante de proportionnalité et  $B_{anc}$  le champ magnétique ancien. Sans cette hypothèse de base, l'étude du paléomagnétisme sur les sédiments serait impossible.

### Les modèles

Le premier modèle a été proposé par Nagata en 1961. Ce modèle prenait juste en compte la rotation des grains magnétiques dans un fluide soumis à un champ magnétique externe. Le champ magnétique a tendance à aligner le moment des particules magnétiques alors que les forces de friction s'opposent à ce mouvement. Ce qui donne, pour une particule avec un moment magnétique  $m$  et avec un angle  $\alpha$ , par rapport au champ magnétique  $B$ :

$$I \frac{d^2\alpha}{dt^2} = -\lambda \frac{dx}{dt} - mB \sin \alpha \quad (1)$$

Avec  $\lambda$ , le coefficient de viscosité du fluide, et  $I$ , le moment d'inertie de la particule. La solution trouvée par Nagata à l'équation 1 (Nagata, 1961) est:

$$\tan \frac{\alpha}{2} = \tan \frac{\alpha_0}{2} e^{(-\frac{mNt}{\lambda})} \quad (2)$$

Où  $\alpha_0$  est l'angle initial entre  $m$  et  $B$ . Avec  $\lambda = 8\pi r^3 \eta$ , où  $r$  est le rayon de la particule et  $\eta$  la viscosité de l'eau ( $\sim 10^{-6}$  kg m<sup>-1</sup> s<sup>-1</sup>). La constante de temps de l'équation (2) avec  $\alpha_0$  réduit à 1/e:

$$\tau = \frac{\lambda}{mB} = \frac{6\eta}{MB} \quad (2)$$

Où  $M$  est le moment normalisé par le volume.

En conséquence, en prenant des valeurs d'aimantation pour un grain mono-domaine (SD)  $M \approx 4,8 \times 10^5$  A/m dans un champ de 50 µT ( $\approx$  champ terrestre), on obtient pour la valeur  $\tau$  quelques millisecondes (Tauxe et al., 2006). Ce même calcul, en prenant en compte l'aimantation de l'hématite ( $M \approx 200$  A/m), aura pour solution  $\tau < 1$  s. Cette valeur impliquerait qu'en l'espace de quelques secondes l'ensemble des grains magnétiques serait aligné avec le champ magnétique ambiant. Cela supposerait que la DRM résultante serait toujours saturée car la durée de chute dans une colonne d'eau est de  $t \gg \tau$ , soit  $DRM = SIRM$  (aimantation rémanente isothermale à saturation). Or, de nombreuses mesures de sédimentation en laboratoire (Tauxe, 1993; Tauxe et al., 2006; Spassov et Valet, 2012; Roberts et al., 2013) présentent une dépendance linéaire entre la DRM et le champ magnétique ambiant. Cela prouve donc que ce premier modèle ne considère pas toutes les interactions liées à l'acquisition de l'aimantation par les sédiments. De plus, s'il était exact, l'hypothèse de base du paléomagnétisme ne serait plus valide étant donné qu'il n'y aurait plus de proportionnalité entre la DRM et le champ magnétique terrestre. Cela empêcherait, par la même occasion, de faire une étude paléomagnétique sur des sédiments.

Il est alors nécessaire de rajouter d'autres paramètres à cette équation du premier ordre pour prendre en compte tous les éléments liés à l'acquisition de la DRM. Ces paramètres sont ceux qui augmentent le temps d'alignement des grains. L'un des premiers

paramètres proposés, faisant appel au mouvement brownien, est l’agitation thermique (Collinson, 1965; Stacey, 1972; Tauxe et al., 2006). Ainsi, Collinson (1965) propose de rajouter ce phénomène d’agitation thermique à l’équation (1). Mais cet effet n’affecte que les fines particules qui sont plus sensibles à l’agitation thermique, les retardant ainsi à s’aligner instantanément (comparativement au temps de chute dans la colonne d’eau). Cependant, cela ne suffit pas à expliquer complètement la DRM. En effet, les gros grains ne sont pas affectés par ce mécanisme et seraient donc rapidement saturés.

La dernière hypothèse proposée est l’impact de la floculation (Tauxe, 1993; Katari et Bloxham, 2001; Tauxe et al., 2006; Shcherbakov et Sycheva, 2010; Roberts et al., 2013). La floculation crée un agglomérat de particules sédimentaires et augmente la taille des particules, ce qui augmente, par la même, leur temps d’alignement. En effet, dans un agrégat (floc), les grains magnétiques ne sont pas tous alignés dans la même direction, ce qui a pour conséquence un agrégat possédant une aimantation plus faible et différente de la somme de tous les moments magnétiques de tous les grains dans une même direction. La taille du floc augmente considérablement le temps d’alignement, permettant l’enregistrement d’une DRM proportionnelle au champ magnétique.

Une fois le sédiment déposé, d’autres paramètres interviennent pour modifier l’aimantation, comme la bioturbation ou la compaction. Cette aimantation résultante s’appelle la *post Detrital remanent magnetization* (pDRM). La bioturbation est un mécanisme créant une zone de mélange due à la présence et l’action d’organismes benthiques. Il s’agit d’un phénomène aléatoire difficile à modéliser précisément. La compaction intervient sur une épaisseur limitée jusqu’à la *lock-in depth*. Elle joue un rôle sur l’orientation des grains magnétiques. Le changement et la manière, dont le blocage des grains magnétiques s’effectue entre l’interface eau-sédiment jusqu’à la *lock-in depth*, restent mal connus, mais des modèles d’évolution ont été proposés (Figure 3) (Roberts et Winklhofer, 2004; Roberts et al., 2013).

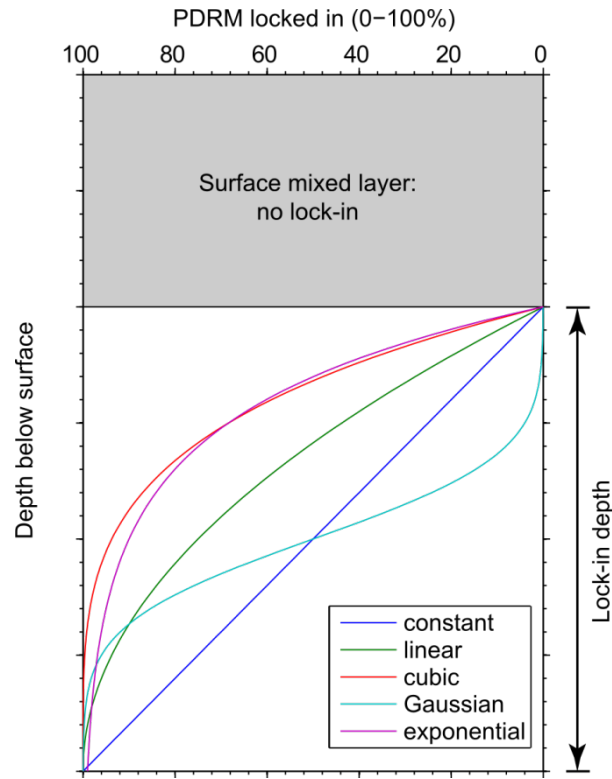


Figure 3: Illustration des filtres du blocage des grains magnétiques lors de l’acquisition de la pDRM (Roberts et Winklhofer, 2004).

Ces résultats restent des modèles pour expliquer l’enregistrement du champ magnétique terrestre par les sédiments. Il est nécessaire de faire des expériences de sédimentation en laboratoire ainsi que des études de cas naturels pour valider et améliorer ces modèles.

### **Les expériences**

Quelques expériences ont été menées ces dernières années dans le but de recréer une acquisition naturelle de l’aimantation par le sédiment. Ces expériences visaient à mieux comprendre l’acquisition de l’aimantation. Elles ont permis notamment de montrer une relation linéaire entre l’aimantation et le champ magnétique ambiant (Spassov et Valet, 2012) quand ce dernier est de l’ordre de grandeur du champ magnétique terrestre.

Cependant, cette relation n'est plus linéaire dans le cas de forts champs magnétiques ambients (Yoshida et Katsura, 1985; Tauxe, 1993; Tauxe et al., 2006).

Par ailleurs, d'autres expériences de sédimentation, menées par Spassov et Valet (2012), cette fois-ci dans une colonne d'eau, montrent l'impact de la flocculation. Des échantillons naturels de sédiments avec une forte teneur en carbonate et en argile sont sédimentés avec et sans défloculant. Pour les échantillons carbonatés, l'augmentation de la flocculation accroît légèrement l'aimantation acquise, alors que pour les sédiments riches en argile, la flocculation diminue l'aimantation acquise (Spassov et Valet, 2012). Ces résultats expérimentaux semblent dévoiler l'impact de la flocculation dans les mécanismes d'acquisition de l'aimantation. De plus, cet effet de la flocculation paraît toucher principalement les sédiments riches en argile et a tendance, en augmentant la taille des agrégats, à induire des dérivations dans les directions. Ainsi, les résultats de Spassov et Valet (2012) montrent que la flocculation n'affecte pas la structure magnétique des grains mais la vitesse de rotation dans le sens du champ magnétique, ce qui en fait un mécanisme important dans l'acquisition de l'aimantation.

Avec ce type d'expérience, recréer la compaction demeure la partie la plus compliquée du processus. En effet, la sédimentation est relativement rapide, car elle dépend, s'il n'y a pas de courant, de la taille des grains/agrégats et de la hauteur de la colonne d'eau. La compaction, quant à elle, est un processus lent d'évacuation de l'eau par diffusion vers le haut et dépend de la vitesse de sédimentation et de la densité/porosité des sédiments. Il est donc nécessaire d'accélérer ce mécanisme et de bloquer les grains autrement. L'une des méthodes utilisées consistait à bloquer artificiellement les grains. Une première méthode utilisée par Spassov et Valet (2012) consistait en l'utilisation d'une gélatine alimentaire pour bloquer la déposition. Cette méthode permet en effet de figer les grains magnétiques, mais ne permet pas de recréer une compaction. De plus, ce fluide (eau + gélatine) ne se comporte pas comme l'eau; la viscosité est différente. Une autre méthode consistait à faire sécher les échantillons (Mao et al., 2014). Cette méthode reste discutable,

car elle entraînerait une déformation des échantillons et donc de l'alignement des grains magnétiques, d'autant plus si l'échantillon contient des argiles.

En résumé, de nombreux paramètres interviennent dans l'acquisition de l'aimantation des sédiments, notamment la coagulation des grains (Tauxe, 1993; Tauxe et al., 2006; Spassov et Valet, 2012) et la rotation des grains pour s'aligner selon le champ magnétique. Une fois déposés, les grains peuvent également subir une bioturbation ou une remobilisation en cas de présence d'organismes ou de courants de fond. Enfin, il y a un blocage progressif des sédiments. Tous ces mécanismes sont représentés sur la Figure 4.

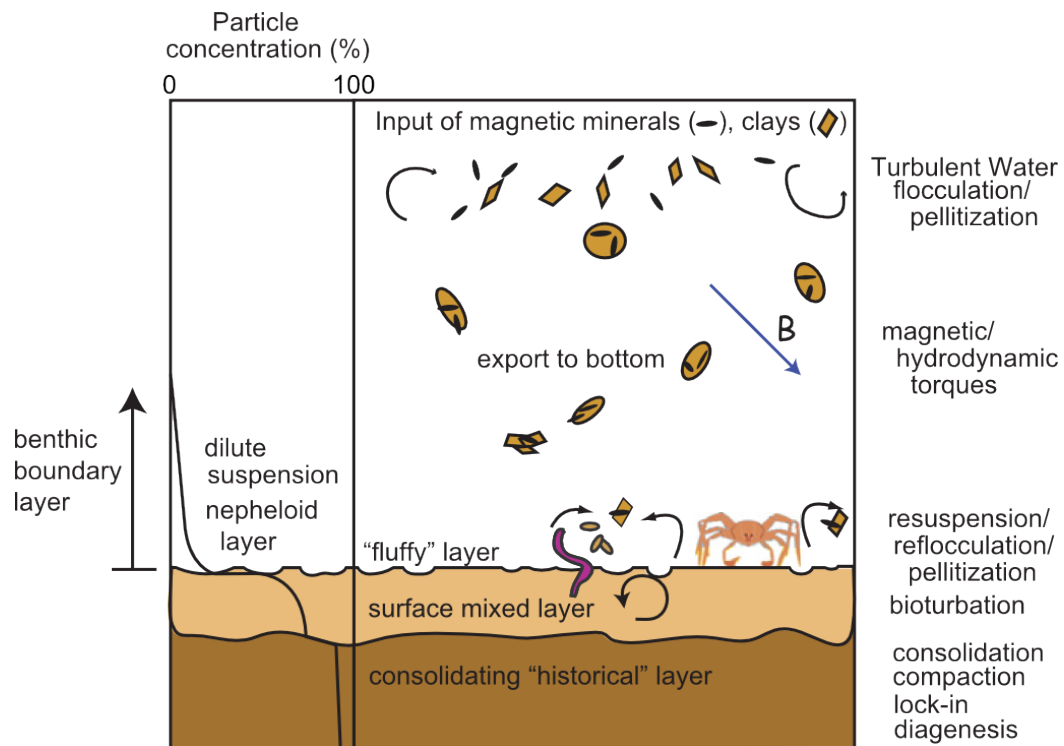


Figure 4: Processus d'acquisition de l'aimantation par les sédiments (Roberts et al., 2013).

L'acquisition du champ magnétique terrestre par les sédiments est partiellement comprise. Il est connu que différents mécanismes sédimentaires comme la compaction, la minéralogie ou la taille des grains affectent l'acquisition de la DRM et de la pDRM, mais leur rôle reste à définir.

## LES VARVES ET LES TURBIDITES

Pour étudier l'impact de la variation sédimentaire sur l'enregistrement magnétique via des échantillons naturels, il est nécessaire, en faisant une analogie avec les expériences sédimentaires, d'avoir des échantillons naturels dont le champ magnétique ambient est fixe, avec une forte variation sédimentaire. Dans la nature, de tels échantillons sont rares, et il est encore plus rare que l'enregistrement magnétique soit de bonne qualité pour pouvoir mener à bien une telle étude. Par ailleurs, ce type d'événement est souvent exempt de bioturbation, supprimant ainsi la composante aléatoire de ce mécanisme de l'équation. Pour réunir de telles conditions, il faut avoir une variation lithologique sans bioturbation sur une période de temps inférieure à une dizaine d'années. Pour cela, nous avons étudié des échantillons varvés et des turbidites, cela sera abordé plus en détails dans les chapitres 2 et 3.

## LIEU D'ÉTUDE

Au cours de ce doctorat, différentes carottes ont été étudiées car elles présentaient des varves ou des turbidites. Dans le Tableau 1 ainsi que sur la Figure 5 sont représentés la localisation de ces dernières.

Tableau 1: Localisation des sédiments étudiés

Nom de la carotte	Localisation	Type de dépôt étudié
G1 à G7	49°56'43.494" N, 77°13'4.663" O	Varves
MD 99-222	48°18.28' N, 70°15.44' O	6 Turbidites 6 Hyperpycnite et 2 RDL
MD 12-3418	16°30.27 N, 87°47.92 E	2 Turbidites
MD 01-2477	38°.133 N, 22°.333 E	1 Turbidite
MD 98-2194	28°06' N; 127°22' E	1 Turbidite

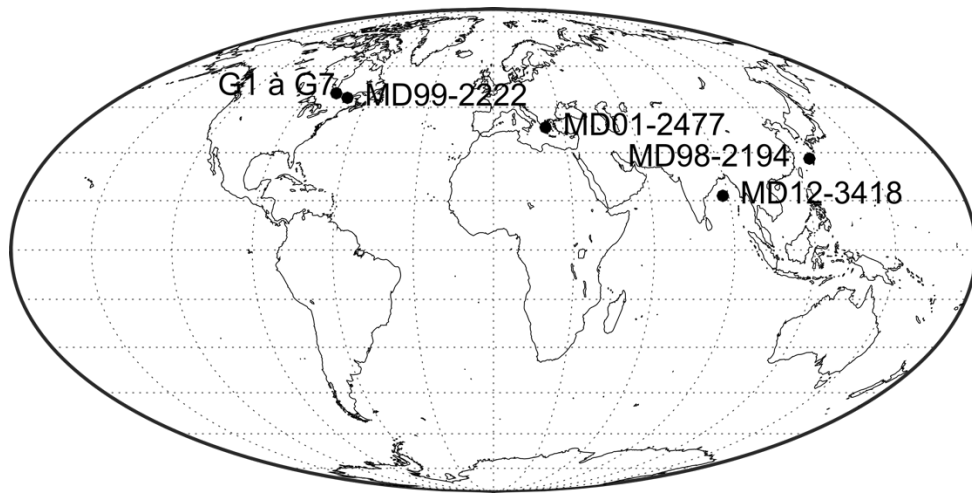


Figure 5: Localisation des zones d'échantillonnage des carottes G1 à G7 (lac Ojibway, Canada), MD01-2477 (Golfe de Corinthe), MD12-3418 (Golfe du Bengale), MD98-2194 (Mer de Chine) and MD99-2222 (Fjord du Saguenay, Canada).

Les varves étudiées proviennent de l'ancien lac proglaciaire Ojibway. Les turbidites étudiées proviennent de 4 carottes différentes. La carotte MD99-2222 provient de l'étude de St-Onge et al. (2004), alors que les carottes MD12-3418, MD01-2477 et MD98-2194 ont été étudiées dans la précédente étude de Tanty et al. (2016). Plus de détails sur l'ensemble de ces données sont abordés dans les chapitres 2 et 3.

### **ÉCHANTILLONNAGE ET MESURE DE L'AIMANTATION DANS LES SÉDIMENTS**

Quand on fait référence aux études paléomagnétiques sédimentaires, il est aussi important de penser à l'échantillonnage de la carotte sédimentaire ainsi qu'à la mesure de l'échantillon.

#### **Échantillonnage**

L'échantillonnage sédimentaire pour une analyse magnétique consiste à un sous-échantillonnage de la carotte sédimentaire. De plus, la taille de l'échantillon joue un rôle important sur la résolution de la mesure. Pour les sédiments, il existe l'échantillonnage par U-channel (Figure 6), de longs tubes de section carrée qui permettent un échantillonnage

pour une mesure dite continue. Ou encore l'échantillonnage ponctuel, qui est souvent réalisé avec des cubes de plastique (Figure 6), mais d'autres formats d'échantillons ponctuels existent également.



Figure 6: Échantillonnage de U-channels et de cubes.

L'échantillonnage est un moment délicat qui nécessite la plus grande minutie. En effet, comme l'objectif est de reconstituer le champ magnétique ancien, son orientation et son intensité, il est nécessaire d'éviter le plus possible de déformer le sédiment durant l'échantillonnage, ainsi que de prendre soin d'orienter les échantillons.

### **Mesure d'aimantation**

L'aimantation dans les sédiments étant plus faible que dans les poteries ou les laves volcaniques, sa mesure nécessite la plupart du temps l'utilisation d'un magnétomètre cryogénique (Figure 7). Actuellement, une seule compagnie fournit l'ensemble des laboratoires de paléomagnétisme. Il s'agit de *2G Enterprises*. Plusieurs modèles existent. Ils ont chacun leurs propres caractéristiques, notamment une fonction de réponse propre qui a un impact lors de la mesure. Cela sera abordé plus en détails dans le chapitre 1.

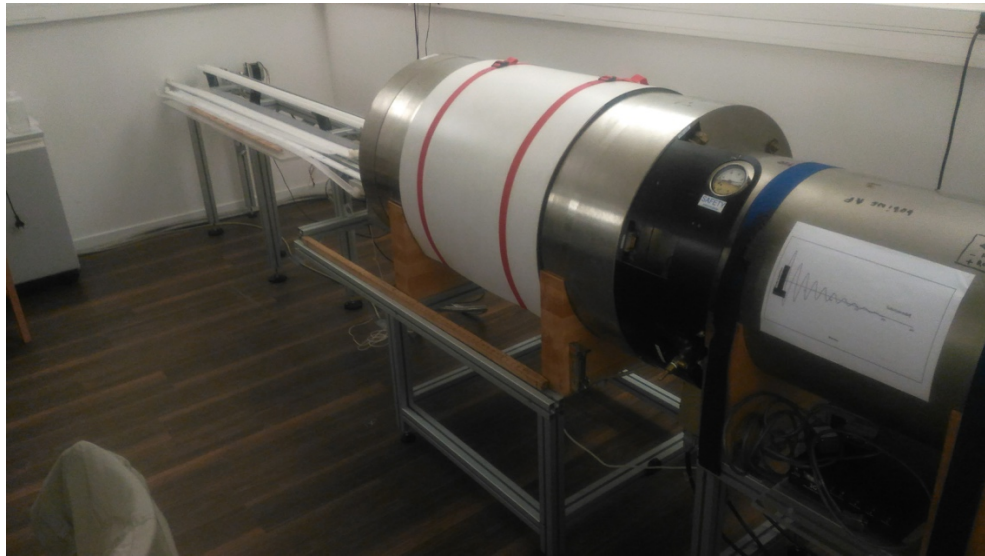


Figure 7: Magnétomètre cryogénique 2G Enterprises de l'IPGP.

La mesure des deux types d'échantillons suit la même méthodologie. Pour reconstituer le champ magnétique terrestre enregistré dans les sédiments, il est nécessaire de désaimanter les échantillons étape par étape à l'aide de la désaimantation par champ alternatif (AF). Une étude d'échantillonnage continu de 10 m de sédiment représente 450 échantillons ponctuels et les mesures couplées à une désaimantation successive requièrent 2 mois de laboratoire, alors que la même étude réalisée avec des U-channels ne prendrait que quelques jours (Nagy & Valet, 1993; Weeks et al., 1993). C'est pour cette raison que les études sur des U-channels sont devenues plus courantes, car elles permettent d'étudier de longues séquences sédimentaires en un minimum de temps. Mais, comme cela sera abordé plus en détails dans le chapitre 1, l'utilisation des U-channels est moins adaptée pour la reconstitution de certaines variations paléomagnétiques tel que le comportement du champ magnétique durant les inversions de polarité.

## OBJECTIFS DE RECHERCHE

L'objectif général de cette thèse est de mieux comprendre les mécanismes d'acquisition du champ magnétique terrestre dans les sédiments. Pour ce faire, cette thèse s'appuie sur trois objectifs spécifiques dans le but d'écrire trois articles scientifiques qui forment les trois chapitres de la thèse.

### **Objectif 1. Définir la limite d'utilisation des U-channels pour l'étude de la variation du champ magnétique terrestre, notamment dans le cas des excursions et des inversions**

Une étude continue au U-channel est beaucoup plus rapide qu'une étude faite avec des échantillons discrets. Cependant, on constate une perte de résolution due au lissage du capteur qui est d'autant plus visible lors de fortes variations rapides du champ magnétique terrestre, notamment lors d'une excursion ou d'une inversion. C'est pourquoi, une comparaison entre échantillons ponctuels et continus est nécessaire pour différents types et épaisseur d'événements. Cette étude sera menée avec l'utilisation d'échantillons artificiels qui permettront, en créant différentes tailles et types d'événements, de définir, en fonction du modèle de magnétomètre cryogénique utilisé, la limite d'utilisation des U-channels. Cette étude vise à répondre aux questions suivantes :

Quelle est la limite d'utilisation des U-channels? Sont-ils adaptés pour l'étude des variations rapides du champ magnétique comme les inversions ou les excursions géomagnétiques?

### **Objectif 2. Déterminer l'influence d'un changement lithologique important sur l'enregistrement magnétique**

La lithologie a un impact sur l'enregistrement magnétique et il est nécessaire de mieux quantifier cet impact. Pour mener à bien cet objectif, il faut réfléchir au problème

mathématique suivant avec l'équation simplifiée de l'aimantation ( $M$ ) dans les sédiments  $M = m * B_{anc}$  (avec  $m$  qui représente la lithologie et  $B_{anc}$  le champ magnétique ancien). Il est nécessaire pour répondre à cette question d'avoir un champ  $B_{anc}$  fixe tout en faisant varier la lithologie ( $m$ ) pour voir l'impact sur l'aimantation mesurée  $M$ . Pour cela, il faut des échantillons naturels qui présentent ce type de caractéristiques. Le champ magnétique terrestre variant à l'échelle du siècle, celui-ci ne varie quasiment pas sur une dizaine d'années, en dehors de toute excursion et inversion, avec une vitesse de sédimentation suffisamment importante pour faciliter l'échantillonnage ponctuel. De plus, cet échantillon doit présenter de fortes variations lithologiques. Pour cela, des échantillons varvés provenant de l'ancien lac proglacière Ojibway ont été étudiés. Ces varves ont l'avantage de présenter, à l'échelle d'une année, deux couches lithologiques différentes. Ainsi, la variation de la mesure de l'aimantation dans les varves est due à la variation lithologique. Il est alors possible de quantifier cet impact. Cette étude vise donc à répondre aux questions suivantes :

Quel est l'impact sur le signal magnétique du changement entre lit d'été et lit hiver ?  
Quels paramètres sont à l'origine de cette variation?

### **Objectif 3. Déterminer l'impact d'une sédimentation rapide sur l'enregistrement magnétique**

Les couches déposées rapidement (RDL), telles que les turbidites, sont rarement étudiées en paléomagnétisme, car l'acquisition de l'aimantation dans les turbidites reste très complexe et semble principalement influencée par la variation de la taille des grains et la dynamique du dépôt (Tanty et al., 2016). Les turbidites sont un type de dépôt ayant comme caractéristique de ne pas avoir subi la bioturbation grâce à leur déposition rapide et leur épaisseur. De plus, comme pour le cas les varves, le dépôt se fait sur un laps de temps suffisamment court (quelques jours ou semaines) pour que le champ magnétique soit fixe. Il représente un cas intéressant pour améliorer la compréhension des mécanismes

d'acquisition du champ magnétique terrestre dans les sédiments. Pour cela, une étude statistique sera effectuée sur une base de données de plusieurs RDL, notamment des hyperpicnites et turbidites provenant de la carotte MD99-2222 (St-Onge et al., 2004) et de l'étude de Tanty et al. (2016). Cette étude vise à répondre aux questions suivantes :

Quel est l'impact d'une couche déposée rapidement sur l'enregistrement magnétique ? Quels paramètres jouent un rôle majeur sur l'enregistrement magnétique durant ce type d'événement?

## ORGANISATION DE LA THÈSE

Cette thèse est structurée sous forme de trois articles scientifiques qui ont pour but de répondre à un des objectifs scientifiques mentionnés ci-dessus. À noter que les références bibliographiques de chaque partie sont à la fin de chacune d'elle.

**Le premier chapitre** présente les limites d'utilisation des U-channels notamment dans le cas de fortes variations du champ magnétique terrestre telles que les excursions et les inversions. Les résultats ont été publiés en septembre 2018 dans la revue *Geochemistry, Geophysics, Geosystems*.

**Philippe, É. G. H.**, Valet, J.-P., St-Onge, G., Thevarasan, A. (2018). *Are paleomagnetic records from U-channels appropriate for studies of reversals and excursions?* *Geochemistry, Geophysics, Geosystems*, 19, 4130–4142.

**Le deuxième chapitre** présente les résultats des mesures sédimentaires et magnétiques sur les varves du lac Ojibway. Celui-ci compare l'impact d'une forte variation sédimentaire sur l'enregistrement magnétique.

**Philippe, É. G. H.**, St-Onge, G., Valet, J.-P., Godbout, P.-M., Egli, R., Francus, P., Roy, M. *Influence of lithology on the remanent magnetization as recorded in varved sediments from the glacial Lake Ojibway (Canada)*. Le manuscrit sera soumis prochainement à la revue *Earth and Planetary Science Letters*.

**Le troisième chapitre** présente finalement une étude statistique sur plusieurs couches sédimentaires déposées rapidement.

**Philippe, É. G. H.**, Valet, J.-P., Egli, R., St-Onge, G. *Impact of turbulence on magnetic alignment in sediments*. Le manuscrit sera soumis prochainement à la revue *Geochemistry, Geophysics, Geosystems*.

Finalement, les principales conclusions des différents articles seront présentées après les trois chapitres. Celles-ci sont présentées sous forme d'une discussion générale qui

aborde l'ensemble des questions scientifiques posées en paléomagnétisme lors de ce doctorat ainsi que leurs liens. De plus, une conclusion générale ainsi que quelques perspectives futures seront présentées.

## AUTRES RÉALISATIONS ET COLLABORATIONS

Cette thèse est en cotutelle entre le laboratoire de paléomagnétisme de l'IPGP en France et le laboratoire de paléomagnétisme et géologie marine de l'ISMER au Canada. Une étroite collaboration a eu lieu entre les deux laboratoires ce qui m'a permis d'utiliser les meilleurs instruments disponibles dans les deux laboratoires et mener mes recherches dans les deux pays tout au long de mon doctorat. De plus, j'ai eu l'occasion de participer à plusieurs activités reliées à mon projet de thèse. J'ai notamment participé à trois congrès internationaux (*International Conference on Tomography of Materials and Structures* (ICTMS) en 2015, *European Geosciences Union* (EGU) en 2016 et *American Geophysical Union* (AGU) en 2017) et quatre congrès nationaux (congrès annuel du GEOTOP en 2015 et 2018, ACFAS 2015 et le congrès des doctorants de l'IPGP en 2016) durant lesquels j'ai présenté mes résultats de recherche. De plus, lors de mon doctorat, j'ai participé à deux missions de terrain sur le lac Walker sur la Côte Nord du Québec en 2014 et en 2015 qui ont permis l'élaboration de différents articles scientifiques (collaborations).

### Articles

Nzekwe, O.P., Francus, P., St-Onge, G., Lajeunesse, P., Fortin, D., Gagnon-Poiré, A., **Philippe, É.G.H.**, Normandeau, A. (2018). *Recent sedimentation in three adjacent fjord-lakes on the Québec North Shore (eastern Canada): facies analysis, laminae preservation, and potential for varve formation*. *Canadian Journal of Earth Sciences*, 55(2), 138–153. <https://doi.org/10.1139/cjes-2017-0070>

Nzekwe, O.P., Francus, P., Gagnon-Poiré, A., Lajeunesse, P., St-Onge, G., Fortin, D., **Philippe, É.G.H.**, Normandeau, A., Brice, C., Jenny, J.-P., Lemieux, J.-M. *Late-Quaternary glacial to postglacial depositional transition in fjord-lakes Pentecôte and Walker, Québec North Shore (eastern Canada): A multi-proxy approach.* Le manuscrit sera soumis prochainement.

## Présentations

**Philippe, É.G.H.**, St-Onge, G., Valet, J.-P., Francus, P. (2015). Propriétés sédimentologiques, physiques et magnétiques des sédiments des lacs profonds de la Côte-Nord du golfe Saint-Laurent (Québec, Canada): processus responsables de l'acquisition de l'aimantation des sédiments. Congrès annuel du GEOTOP, Base de plein-air Jouvence, Orford, Can., 13-15 février.

**Philippe, É.G.H.**, St-Onge, G., Valet, J.-P., Francus, P. (2015). Comprendre l'acquisition du signal paléomagnétique dans les sédiments par l'étude des propriétés des sédiments varvés des lacs profonds de la Côte-Nord (Québec, Canada). Colloque sur les variations climatiques au cours du Quaternaire. 83e congrès de l'ACFAS, Rimouski, 28 et 29 mai.

**Philippe, É.G.H.**, St-Onge, G., Valet, J.-P., Francus, P. (2015). *Acquisition of the natural remanent magnetization in varved sediments: laboratory redeposition experiments, CT-Scan imaging and modeling.* 2nd International conference on tomography of materials and structures, Québec, 29 juin au 3 juillet.

**Philippe, É.G.H.**, Valet, J.-P., St-Onge, G. (2016). *Acquisition of the detrital remanent magnetization in turbidites.* congrès des doctorants, Paris, 14-18 mars.

**Philippe, É.G.H.**, Valet, J.-P., St-Onge, G. (2016). *Acquisition of the detrital remanent magnetization in turbidites*, EGU (European Geosciences Union). Vienne, 17-22 avril.

**Philippe, É.G.H.**, Valet, J.-P. (2017). *Are paleomagnetic records from U-channels appropriate for studies of reversals and excursions*. AGU (American Geophysical Union), La Nouvelle Orléans, 11-15 décembre.

**Philippe, É.G.H.**, Valet, J.-P., St-Onge, G, Godbout, P.-M., Egli, R., Roy, M. (2018). *Lithological dependence of the remanent magnetization in varved sediments from the glacial Lake Ojibway (Canada)*. Congrès annuel du GEOTOP, La Malbaie, 21-23 mars.

## Collaborations

Godbout, P.M., Roy, M., **Philippe, É.G.H.**, St-Onge, G. (2015). *Characterizing late-glacial readvances and the drainage of Lake Ojibway through compositional and paleomagnetic analyses of long sediment sequences*. CANQUA meeting, St. John's (NL), 16-19 août 2015

Nzekwe, O.P., Francus, P., St-Onge, G., Lajeunesse, P., Fortin D., Gagnon-Poiré, A., **Philippe, É.G.H.** (2017). *A high-resolution approach to evaluate the occurrence of varved sediments in Lake Walker, Québec North Shore, using image analysis and X-ray microfluorescence*. 47th International Arctic Workshop, New York (NY), USA, 23-25 mars. p. 114.

Nzekwe, O.P., Francus, P., St-Onge, G., Lajeunesse, P., Fortin, D., Gagnon-Poiré, A., **Philippe É.G.H.** (2017). *A high-resolution approach to evaluate the occurrence of varved sediments in Lake Walker, Québec North Shore, using image analysis and X-ray microfluorescence*. Ontario-Quebec Paleolimnology Symposium (PALS) 2017, St-Catherine ,Canada. 24-26 mai.

Nzekwe O.P., Francus, P., St-Onge, G., Lajeunesse, P., Fortin, D., Gagnon Poiré, A., **Philippe, É.G.H.** (2018). *A high-resolution approach to evaluate the occurrence of varved sediments in Lake Walker, Québec North Shore (eastern Canada) using - XRF, CT-scan and thin section image analysis.* 20th International Sedimentological Congress - ICS2018, Québec, Canada, 13-17 août.

## RÉFÉRENCES

- Barletta, F., St-Onge, G., Stoner, J. S., Lajeunesse, P., & Locat, J. (2010). A high-resolution Holocene paleomagnetic secular variation and relative paleointensity stack from eastern Canada. *Earth and Planetary Science Letters*, 298(1–2), 162–174. <https://doi.org/10.1016/j.epsl.2010.07.038>
- Carter-Stiglitz, B., Valet, J.-P., & LeGoff, M. (2006). Constraints on the acquisition of remanent magnetization in fine-grained sediments imposed by redeposition experiments. *Earth and Planetary Science Letters*, 245(1), 427–437.
- Channell, J. E. T., & Kleiven, H. F. (2000). Geomagnetic palaeointensities and astrochronological ages for the Matuyama–Brunhes boundary and the boundaries of the Jaramillo Subchron: palaeomagnetic and oxygen isotope records from ODP Site 983. *Philosophical Transactions of the Royal Society of London A: Mathematical, Physical and Engineering Sciences*, 358(1768), 1027–1047. <https://doi.org/10.1098/rsta.2000.0572>
- Channell, J. E. T., Stoner, J. S., Hodell, D. A., & Charles, C. D. (2000). Geomagnetic paleointensity for the last 100 kyr from the sub-antarctic South Atlantic: a tool for inter-hemispheric correlation. *Earth and Planetary Science Letters*, 175(1–2), 145–160. [https://doi.org/10.1016/S0012-821X\(99\)00285-X](https://doi.org/10.1016/S0012-821X(99)00285-X)
- Collinson, D. W. (1965). Depositional remanent magnetization in sediments. *Journal of Geophysical Research*, 70(18), 4663–4668.

- Denham, C. R., & Chave, A. D. (1982). Detrital remanent magnetization: Viscosity theory of the lock-in zone. *Journal of Geophysical Research: Solid Earth*, 87(B8), 7126–7130.
- Dubois, J., Diament, M., Cogné, J.-P., & Mocquet, A. (2016). Chapitre 6. Le géomagnétisme. In *Géophysique - 5e éd.: Cours, étude de cas et exercices corrigés* (Dunod, pp. 187–230). Dunod.
- Heslop, D., Witt, A., Kleiner, T., & Fabian, K. (2006). The role of magnetostatic interactions in sediment suspensions. *Geophysical Journal International*, 165(3), 775–785. <https://doi.org/10.1111/j.1365-246X.2006.02951.x>
- Katari, K., Tauxe, L., & King, J. (2000). A reassessment of post-depositional remanent magnetism: preliminary experiments with natural sediments. *Earth and Planetary Science Letters*, 183(1), 147–160.
- Katari, Kaushik, & Bloxham, J. (2001). Effects of sediment aggregate size on DRM intensity: a new theory. *Earth and Planetary Science Letters*, 186(1), 113–122.
- Macrì, P., Sagnotti, L., Dinarès-Turell, J., & Caburlotto, A. (2010). Relative geomagnetic paleointensity of the Brunhes Chron and the Matuyama–Brunhes precursor as recorded in sediment core from Wilkes Land Basin (Antarctica). *Physics of the Earth and Planetary Interiors*, 179(1), 72–86. <https://doi.org/10.1016/j.pepi.2009.12.002>
- Mao, X., Egli, R., Petersen, N., Hanzlik, M., & Zhao, X. (2014). Magnetotaxis and acquisition of detrital remanent magnetization by magnetotactic bacteria in natural sediment: First experimental results and theory. *Geochemistry, Geophysics, Geosystems*, 15(1), 255–283. <https://doi.org/10.1002/2013GC005034>
- Mazaud, A., Channell, J. E. T., & Stoner, J. S. (2012). Relative paleointensity and environmental magnetism since 1.2 Ma at IODP site U1305 (Eirik Drift, NW Atlantic). *Earth and Planetary Science Letters*, 357–358, 137–144. <https://doi.org/10.1016/j.epsl.2012.09.037>

- Meynadier, L., Valet, J.-P., Weeks, R., Shackleton, N. J., & Hagee, V. L. (1992). Relative geomagnetic intensity of the field during the last 140 ka. *Earth and Planetary Science Letters*, 114(1), 39–57. [https://doi.org/10.1016/0012-821X\(92\)90150-T](https://doi.org/10.1016/0012-821X(92)90150-T)
- Nagata, T. (1961). Rock Magnetism, 350 pp. Maruzen, Tokyo.
- Nagy, E. A., & Valet, J.-P. (1993). New advances for paleomagnetic studies of sediment cores using U-Channels. *Geophysical Research Letters*, 20(8), 671–674. <https://doi.org/10.1029/93GL00213>
- Quidelleur, X., Valet, J.-P., LeGoff, M., & Boulldoire, X. (1995). Field dependence on magnetization of laboratory-redeposited deep-sea sediments: First results. *Earth and Planetary Science Letters*, 133(3), 311–325.
- Roberts, A. P., & Winklhofer, M. (2004). Why are geomagnetic excursions not always recorded in sediments? Constraints from post-depositional remanent magnetization lock-in modelling. *Earth and Planetary Science Letters*, 227(3), 345–359. <https://doi.org/10.1016/j.epsl.2004.07.040>
- Roberts, A. P., Lehman, B., Weeks, R. J., Verosub, K. L., & Laj, C. (1997). Relative paleointensity of the geomagnetic field over the last 200,000 years from ODP Sites 883 and 884, North Pacific Ocean. *Earth and Planetary Science Letters*, 152(1), 11–23. [https://doi.org/10.1016/S0012-821X\(97\)00132-5](https://doi.org/10.1016/S0012-821X(97)00132-5)
- Roberts, A. P., Tauxe, L., & Heslop, D. (2013). Magnetic paleointensity stratigraphy and high-resolution Quaternary geochronology: successes and future challenges. *Quaternary Science Reviews*, 61, 1–16.
- Shcherbakov, V., & Sycheva, N. (2010). On the mechanism of formation of depositional remanent magnetization. *Geochemistry, Geophysics, Geosystems*, 11(2). Retrieved from <http://onlinelibrary.wiley.com/doi/10.1029/2009GC002830/full>
- Spassov, S., & Valet, J.-P. (2012). Detrital magnetizations from redeposition experiments of different natural sediments. *Earth and Planetary Science Letters*, 351, 147–157.
- Stacey, F. D. (1972). On the role of Brownian motion in the control of detrital remanent magnetization of sediments. *Pure and Applied Geophysics*, 98(1), 139–145.

- Stoner, J. S., Channell, J. E. T., Hillaire-Marcel, C., & Kissel, C. (2000). Geomagnetic paleointensity and environmental record from Labrador Sea core MD95-2024: global marine sediment and ice core chronostratigraphy for the last 110 kyr. *Earth and Planetary Science Letters*, 183(1–2), 161–177. [https://doi.org/10.1016/S0012-821X\(00\)00272-7](https://doi.org/10.1016/S0012-821X(00)00272-7)
- Tauxe, L. (1993). Sedimentary records of relative paleointensity of the geomagnetic field: theory and practice. *Reviews of Geophysics*, 31(3), 319–354.
- Tauxe, L. (2010). Chapter 2 The Geomagntetic Fields. In *Essentials of Paleomagnetism* (pp. 17–32). Univ of California Press.
- Tauxe, L., Steindorf, J. L., & Harris, A. (2006). Depositional remanent magnetization: toward an improved theoretical and experimental foundation. *Earth and Planetary Science Letters*, 244(3), 515–529.
- Valet, J.-P. (2003). Time variations in geomagnetic intensity. *Reviews of Geophysics*, 41(1), 1004. <https://doi.org/10.1029/2001RG000104>
- Valet, J.-P., & Meynadier, L. (1993). Geomagnetic field intensity and reversals during the past four million years. *Nature*, 366(6452), 234–238.
- Weeks, R., Laj, C., Endignoux, L., Fuller, M., Roberts, A., Manganne, R., et al. (1993). Improvements in long-core measurement techniques: applications in palaeomagnetism and palaeoceanography. *Geophysical Journal International*, 114(3), 651–662. <https://doi.org/10.1111/j.1365-246X.1993.tb06994.x>
- Yoshida, S., & Katsura, I. (1985). Characterization of fine magnetic grains in sediments by the suspension method. *Geophysical Journal International*, 82(2), 301–317. <https://doi.org/10.1111/j.1365-246X.1985.tb05139>.

# **CHAPITRE 1**

## **LES ENREGISTREMENTS PALÉOMAGNÉTIQUES DES U-CHANNELS SONT-ILS APPROPRIÉS POUR L'ÉTUDES DES INVERSIONS ET DES EXCURSIONS?**

### **1.1 RÉSUMÉ EN FRANÇAIS DU PREMIER ARTICLE**

L'échantillonnage de carottes sédimentaires à l'aide de U-channels a permis l'acquisition d'enregistrements détaillés de la variation séculaire paléomagnétique, de la polarité géomagnétique, des études magnétiques environnementales, et de la paléointensité relative au cours des derniers millions d'années. Les mesures U-channels offrent le grand avantage de mesures rapides de longues carottes sédimentaires, mais la résolution du signal est atténuee par la fonction de réponse des capteurs du magnétomètre, ce qui limite donc la restauration des variations rapides et de forte amplitude du champ. Nous nous concentrons ici sur l'adéquation de la dynamique des inversions et des excursions dérivées des mesures U-channels. Nous comparons les directions paléomagnétiques individuelles successives d'échantillons ponctuels cubiques de 1,5 cm x 1,5 cm x 1,5 cm avec celles d'un train d'échantillons équivalent de 1,5 m de U-channel obtenu en plaçant les échantillons adjacents les uns aux autres. Nous utilisons différentes longueurs d'excursion et de transition et générerons des directions de transition qui ressemblent à celles des enregistrements paléomagnétiques les plus détaillés. Les excursions avec des directions de polarité opposées enregistrées sur moins de 7,5 cm sont à peine détectées par les mesures U-channels. En ce qui concerne les inversions, les mesures par U-channel lissent le signal des enregistrements à basse résolution et génèrent des directions de transition artificielles. Malgré des similitudes trompeuses avec la structure générale des enregistrements de transition, des intervalles de transition plus longs ne permettent pas non plus de reproduire

la complexité des variations du champ. Enfin, nous testons la convolution de l'aimantation par différentes fonctions de réponse. La simulation montre que même de petites variations de fonction de réponse peuvent générer des différences significatives dans les résultats.

Ce premier article, intitulé « *Are Paleomagnetic Records From U-channels Appropriate for Studies or Reversals and Excursions?* », fut corédigé par moi-même ainsi que par mes deux directeurs Jean-Pierre Valet (IPGP) et Guillaume St-Onge (UQAR-ISMER). Anojh Thevarasan (IPGP) a fortement contribué aux analyses en laboratoire. L'article a également grandement bénéficié des commentaires et des suggestions constructifs d'Andrew Roberts et d'un examinateur anonyme. L'article fut accepté pour publication en ligne dans sa version finale le 9 octobre 2018 par l'éditeur dans la revue *Geochemistry, Geophysics, Geosystems*.

Par ailleurs, une version abrégée de cet article a été présentée sous forme d'affiche au congrès de l'*American Geophysical Union* qui s'est déroulé à la Nouvelle Orléans (É.-U.) en 2017.

## 1.2 ARE PALEOMAGNETIC RECORDS FROM U-CHANNELS APPROPRIATE FOR STUDIES OF REVERSALS AND EXCURSIONS?

Sampling of sediment cores using plastic U-channels has made possible the acquisition of detailed records of paleomagnetic secular variation, geomagnetic polarity, environmental magnetic studies, and relative paleointensity over the past several million years. U-channel measurements provide the great advantage of rapid measurements of long sediment cores, but the signal resolution is attenuated by the response function of the magnetometer sensors, which therefore restrains the recovery of rapid and large-amplitude field changes. Here we focus on the suitability of the dynamics of reversals and excursions derived from U-channel measurements. We compare successive individual paleomagnetic directions of  $1.5\text{ cm} \times 1.5\text{ cm} \times 1.5\text{ cm}$  cubic discrete samples with those of a 1.5-m equivalent U-channel sample train obtained by placing the samples adjacent to each other. We use varying excursion and transition lengths and generate transitional directions that resemble those of the most detailed paleomagnetic records. Excursions with opposite polarity directions recorded over less than 7.5 cm are barely detected in U-channel measurements. Regarding reversals, U-channel measurements smooth the signal of low-resolution records and generate artificial transitional directions. Despite producing misleading similarities with the overall structure of transition records, longer transitional intervals fail also to reproduce the complexity of field changes. Finally, we test the convolution of magnetization by different response functions. The simulation reveals that even small response function changes can generate significant differences in results.

## 1.3 INTRODUCTION

Measurement of 1.5-m-long sedimentary samples enclosed in plastic tubes called U-channels was proposed by Tauxe et al. (1983) as an alternative to the traditional, time-consuming procedure based on single samples extracted from the sediment.

Continuous sampling of 10 m of sediment provides at least 450 discrete samples that are measured and stepwise demagnetized separately. This technique typically requires a 2-month laboratory effort, while it can take only a few days to measure the equivalent U-channel samples (Nagy & Valet, 1993; Weeks et al., 1993). U-channel measurements therefore have become a successful and standard practice, and U-channel facilities have now been developed in many laboratories. The most direct impact has been the proliferation of long and detailed geomagnetic field records and environmental magnetic studies with special interest for obtaining relative paleointensity records over time scales that range from several thousands to millions of years depending on sediment deposition rate (e.g., Barletta et al., 2010; Channell et al., 2000; Channell & Kleiven, 2000; Kissel et al., 1998; Macrì et al., 2010; Mazaud et al., 2012; Meynadier et al., 1992; Roberts et al., 1997; Stoner et al., 2000; Valet, 2003; Valet & Meynadier, 1993).

During measurement, the U-channel is placed on an automated horizontal sample holder and is translated in and out of the sensing region of a cryogenic magnetometer that is equipped with a set of three orthogonal pickup coils. The resolution of U-channel records depends on the accumulation rate of the sediment but also on the width of the magnetometer response function. The response function width depends essentially on the distance between the coils and sediment and is constrained by the diameter of the room temperature access of the instrument. Most laboratories with U-channel magnetometer systems are equipped with a 4.2-cm-diameter access, which is optimal for standard 4-cm<sup>2</sup> square cross-section U-channels. The resolution of the record then depends on the length of sediment detected by the pickup coils.

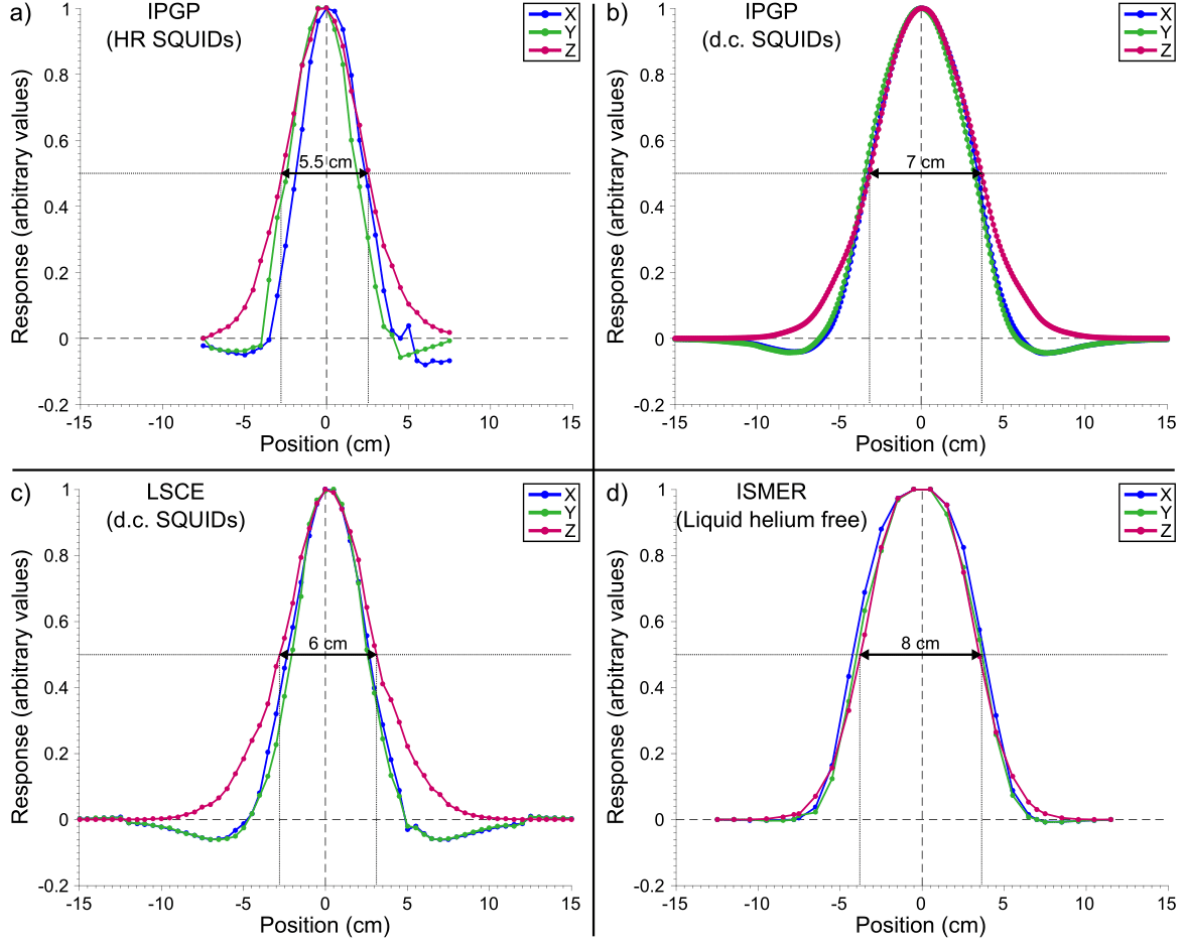


Figure 8: Response functions of model 755-R (2G Enterprises) magnetometers with different sets of sensing coils. The type and location of the magnetometers are mentioned in each panel. IPGP (Institut de Physique du Globe de Paris), LSCE (Laboratoire des Sciences du Climat et de l’Environnement), and ISMER (Institut des sciences de la mer de Rimouski).

#### 1.4 MEASUREMENT RESOLUTION

To our knowledge, all cryogenic magnetometers adapted for U-channel measurements were built by 2G Enterprises, but the length of the response functions differs between different instruments and therefore between laboratories. In Figure 8, we show examples of response curves for various generations of magnetometers. We excluded the large 15–20 cm

half-width response curves inherent to the 760-R series that was designed for whole-core measurements. The optimal resolution was provided by the 755-R series equipped with the so-called high-resolution (HR) sensors with a half-window width as short as 4.5–5.5 cm (Figure 8a; Guyodo et al., 2002; Nagy & Valet, 1993; Weeks et al., 1993) that were initially installed in a few laboratories. The next generation of 2G magnetometers introduced direct current (d.c.) superconducting quantum interference devices (SQUIDs) and was characterized by relatively homogeneous responses with half-widths of 6–7 cm (Figure 8b and Figure 8c). The most recent liquid helium-free magnetometers are characterized by larger smoothing windows of the order of 7–8 cm (Figure 8d). Note that these values can change between magnetometers of the same generation depending on various technical constraints. Summarizing, except the HR coils of the first series, the models presently available on the market do not have half-width response functions shorter than 6–7 cm (Figure 8a and Figure 8c). The magnetometer used for the present measurements was the 2G Enterprises Model 755-R located in the shielded room of the Institut de Physique du Globe de Paris. It is equipped with d.c. SQUIDs with a half-width response function of 7 cm (Figure 8b). We are aware that this is not the optimal available resolution and therefore results presented here are also discussed for smaller window widths.

For the optimal 5.5-cm half-width response functions of the first 755-R series, each sediment magnetization measurement is integrated over an equivalent interval. Consequently, variations with characteristic times longer than several kyr are recorded by U-channel measurements of sediments with deposition rates between 2 and 5 cm/kyr that make up a significant part of the global database. This is the reason why dipolar variations dominate published relative paleointensity records. If we deal with deposition rates between 10 and 15 cm/kyr the resolution is evidently improved (Roberts & Winklhofer, 2004). Only a few long-term studies (e.g., Channell, 2017; Channell & Lehman, 1997; Laj et al., 2006; Verosub et al., 2001) have relied on U-channel measurements of such rapidly deposited sediments to investigate detailed variations associated with geomagnetic excursions and reversals.

The question is to determine the extent to which detailed U-channel records properly document rapid field changes during these periods that are also characterized by low dipole field intensities. In the present study, we investigate this aspect by using a direct approach that relies on testing the coherency of paleomagnetic individual sediment slice records with the corresponding synthetic U-channel record obtained when the discrete samples are placed side by side in a continuous manner. Alternatively, we also calculate the convolution induced by the response curve of the magnetometer on the single sample train and test the results against actual U-channel measurements.

## 1.5 EXPERIMENTAL PROTOCOL

The direct way to compare U-channel measurements is to place a succession of sediment slices adjacent to each other to mimic a 150-cm-long U-channel. A similar approach has been used previously for various purposes (Guyodo et al., 2002; Nagy & Valet, 1993; Roberts et al., 1996; Weeks et al., 1993). In the present case, we used 1.5-cm-wide plastic cubes to optimize the resolution of discrete samples. Each cube was filled with modeling clay to which we added a small amount of pure magnetite powder. Care was taken to fill each cube with a similar amount of magnetite that was weighed so that each specimen has similar magnetic properties. Owing to the difficulties inherent to detrital remanent magnetization acquisition in the laboratory for a large number of specimens, we produced an anhysteretic remanent magnetization (ARM) in the synthetic sediment samples. The ARM was imparted by inserting each cube within the demagnetization coil of a Schönstedt demagnetizer (60 mT) alternating field (a.f.) surrounded by an external coil to produce a d.c. field (50 µT). Each specimen was inserted within a home-made sample holder that can be oriented in the vertical and horizontal planes so that samples can record any field direction and, thus, simulate reversed, intermediate, and normal polarities. Magnetization intensity was controlled by the concentration of

magnetite in the modeling clay. We created eight different magnetite concentrations in more than 700 cubes, which allowed us to generate any combination of intensity variations.

The ARM for each cube was measured in the same conditions within the same 2G Enterprises magnetometer system used for the U-channel measurements. As a first step, the discrete samples were measured separately and spaced from each other by a distance of 30 cm on the sample holder to avoid any interaction. The samples were then positioned adjacent to each other along the magnetometer sample tray to mimic a U-channel and were measured again. Data treatment consisted of comparing the directions and intensities obtained from single samples before and after they were measured as a synthetic U-channel.

Magnetization stability was tested by monitoring the evolution of magnetic directions and intensities of the samples over a 1-day period. The procedure is analogous to a viscosity test and was aimed at checking that the magnetization did not change between successive measurements that were never separated by more than 3 hr. The magnetization remained largely unchanged except for a few variations (Figure 9a) that were likely due to a small viscous component. The sample magnetization is an ARM with coercivity as high as 60 mT, so some samples were demagnetized by a.f. The results (Figure 9b) confirm the overall stability of the magnetization that is removed at the same peak a.f. as used for ARM acquisition.

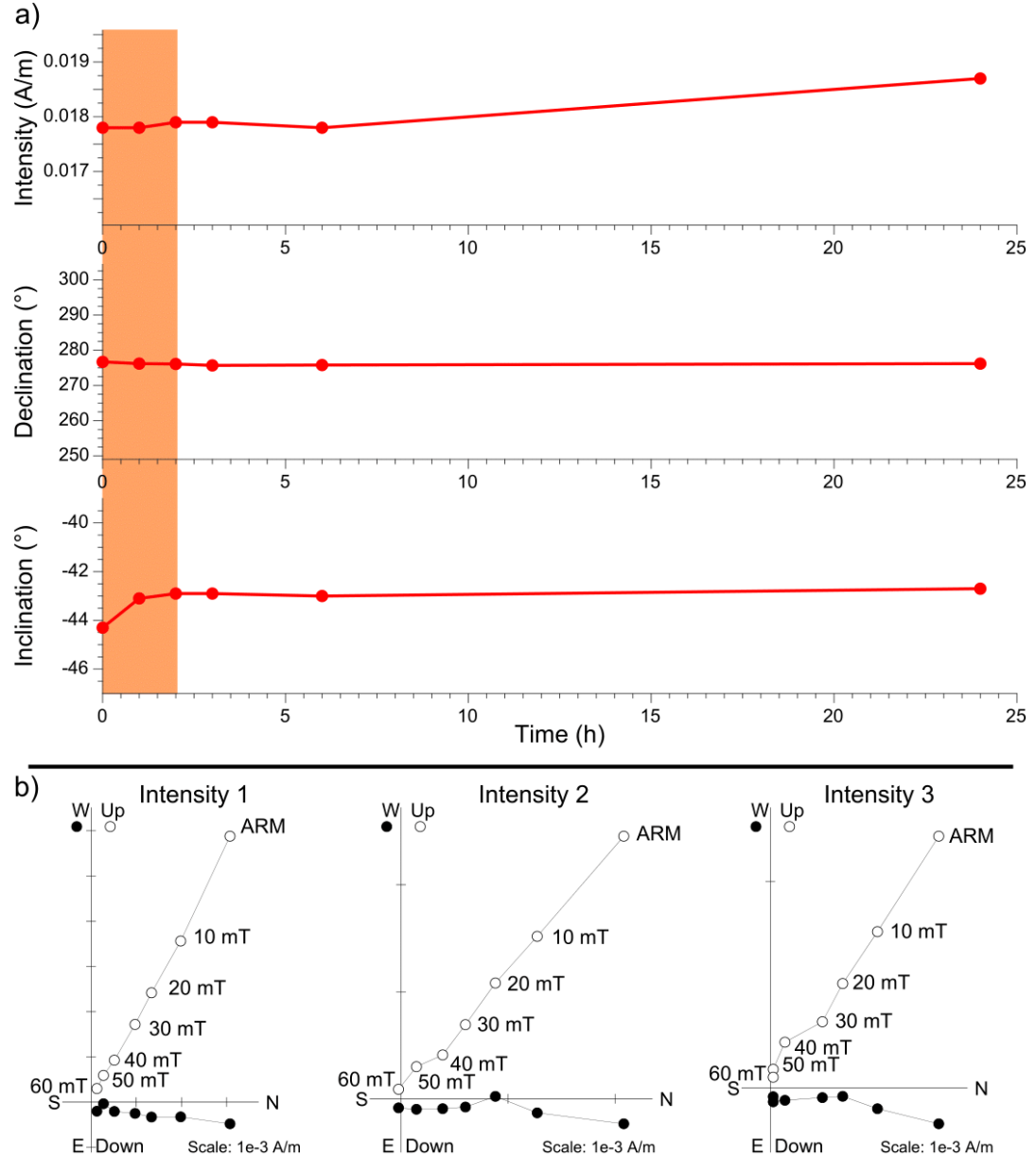


Figure 9: (a) Evolution of the remanent magnetization (intensity, declination, and inclination) of the synthetic samples as a function of time. The maximum duration of the experiments (3 hr) is indicated by the orange zone. (b) Alternating field demagnetization diagrams of the anhysteretic remanent magnetization (ARM) imparted to the synthetic samples. The solid symbols correspond to projections onto the horizontal plane, while the open symbols represent projections onto the vertical plane.

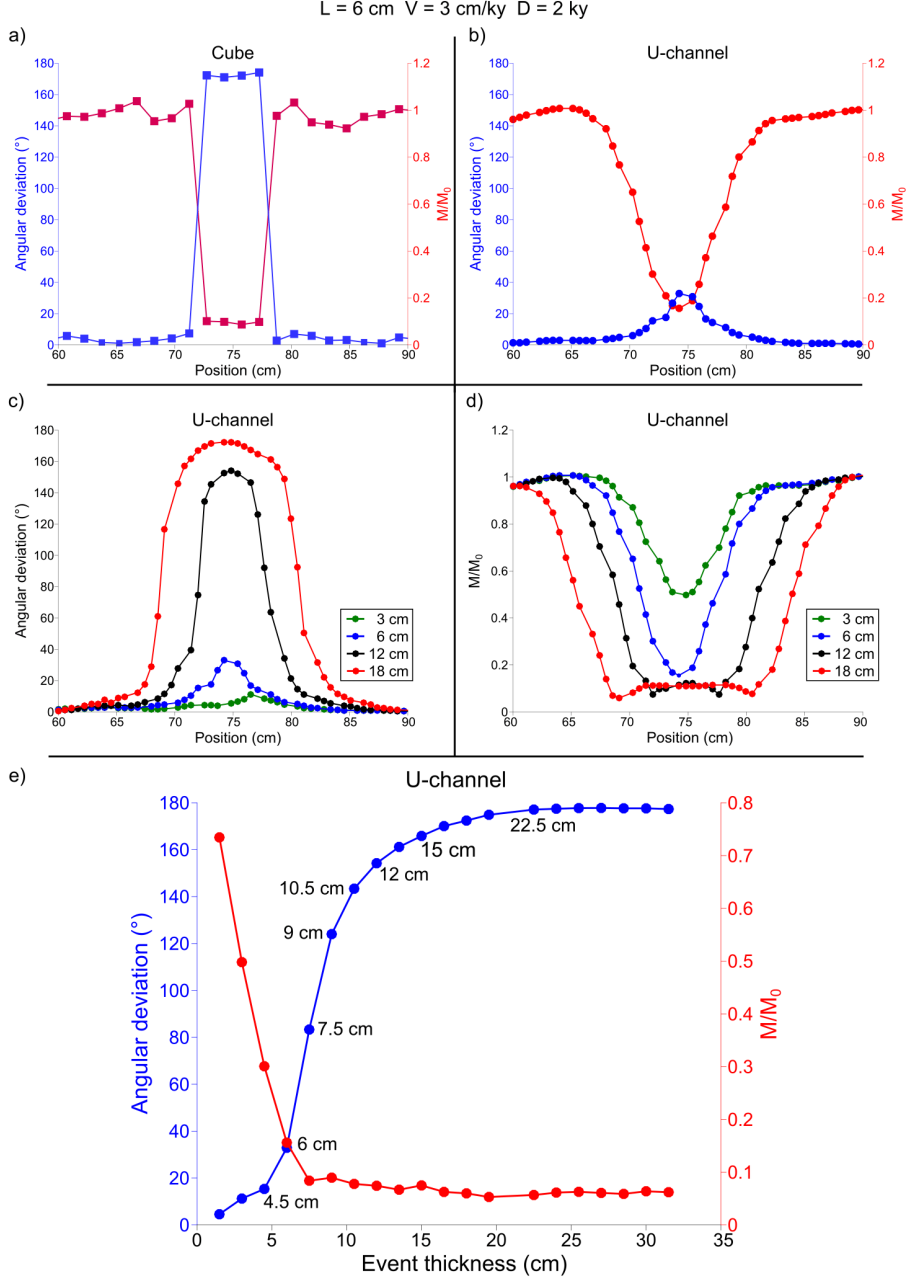


Figure 10: (a) Angular variation (blue squares) and intensity (red squares) changes measured for individual cubes for a 6-cm-long excursion simulated by four reversely magnetized cubes. (b) Same as (a) for the equivalent U-channel. (c) Angular deviation for excursions recorded over increasing length intervals. (d) Same as (c) for magnetization intensity. (e) Maximum angular deviation from the original polarity and minimum moment variation measured in U-channel samples as a function of excursion length. The maximum angular deviation does not reach 180 $^{\circ}$  for events smaller than 20 cm.

## 1.6 SIMULATION OF GEOMAGNETIC EXCURSIONS

### 1.6.1 Previous Studies

Intermediate or reverse polarity directions that correspond to geomagnetic excursions have been rarely detected in sedimentary records with accumulation rates lower than 5-6 cm/kyr, but the intensity minimum that accompanies these rapid events is frequently present. The reason for this is that directional changes occur over a short time period and in the presence of weak fields. In such conditions, even minor smoothing linked to magnetization acquisition in addition to resolution limits imposed by the sediment accumulation rate erases the imprint of reverse polarity or intermediate directions.

Nagy and Valet (1993) and Weeks et al. (1993) compared single sample results with U-channel measurements and reported that a few abrupt directional changes were smoothed out by pass-through measurements with high-resolution coils. Roberts et al. (1996) compared long-core measurements of Ocean Drilling Program core halves and the equivalent set of discrete samples in a cube train. The magnetometer used for the experiments was the 2G Enterprises Model 760-R with a more than 15-cm-wide half-window response curve that is the consequence of the large diameter access needed for whole core measurements. It is, thus, considerably larger than the magnetometers mentioned above for U-channel measurements. Roberts et al. (1996) reported directional artifacts that were introduced by convolution of the intensity changes, especially for regions characterized by large intensity changes.

Roberts and Winklhofer (2004) simulated the effects of postdepositional remanent magnetization (pDRM) lock-in on a high-frequency geomagnetic signal characterized by a succession of excursions with a 4.5-cm half-width response function for single samples and for U-channel measurements. For a pDRM lock-in depth of 10 cm where 95% of the signal is locked within 5 cm, a deposition rate of 8 cm/kyr is required to detect a 1-kyr-long event using 2-cm-length single samples. The results from the study of Roberts and Winklhofer

(2004) involved that smoothing associated with enhance acquisition and U-channel measurement makes it ideal to study sediments deposited at rates  $>10$  cm/kyr in order to detect the presence of excursions. In stating this, however, they did not consider whether U-channel measurements introduce directional artifacts.

Here we used a similar approach, but with a 7-cm half-width response curve (Figure 8b). Before investigating the suitability of transitional directions derived from U-channel measurements, we focused on the detection of excursions. We did not consider smoothing effects due to pDRM acquisition.

### **1.6.2 Artifacts Induced by U-channel Measurements**

Following the previous studies mentioned above, we placed plastic cubes with opposite polarities next to each other. Normal (and reverse) polarity directions were given a declination close to  $0^\circ$  (and  $180^\circ$ , respectively) and inclinations of  $45^\circ$  (and  $-45^\circ$ , respectively). We deliberately did not produce any intermediate direction in order to be in the most favorable situation, that is, a complete  $180^\circ$  directional change, to detect the event. A progressive intensity drop with magnetization intensity equal to 10% of the original normal polarity field was also generated for the excursion.

A first example involves four magnetized 1.5-cm reverse polarity cubes inserted within strongly magnetized specimens with the opposite polarity to simulate a 6-cm-long excursion (Figure 10a and Figure 10b). The U-channel measurements (Figure 10b) fail to reproduce the magnetization changes of the discrete samples (Figure 10a). The directions do not deviate by more than  $35^\circ$  from the initial polarity direction in the U-channel measurements even though the magnetization intensity changed considerably. The U-channel intensity minimum is much longer and incorporates a succession of intermediate intensity values. If these results are interpreted in terms of duration based on sediment deposition rate, they indicate that 1- or 2-kyr-long events are difficult to detect with U-channel measurements for sediment accumulation rates lower than 6 cm/kyr or 3 cm/kyr, respectively, and that detection of 2-kyr-long events require deposition rates above

10 cm/kyr. Similar conclusions were reached by Roberts and Winklhofer (2004). However, the data also illustrate that events can be identified easily with sedimentation rates above 10 cm/yr for 2-kyr-long events.

Results for increasing excursion lengths are plotted in Figure 10c and Figure 10d, which demonstrate the evolution of angular deviation and magnetization intensity changes with measurement position. No significant polarity change is detected for intervals up to at least 6 cm, and in all cases the U-channel measurements generate artificial directions and magnetization intensities. The situation is summarized by changes in the angular deviation (defined as the angular change from the original normal polarity direction) in each U-channel record as a function of excursion length (Figure 10e). Large-scale deviations are not detected in U-channel measurements for excursion intervals lower than 7.5 cm. Above this value, U-channel measurements document the excursion, but the directional amplitude of the changes is considerably lower than the real changes. The opposite polarity is only detected for intervals larger than 15 cm. In contrast, a significant intensity minimum is observed for excursions as short as 3 cm in the U-channel records. This characteristic is consistent with the fact that transitional or reverse polarity directions are rarely detected in sedimentary excursion records, but significant intensity minima are observed frequently.

In summary, with the 7-cm half-width of the response curve used for our experiments, U-channel measurements do not reveal significant polarity changes for events recorded over  $<7.5$  cm intervals and they contain no evidence for a  $180^\circ$  directional change for intervals  $<20\text{--}25$  cm. These results indicate that sedimentation rates  $>20$  cm/kyr are necessary to provide evidence for a 1-kyr-long event, while values  $>10$  cm/kyr would be required for a 2-kyr event. Our most significant finding concerns the systematic lack of fidelity with respect to detecting the original magnetic directions of individual cubes.

In our cube-train measurements, no transitional direction was induced in the cube magnetizations, so virtual geomagnetic poles (VGP) lie to the north before and after simulated excursions and to the south during excursions. All simulated records, including the most detailed ones, are characterized by artificial transitional directions with VGPs that

are absent from the initial data. In Figure 11, we plot VGP paths derived from measurements of excursions simulated over 4.5- and 24-cm intervals. The VGP trajectories define the transit to the opposite polarity and the return to the initial state. During these two phases the VGPs are almost antipodal and progress through a large loop. The length of the excursion controls the amplitude of the loop. For increasing excursion lengths, the VGPs reach higher southern latitudes and therefore produce a larger loop. Recurring loops with different amplitudes and similar VGP paths can, thus, be artificially generated by U-channel measurements.

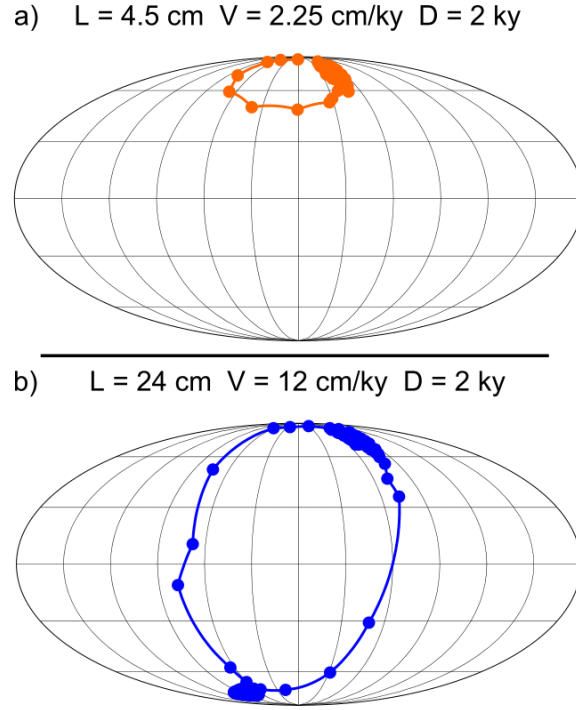


Figure 11: Artificial VGP paths derived from U-channel measurements for (a) 4.5-cm and (b) 12-cm events.

In this first experiment, we did not use cubes with transitional magnetic directions. However, the smearing of weakly magnetized transitional directions by U-channel measurements raises questions about intermediate or transitional directions even in high-resolution records. This aspect is investigated below from simulations of polarity transitions.

## 1.7 SIMULATIONS OF POLARITY TRANSITIONS

Following the same approach, we investigated the evolution of transitional directions induced in different sample sets sandwiched between intervals with normal and reverse polarity. We generated successive transitional directions that are similar to the most detailed volcanic records of reversals, keeping in mind that these changes may be distinct from reality because the magnetization of each 1.5-cm cube represents a time-averaged direction that integrates a significant field history, including possibly rapid changes. However, this is not critical for investigating the effect of U-channel measurements on successions of rapidly changing directions during transitional periods and determining whether suitable transitional directions can be obtained.

From the above results, we emphasize the importance of a long transition interval to recover transitional directions that are not generated artificially by signal smearing. We simulated reverse to normal polarity reversals (the sense of the transition is not critical). The first reversal was defined by eight transitional cubes (for a 12-cm transitional interval) with angular deviations more than  $10^\circ$  away from full polarity (Figure 12a) and identified also the intermediate VGP positions. Associated field intensity variations involve 12 cubes over an 18-cm interval. Smoothing generated by the U-channel has changed the intermediate directions (Figure 12b) and their latitudinal distribution with evident consequences for the limits of the reversal. The initial VGP path (Figure 12c) is characterized by two deviations across a large range of longitudes that resemble features found in paleomagnetic records. VGPs for the U-channel (Figure 12d) fail to duplicate the short-period changes and evolve smoothly and gradually in latitude between the two polarities. The apparent duration (or interval length) of the transition is unchanged.

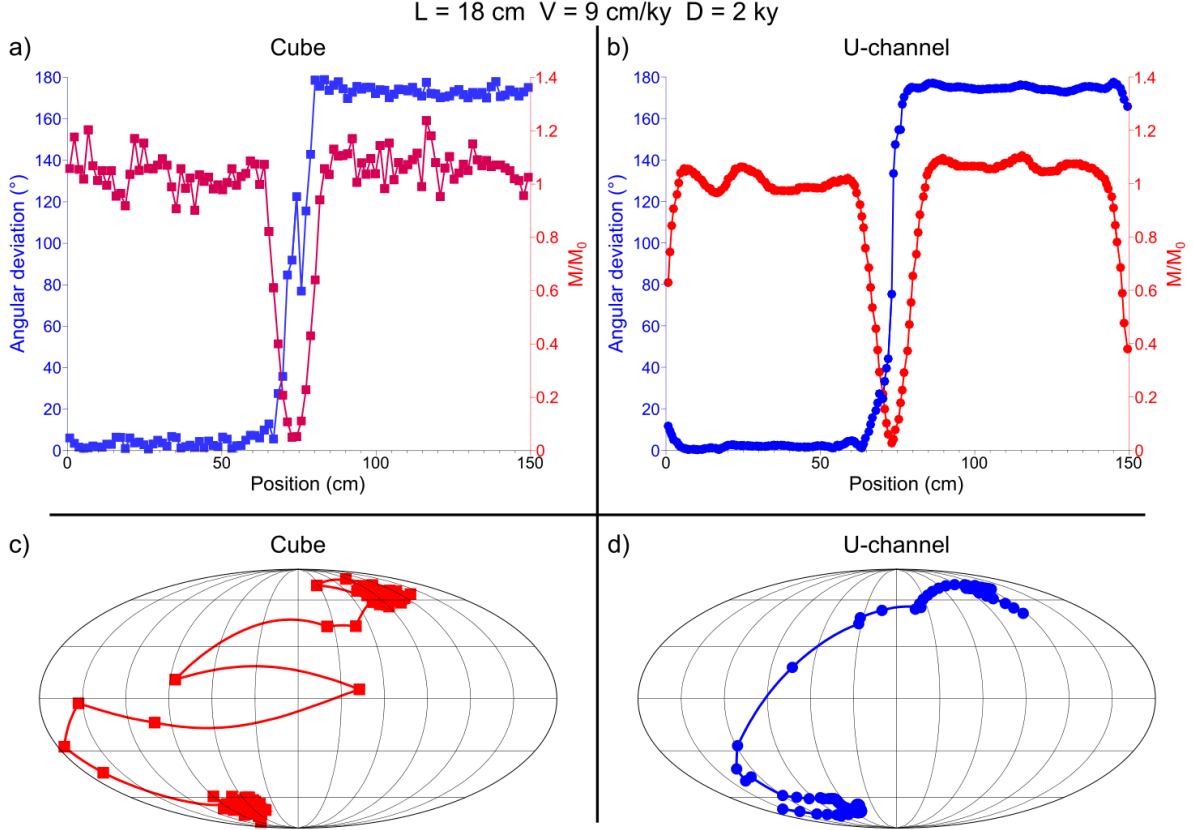


Figure 12: Simulations of a 2-kyr polarity transition recorded over an 18-cm stratigraphic interval. (a) Angular deviation (blue squares) and magnetization intensity (red squares) of individual cubes as a function of their position in the simulated sequence, and (b) angular deviation (blue dots) and magnetization intensity (red dots) derived from the corresponding U-channel. (c) Initial VGP path derived from the single samples, and (d) VGP path obtained from the U-channel measurements.

A second reversal was simulated over a 30-cm-long interval of sediment with 20 transitional directions (Figure 13a). It represents a 2-kyr transition duration recorded by sediment with a 15 cm/kyr accumulation rate (or a 3-kyr transition at 10 cm/kyr). As in the previous case, successive transitional directions (Figure 13b) are heavily smoothed and their number has increased. The initial VGPs (Figure 13c) have a smoother variation than in the previous case, with two small amplitude loops in the southern hemisphere and a cluster at mid- northern latitudes. The VGP path derived from the U-channel measurements is confined strictly in longitude with no VGP looping and no significant VGP clustering (Figure 13d). Again, the apparent transition duration is unchanged. In both situations,

smearing of transitional directions by U-channel measurements generates smooth VGP paths. The degree of longitudinal confinement evidently depends on the initial VGP configuration. U-channel measurements of transitions with poorly scattered VGPs in longitude produce a smooth and regular transit between the two polarities that resemble a simple dipole rotation, while they tend to reduce the longitudinal confinement of transitions with scattered VGPs, but still have a smooth change in latitude. In all cases, the apparent complexity of field changes has been smoothed in the U-channel records.

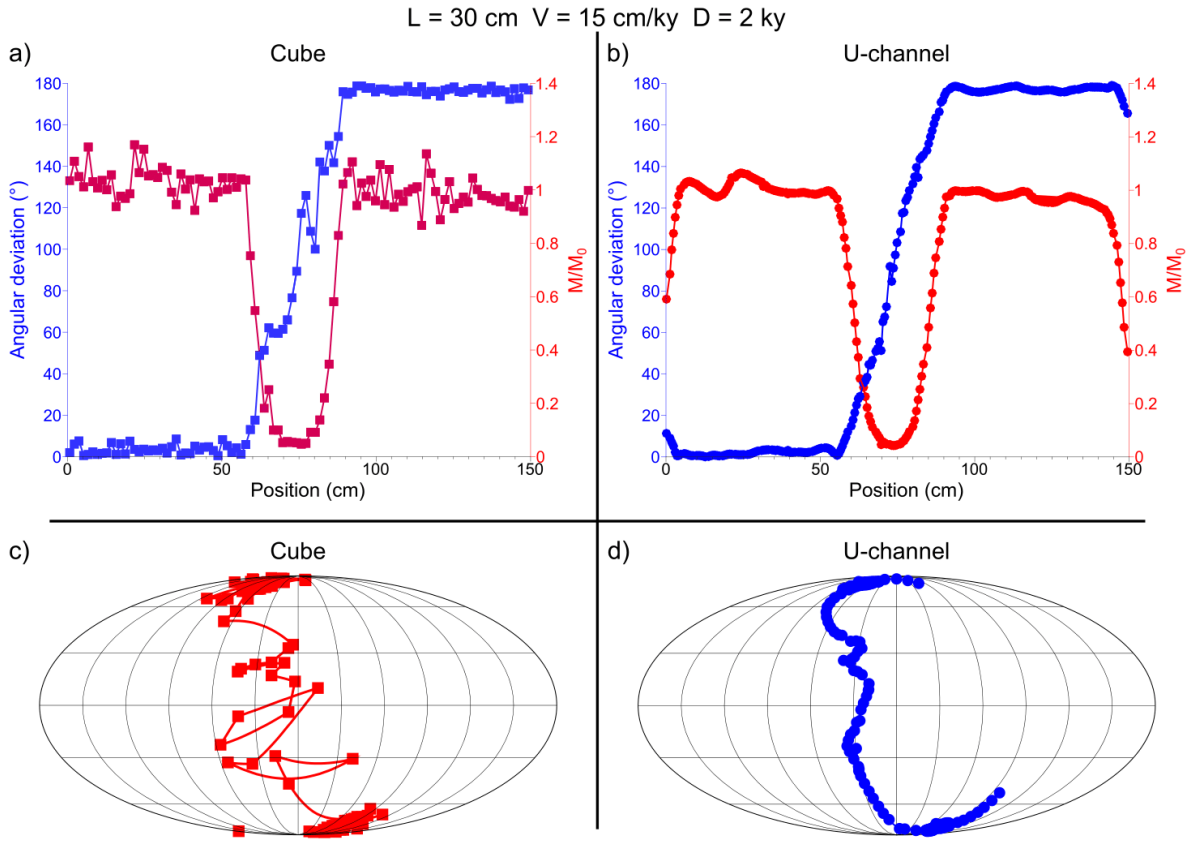


Figure 13: Same as Figure 12 for a 30-cm simulated transitional interval recorded in sediment with 15 cm/kyr deposition rate and a 2-kyr transition.

The third simulation applies to a reversal recorded over the same interval thickness, but with a more complex dynamical structure (Figure 14a). The directions of the cubes are characterized by rapid and large amplitude changes that have completely disappeared in the U-channel record (Figure 14b). The transitional VGPs (Figure 14c) cross a wide range of

longitudes and are characterized by large latitudinal variations that can be described roughly by two latitudinal loopings referred to as loops 1 and 2 in Figure 14c. At first glance, the U-channel results (Figure 14d) bear some similarities to the initial record, but in reality, they do not reproduce any major feature of the transition and they alter its dynamical pattern. Overall, the VGP trajectory has a regular transit from south to north followed by a large loop that could be erroneously interpreted as a rebound. Neither the amplitude of the changes nor the overall geometry of the path is reproduced. U-channel measurements fail to recover the first loop, and they amplify considerably the second loop. They have also artificially generated VGP clusters (e.g., at 30°N and within the VGP loop).

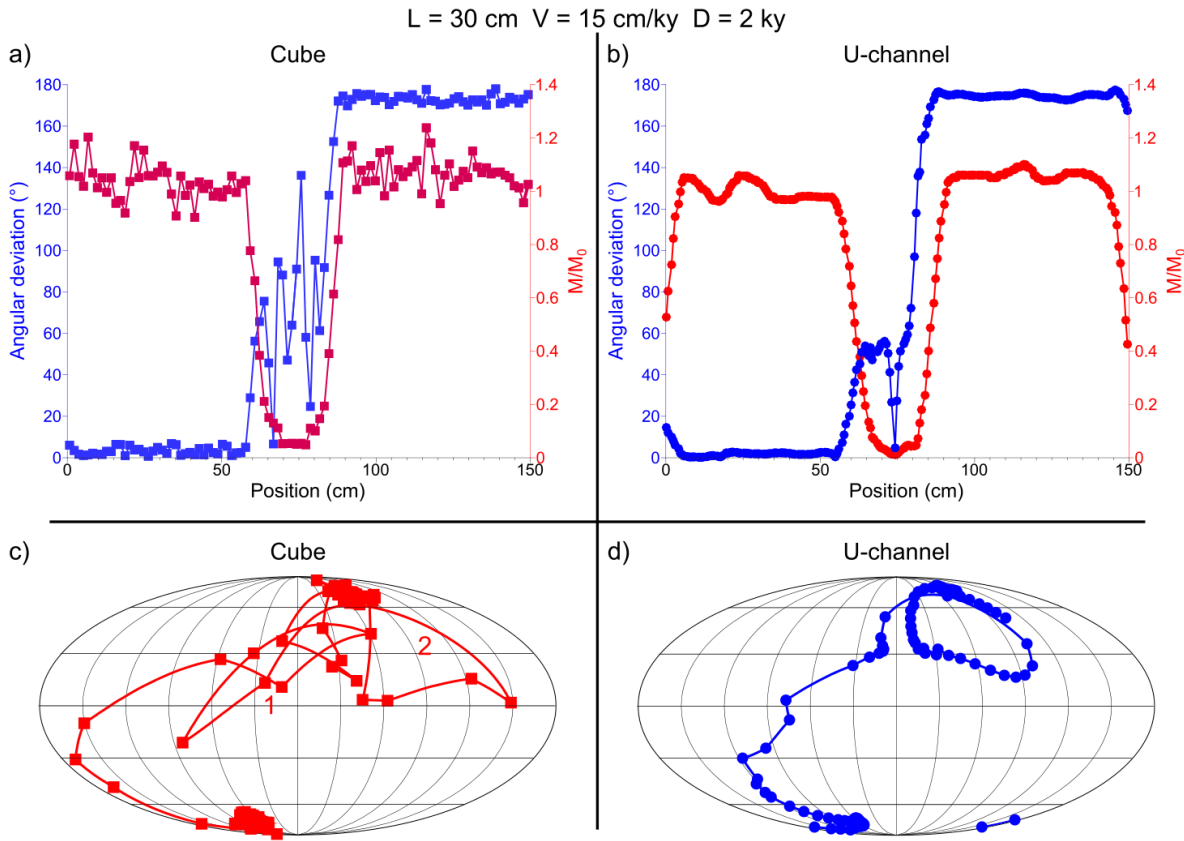


Figure 14: Same as Figure 13 for a more complex 2-kyr transition over a 30-cm transitional interval with a 15 cm/kyr deposition rate.

Based on the results in Figure 13, an optimistic view would be to consider that provided that sedimentation rates are high enough, U-channel measurements can

discriminate between simple transitional paths and more complex dynamic transitional behavior, but any interpretation remains uncertain and dependent on the amount of smoothing, which is generated by the geometry of the SQUIDs. It is worth noting that U-channel measurements amplify the distortion generated by changes in deposition rates during the short transitional period.

## 1.8 U-CHANNEL MEASUREMENTS AND SIGNAL CONVOLUTION

Each magnetometer has characteristics that yield different measurement resolutions, so it is useful to investigate further the sensitivity to the width of the response curve. In this test, we compare whether transitional directions derived from U-channel measurements are identical to those obtained after convolution of the cube train by the magnetometer response. We simply use each response curve to simulate the measurement of the equivalent U-channel. We used the discrete sample measurements of the third simulation, which is characterized by the most complex dynamical transition structure (Figure 14 and Figure 15a). We added a 20-cm-long void on both sides of the mimicked U-channel and convolved the measured data by the response function of the magnetometer (Figure 8b). The U-channel measurements and convolution results are compared in Figure 15 and Figure 16 in terms of intensity, angular variation, and VGPs, respectively.

The good (expected) coherence between the measured and simulated U-channels indicates that this simple convolution has captured the required details and therefore that it can be used further to test the impact of other response curves. We first used the response functions of the HR magnetometer at Institut de Physique du Globe de Paris (IPGP) with a 5.5-cm half-width response curve (Figure 8a), then the d.c. SQUIDs of the later IPGP (Figure 8b) and Laboratoire des Sciences du Climat et de l’Environnement (LSCE) magnetometers (Figure 8c), which have similar 6- to 7-cm half-width response curves, and finally the response of the liquid helium free magnetometer from the Institut des sciences de la mer de Rimouski (ISMER) paleomagnetic laboratory (Figure 8d). As expected, the

resolution of the HR SQUIDs provides the best agreement with the original samples but fails to reproduce the complexity of the directional changes (Figure 15c). The convolution distorted the VGP path and considerably amplified the c2 loop (Figure 16c). The half-width response curve of the HR IPGP magnetometer is 1.5 cm smaller than with the d.c. SQUIDs at IPGP and 0.5 cm for LSCE, while the ISMER (Rimouski) magnetometer has a 1-cm wider response (Figure 8). Our simulation reveals that intensity (Figure 15d and Figure 15e) changes are similar for both kind of magnetometers, but that angular deviations (Figure 15d and Figure 15e) and VGP trajectories (Figure 16d and Figure 16e) obtained for IPGP and LSCE benefit from the 1-cm difference in resolution (Figure 16e). Notwithstanding this, both magnetometers fail to reproduce the complexity of the original single sample measurements. Therefore, despite improvement of resolution, the major characteristics of transitional changes are not correctly reproduced by U-channel measurements. As expected, the measurements obtained with the larger response of the ISMER magnetometer amplified the smearing (Figure 15f) and generated a much smoother VGP trajectory (Figure 16f). The loop has almost disappeared and looks more like a small hairpin, while the existence of VGP clusters is less obvious.

Overall, our simulations illustrate the sensitivity of U-channel transitional directions to the width of the magnetometer response function. Differences, as small as 1 cm in the half-width of the response function, can generate different VGP paths with different configurations that are also different from the original field and, thus, lead to erroneous interpretations in terms of field behavior. Deconvolution of U-channel data is commonly considered as an alternative way to recover original directions and to improve resolution. Several deconvolution techniques have been proposed with various levels of success (Constable & Parker, 1991; Guyodo et al., 1999; Jackson et al., 2010; Oda & Shibuya, 1996; Oda & Xuan, 2014; Weeks et al., 1993). The difficulty inherent to this approach is to restore variations with durations that are shorter than the window length of the magnetometer sensors but also to account for rapid changes in magnetization intensity. The most recent and successful method by Xuan and Oda (2015) proposes a statistical correction that addresses these aspects.

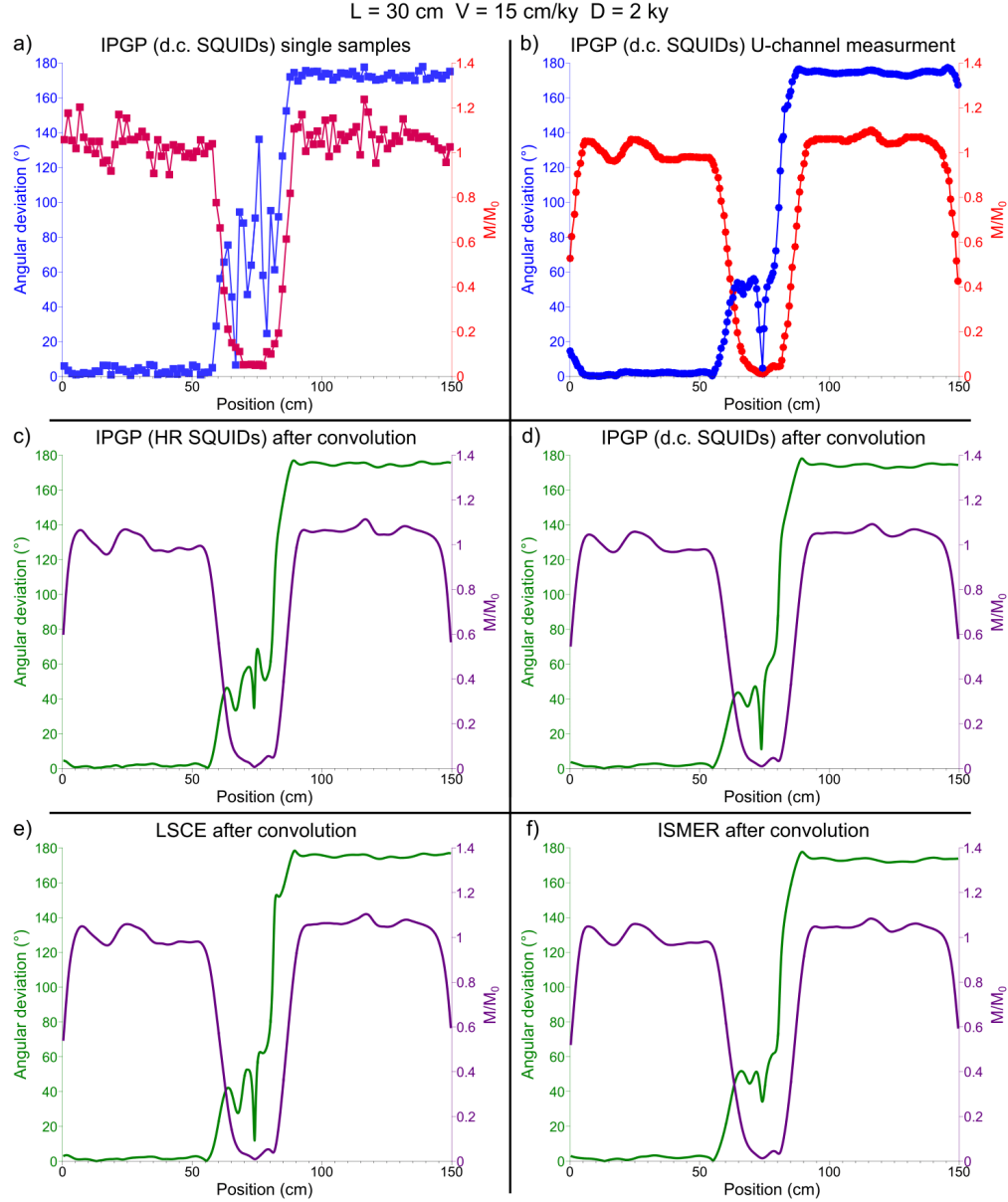


Figure 15: Convolution of measurements for successive discrete samples recording a 2-kyr polarity transition over 30 cm. (a) Angular deviation (blue dots) and magnetization intensity (red dots) for measurements of individual 1.5-cm samples. (b) Angular deviation (blue dots) and magnetization intensity (red dots) obtained from U-channel measurements. (c) Angular deviation (green) and magnetization intensity (purple) after convolution of discrete sample measurements by the Institut de Physique du Globe de Paris (IPGP) high-resolution (HR) superconducting quantum interference device (SQUID) response functions. (d) Same as (c) with the IPGP direct current SQUIDS. (e) Same as (c) using the Laboratoire des Sciences du Climat et de l'Environnement (LSCE) magnetometer response. (f) Same as (c) using the Institut des sciences de la mer de Rimouski (ISMER) magnetometer response.

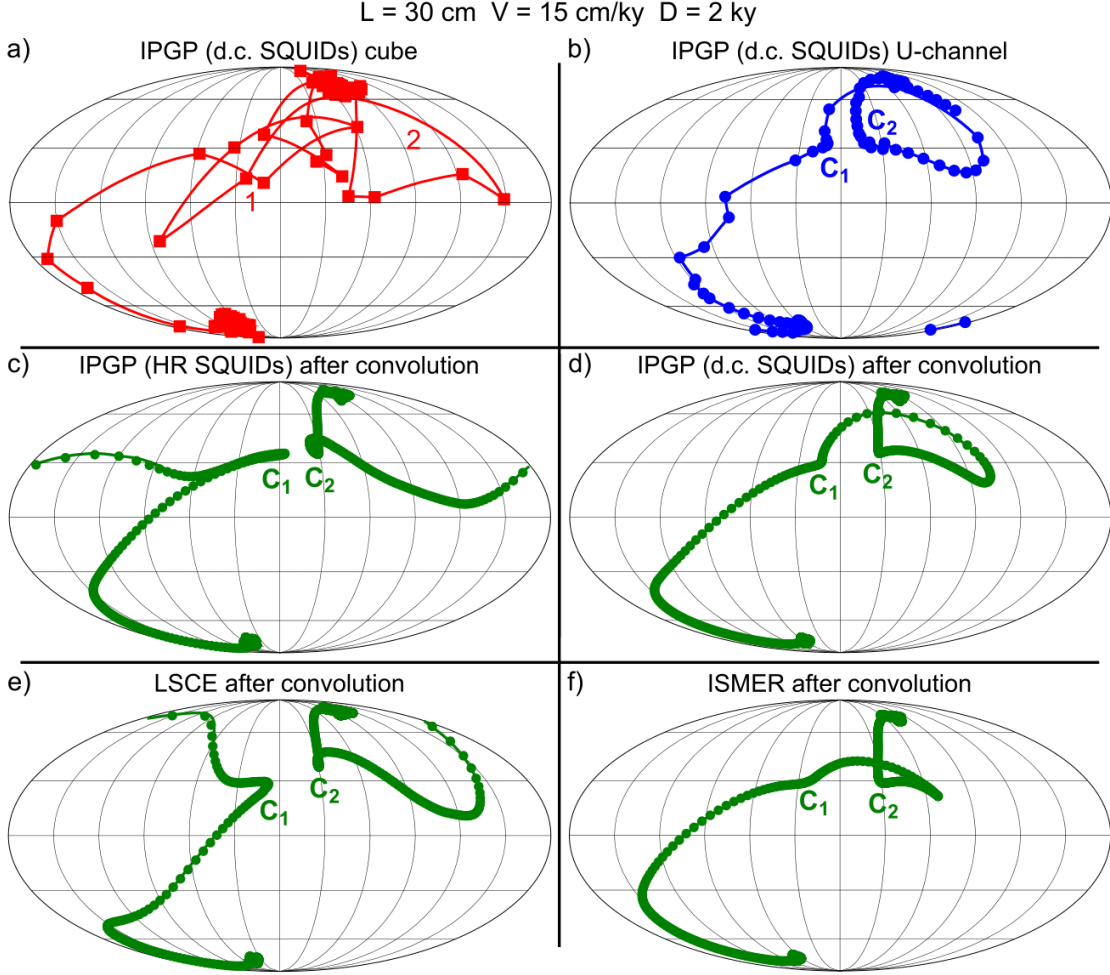


Figure 16: VGP paths shown in Figure 15 for the measurements and calculated convolutions.

## 1.9 CONCLUSIONS

We have investigated whether U-channel samples are appropriate for recovering high-fidelity records of large-amplitude rapid geomagnetic field changes that are typical of excursions or polarity reversals. We used a direct approach that consisted of testing successive measurements of individual 1.5-cm synthetic samples against measurements of equivalent synthetic U-channels constructed by placing the same samples in a continuous

row using a 2G Enterprises magnetometer with 7-cm half-length response function. This experiment was exempt from disturbances due to sampling and did not take into account any additional smearing induced by magnetization acquisition. We simulated excursions (including at least four directions with opposite polarity) over increasingly thicker intervals. Events shorter than 7.5 cm were not revealed by U-channel measurements. Longer events were detected, but the amplitude of variations was attenuated considerably. We found that a 20-cm excursion interval was required to detect paleomagnetic directions with opposite polarity. The remanence intensity for U-channel measurements decreases within excursion thickness, which could be used to indicate the presence of an excursion, but lack of detection of directional changes prevents interpretation of directional behavior. When available, VGP paths describe a large looping during excursions that result from smoothing of preexcursional and postexcursional directions.

Reversal simulations also failed to reproduce the original VGPs, even for long transitional intervals. Signal smoothing inherent to U-channel measurements tends to constrain VGPs in longitude and generates artificial directions. VGP loops are not reproduced, while a few geographically nearby VGPs can give the appearance of a VGP cluster.

Results of U-channel measurements are consistent with a simple convolution of a discrete sample train by the IPGP magnetometer response curves. We tested further the impact of other magnetometer response curves and found that transitional directions and therefore the pattern of the transition are sensitive to the widths of the response curves, even for differences as small as 1 cm.

Even though U-channel measurements are appropriate and extremely useful for documenting long-term dipolar field features and provide excellent records of field behavior (magnetostratigraphy, relative paleointensity) and pertinent environmental studies, for sedimentation rates lower than  $\sim$ 10 cm/kyr, they fail to detect directional changes inherent to excursions or polarity transitions. Smearing of directions with opposite and/or intermediate polarities generate directional artifacts that are not representative of the

magnetic vector. High-frequency field changes are recovered better in high deposition rate records, but transitional directions are also affected by smoothing.

Finally, we demonstrate that U-channel measurements fail to duplicate rapidly changing field features during polarity transitions, even for rapid deposition rates and are therefore not appropriate for reversal studies. This is exemplified by dissimilarities between single samples and U-channel directions reported in detailed high-resolution records of excursions (Channell, 2017; Laj et al., 2006) and reversals (Channell et al., 2017). We do not deny that there are situations with high sedimentation rates where U-channel measurements do not appear to provide large distortions. However, there is no other way to assess the reliability of the directional changes than by comparing the U-channel results with single sample measurements. We infer that the U-channel measurement technique is not appropriate for extracting significant information about detailed field morphologies during reversals and excursions and that such records should be systematically accompanied by discrete samples provided that the resolution of the record is sufficient and tested against the deconvolution of U-channel measurements (Channell, 2017).

## 1.10 ACKNOWLEDGMENTS

This study was supported by the ERC Advanced grant GA 339899-EDIFICE under the ERC's 7th Framework Program (FP7-IDEAS-ERC) and by an NSERC Discovery Grant. The authors acknowledge Fernando Lopes and Nabil Garoum for contributions at various stages of the study. We are deeply grateful to Andrew Roberts for his exhaustive review and for considerably improving the manuscript and acknowledge an anonymous reviewer. Data are available in the supporting information. This is IPGP contribution number 3984.

## 1.11 REFERENCES

- Barletta, F., St-Onge, G., Stoner, J. S., Lajeunesse, P., & Locat, J. (2010). A high-resolution Holocene paleomagnetic secular variation and relative paleointensity stack from eastern Canada. *Earth and Planetary Science Letters*, 298(1–2), 162–174. <https://doi.org/10.1016/j.epsl.2010.07.038>
- Channell, J. E. T. (2017). Complexity in Matuyama–Brunhes polarity transitions from North Atlantic IODP/ODP deep-sea sites. *Earth and Planetary Science Letters*, 467, 43–56. <https://doi.org/10.1016/j.epsl.2017.03.019>
- Channell, J. E. T., & Kleiven, H. F. (2000). Geomagnetic palaeointensities and astrochronological ages for the Matuyama–Brunhes boundary and the boundaries of the Jaramillo Subchron: Palaeomagnetic and oxygen isotope records from ODP Site 983. *Philosophical Transactions of the Royal Society of London A: Mathematical, Physical and Engineering Sciences*, 358(1768), 1027–1047. <https://doi.org/10.1098/rsta.2000.0572>
- Channell, J. E. T., & Lehman, B. (1997). The last two geomagnetic polarity reversals recorded in high-deposition-rate sediment drifts. *Nature*, 389(6652), 712–715. <https://doi.org/10.1038/39570>
- Channell, J. E. T., Stoner, J. S., Hodell, D. A., & Charles, C. D. (2000). Geomagnetic paleointensity for the last 100 kyr from the sub-antarctic South Atlantic: A tool for inter-hemispheric correlation. *Earth and Planetary Science Letters*, 175(1–2), 145–160. [https://doi.org/10.1016/S0012-821X\(99\)00285-X](https://doi.org/10.1016/S0012-821X(99)00285-X)
- Channell, J. E. T., Vázquez Riveiros, N., Gottschalk, J., Waelbroeck, C., & Skinner, L. C. (2017). Age and duration of Laschamp and Iceland Basin geomagnetic excursions in the South Atlantic Ocean. *Quaternary Science Reviews*, 167, 1–13. <https://doi.org/10.1016/j.quascirev.2017.04.020>

- Constable, C., & Parker, R. (1991). Deconvolution of long-core palaeomagnetic measurements—Spline therapy for the linear problem. *Geophysical Journal International*, 104(3), 453–468. <https://doi.org/10.1111/j.1365-246X.1991.tb05693.x>
- Guyodo, Y., Channell, J. E. T., & Thomas, R. G. (2002). Deconvolution of u-channel paleomagnetic data near geomagnetic reversals and short events. *Geophysical Research Letters*, 29(17), 1845. <https://doi.org/10.1029/2002GL014927>
- Guyodo, Y., Richter, C., & Valet, J.-P. (1999). Paleointensity record from Pleistocene sediments (1.4–0 Ma) off the California Margin. *Journal of Geophysical Research*, 104, 22,953–22,964. <https://doi.org/10.1029/1999JB900163>
- Jackson, M., Bowles, J. A., Lascu, I., & Solheid, P. (2010). Deconvolution of u channel magnetometer data: Experimental study of accuracy, resolution, and stability of different inversion methods. *Geochemistry, Geophysics, Geosystems*, 11, Q07Y10. <https://doi.org/10.1029/2009GC002991>
- Kissel, C., Laj, C., Mazaud, A., & Dokken, T. (1998). Magnetic anisotropy and environmental changes in two sedimentary cores from the Norwegian Sea and the North Atlantic. *Earth and Planetary Science Letters*, 164(3-4), 617–626. [https://doi.org/10.1016/S0040-1951\(98\)00223-6](https://doi.org/10.1016/S0040-1951(98)00223-6)
- Laj, C., Kissel, C., & Roberts, A. P. (2006). Geomagnetic field behavior during the Iceland Basin and Laschamp geomagnetic excursions: A simple transitional field geometry? *Geochemistry, Geophysics, Geosystems*, 7, Q03004. <https://doi.org/10.1029/2005GC001122>
- Macrì, P., Sagnotti, L., Dinarès-Turell, J., & Caburlotto, A. (2010). Relative geomagnetic paleointensity of the Brunhes Chron and the Matuyama–Brunhes precursor as recorded in sediment core from Wilkes Land Basin (Antarctica). *Physics of the Earth and Planetary Interiors*, 179(1-2), 72–86. <https://doi.org/10.1016/j.pepi.2009.12.002>

- Mazaud, A., Channell, J. E. T., & Stoner, J. S. (2012). Relative paleointensity and environmental magnetism since 1.2 Ma at IODP site U1305 (Eirik Drift, NW Atlantic). *Earth and Planetary Science Letters*, 357-358, 137–144. <https://doi.org/10.1016/j.epsl.2012.09.037>
- Meynadier, L., Valet, J.-P., Weeks, R., Shackleton, N. J., & Hagee, V. L. (1992). Relative geomagnetic intensity of the field during the last 140 ka. *Earth and Planetary Science Letters*, 114(1), 39–57. [https://doi.org/10.1016/0012-821X\(92\)90150-T](https://doi.org/10.1016/0012-821X(92)90150-T)
- Nagy, E. A., & Valet, J.-P. (1993). New advances for paleomagnetic studies of sediment cores using U-channels. *Geophysical Research Letters*, 20, 671–674. <https://doi.org/10.1029/93GL00213>
- Oda, H., & Shibuya, H. (1996). Deconvolution of long-core paleomagnetic data of Ocean Drilling Program by Akaike's Bayesian Information Criterion minimization. *Journal of Geophysical Research*, 101, 2815–2834. <https://doi.org/10.1029/95JB02811>
- Oda, H., & Xuan, C. (2014). Deconvolution of continuous paleomagnetic data from pass-through magnetometer: A new algorithm to restore geomagnetic and environmental information based on realistic optimization. *Geochemistry, Geophysics, Geosystems*, 15, 3907–3924. <https://doi.org/10.1002/2014GC005513>
- Roberts, A. P., Lehman, B., Weeks, R. J., Verosub, K. L., & Laj, C. (1997). Relative paleointensity of the geomagnetic field over the last 200,000 years from ODP Sites 883 and 884, North Pacific Ocean. *Earth and Planetary Science Letters*, 152(1-4), 11–23. [https://doi.org/10.1016/S0012-821X\(97\)00132-5](https://doi.org/10.1016/S0012-821X(97)00132-5)
- Roberts, A. P., Stoner, J. S., & Richter, C. (1996). Coring-induced magnetic overprints and limitations of the long-core paleomagnetic measurement technique: some observations from Leg 160, Eastern Mediterranean Sea. In K.-C. Emeis, A. H. F. Robertson, & C. Richter (Eds.), *Proceedings of ODP initial reports* (Vol. 160, pp.

497–505). College Station, TX: Texas A & M University Ocean Drilling Program.  
<https://doi.org/10.2973/odp.proc.ir.160.115.1996>

Roberts, A. P., & Winklhofer, M. (2004). Why are geomagnetic excursions not always recorded in sediments? Constraints from post- depositional remanent magnetization lock-in modelling. *Earth and Planetary Science Letters*, 227(3-4), 345–359.  
<https://doi.org/10.1016/j.epsl.2004.07.040>

Stoner, J. S., Channell, J. E. T., Hillaire-Marcel, C., & Kissel, C. (2000). Geomagnetic paleointensity and environmental record from Labrador Sea core MD95-2024: Global marine sediment and ice core chronostratigraphy for the last 110 kyr. *Earth and Planetary Science Letters*, 183(1–2), 161–177. [https://doi.org/10.1016/S0012-821X\(00\)00272-7](https://doi.org/10.1016/S0012-821X(00)00272-7)

Tauxe, L., LaBrecque, J. L., Dodson, R., & Fuller, M. (1983). U-channels-a new technique for paleomagnetic analysis of hydraulic piston cores. *Eos, Transactions American Geophysical Union*, 64, 219.

Valet, J.-P. (2003). Time variations in geomagnetic intensity. *Reviews of Geophysics*, 41(1), 1004. <https://doi.org/10.1029/2001RG000104> Valet, J.-P., & Meynadier, L. (1993). Geomagnetic field intensity and reversals during the past four million years. *Nature*, 366(6452), 234–238. <https://doi.org/10.1038/366234a0>

Verosub, K. L., Harris, A. H., & Karlin, R. (2001). Ultrahigh-resolution paleomagnetic record from ODP Leg 169S, Saanich Inlet, British Columbia: Initial results. *Marine Geology*, 174(1–4), 79–93. [https://doi.org/10.1016/S0025-3227\(00\)00143-2](https://doi.org/10.1016/S0025-3227(00)00143-2)

Weeks, R., Laj, C., Endignoux, L., Fuller, M., Roberts, A., Manganne, R., et al. (1993). Improvements in long-core measurement techniques: Applications in palaeomagnetism and palaeoceanography. *Geophysical Journal International*, 114(3), 651–662. <https://doi.org/10.1111/j.1365-246X.1993.tb06994.x>

Xuan, C., & Oda, H. (2015). UDECON: Deconvolution optimization software for restoring high-resolution records from pass-through paleomagnetic measurements. *Earth, Planets and Space*, 67(1), 183. <https://doi.org/10.1186/s40623-015-0332-x>



## CHAPITRE 2

# **INFLUENCE DE LA LITHOLOGIE SUR L'AIMANTATION RÉMANENTE ENREGISTRÉE DANS LES SÉDIMENTS VARVÉS DU LAC GLACIAIRE OJIBWAY (CANADA)**

### **2.1 RÉSUMÉ EN FRANÇAIS DU DEUXIÈME ARTICLE**

L'aimantation naturelle rémanente (NRM) de sédiments à hautes vitesses de sédimentation fournit des informations pertinentes sur la variation séculaire du champ magnétique terrestre et peut aussi être potentiellement utilisée pour la stratigraphie. Cependant, l'acquisition de la NRM dépend des conditions inhérentes à l'environnement sédimentaire. Les sédiments varvés, en plus de fournir une chronologie annuelle, sont typiquement caractérisés par des changements sédimentaires importants durant une même année. Puisque le champ magnétique de la Terre ne varie pas significativement au cours d'une telle période, les changements magnétiques enregistrés par les varves reflètent alors l'influence des paramètres sédimentaires sur l'enregistrement paléomagnétique. La présente étude se concentre sur des sédiments de l'ancien lac proglaciaire Ojibway ( $\sim 8.5$  ka cal BP), qui était recouvert de glace en hiver. Elle se concentre sur une série de lits d'été et d'hiver d'un centimètre d'épaisseur, échantillonnés individuellement à l'aide de petits cubes de 1 cm<sup>3</sup>. Des analyses paléomagnétiques, granulométriques et géochimiques ont été réalisées sur chaque lit. Les déclinaisons magnétiques ne montrent pas de déviations systématiques par rapport à la direction du champ attendue, contrairement aux inclinations, qui sont beaucoup plus faibles que celles attendues à la latitude du site, sur la base d'un modèle dipolaire axial géocentrique. Un aplatissement de l'inclinaison de 13° est systématiquement observé dans les lits d'hiver. Les lits d'été sont plus épais que les lits d'hiver et se caractérisent par une susceptibilité magnétique plus forte, un rapport Ca/Fe plus élevé et des grains sédimentaires et magnétiques plus grossiers. Cette configuration

granulométrique reflète l'apport de particules détritiques plus grossières pendant l'été, tandis que la fraction plus fine est restée en suspension jusqu'au dépôt en hiver. Les différences observées pourraient être attribuables au compactage différentiel des lits d'hiver et d'été et aux variations de la composition des grains magnétique. Ces résultats indiquent que les variations lithologiques peuvent jouer un rôle dominant sur les enregistrements magnétiques des sédiments.

Cet article, intitulé « *Influence of lithology on the remanent magnetization as recorded in varved sediments from the glacial Lake Ojibway (Canada)* », fut corédigé par moi-même ainsi que par mes deux directeurs Guillaume St-Onge (UQAR-ISMER) et Jean-Pierre Valet (IPGP). Pierre-Marc Godbout, étudiant au doctorat à l'UQAM, a fait les principales analyses sédimentaires et a apporté ses connaissances sur le lac Ojibway. Ramon Egli, chercheur du *Central Institute for Meteorology and Geodynamics* a contribué aux analyses et à l'interprétation des mesures des *first-order reversal curve* (FORC). Mon co-directeur, Pierre Francus a supervisé la rédaction de l'article et a apporté ses connaissances sur l'étude des varves. Martin Roy, professeur à l'UQAM, a apporté ses connaissances sur le lac Ojibway. Le manuscrit sera soumis prochainement à la revue *Earth and Planetary Science Letters*.

Une version abrégée de cet article a été présentée à l'oral au congrès annuel du GEOTOP qui s'est déroulé à La Malbaie (QC, Canada) en 2018.

## **2.2 INFLUENCE OF LITHOLOGY ON THE REMANENT MAGNETIZATION AS RECORDED IN VARVED SEDIMENTS FROM THE GLACIAL LAKE OJIBWAY (CANADA)**

Natural Remanent Magnetization (NRM) of high sedimentation rate sediments provides pertinent information about the paleomagnetic secular variation of the Earth's magnetic field and can also potentially be used for stratigraphy. However, NRM acquisition depends on conditions inherent to the depositional environment. Besides recording a precise annual chronology, varved sediments are typically characterized by marked sedimentary changes within the same year. Since the Earth's magnetic field does not vary significantly over such short period, magnetic changes recorded by varves reflect the influence of sedimentary parameters on the recording process. The present study focuses on sediments from the former proglacial Lake Ojibway (~ 8.5 ka cal BP), which was ice covered in winter. It concentrates on a sequence of centimetre-thick summer and winter beds that were sampled individually using small 1 cm<sup>3</sup> plastic cubes. Paleomagnetic, granulometric and geochemical analyses were conducted on each individual layer. Magnetic declinations do not show systematic deviations from the expected field direction, contrary to inclinations, which are much shallower than expected at the site latitude based on a geocentric axial dipole model. An inclination shallowing of 13° is systematically observed in winter beds. Summer beds are thicker than winter beds and characterized by stronger magnetic susceptibility, higher Ca/Fe ratios and coarser sedimentary and magnetic grains. This grain size pattern reflects the input of coarser detrital particles during summer, while the finer fraction remained in suspension until deposition in winter. Differential compaction of the winter and summer beds and variations of magnetic grain composition might be responsible for the observed differences. These results indicate that lithological changes can play a dominant role on magnetic records of sediments.

## **2.3 INTRODUCTION**

Acquisition of detrital remanent magnetization (DRM) by sediments is a complex phenomenon that results from the alignment of magnetic grains by the local geomagnetic

field ( $DRM \approx f^*B$ , where  $f$  is the sediment response function and  $B$  the geomagnetic field). The sediment response function depends on several parameters related to the depositional environment, the sediment matrix, and the nature of magnetic grains. Numerous experiments aimed at simulating depositional processes as well as models of sediment magnetization have been proposed during the last 50 years (Nagata, 1961; Yoshida and Katsura, 1985; Tauxe, 1993; Tauxe et al., 2006; Spassov and Valet, 2012; Tanty et al., 2016). However, a major limitation of laboratory redeposition experiments is the impossibility to simulate the natural conditions of sedimentation in absence of adequate scaling that accounts for the much longer duration of the magnetization process in nature (Yoshida and Katsura, 1985; Tauxe, 1993; Katari et al., 2000; Tauxe et al., 2006; Spassov and Valet, 2012; Valet et al., 2017). The experiments are also constrained by the limited size of containers used for deposition, which impose a high concentration of suspended sediment, and the lack of adequate simulation of the hydrodynamic environment (Yoshida and Katsura, 1985; Spassov and Valet, 2012; Valet et al., 2017). Despite these limitations, it is possible to constrain the role of specific parameters on magnetic alignment using artificial mixtures that are deposited in laboratory (Valet et al., 2017). It is also possible to compare the results of laboratory experiments with natural analogues of very rapidly deposited sediments. The role of lithology and grain size on the magnetization process can be studied in turbidite sequences that provide useful indications about the influence of the hydrodynamic conditions and the role played by magnetic and sedimentary granulometry (Tanty et al., 2016). Another interesting approach is to investigate the magnetism of varved sediments (Mellström et al., 2015; Nilsson et al., 2018), which can potentially provide highly detailed magnetic records with an annual temporal resolution. Another advantage is that they can frequently be correlated over a relatively large geographical area (Antevs, 1925, 1928).

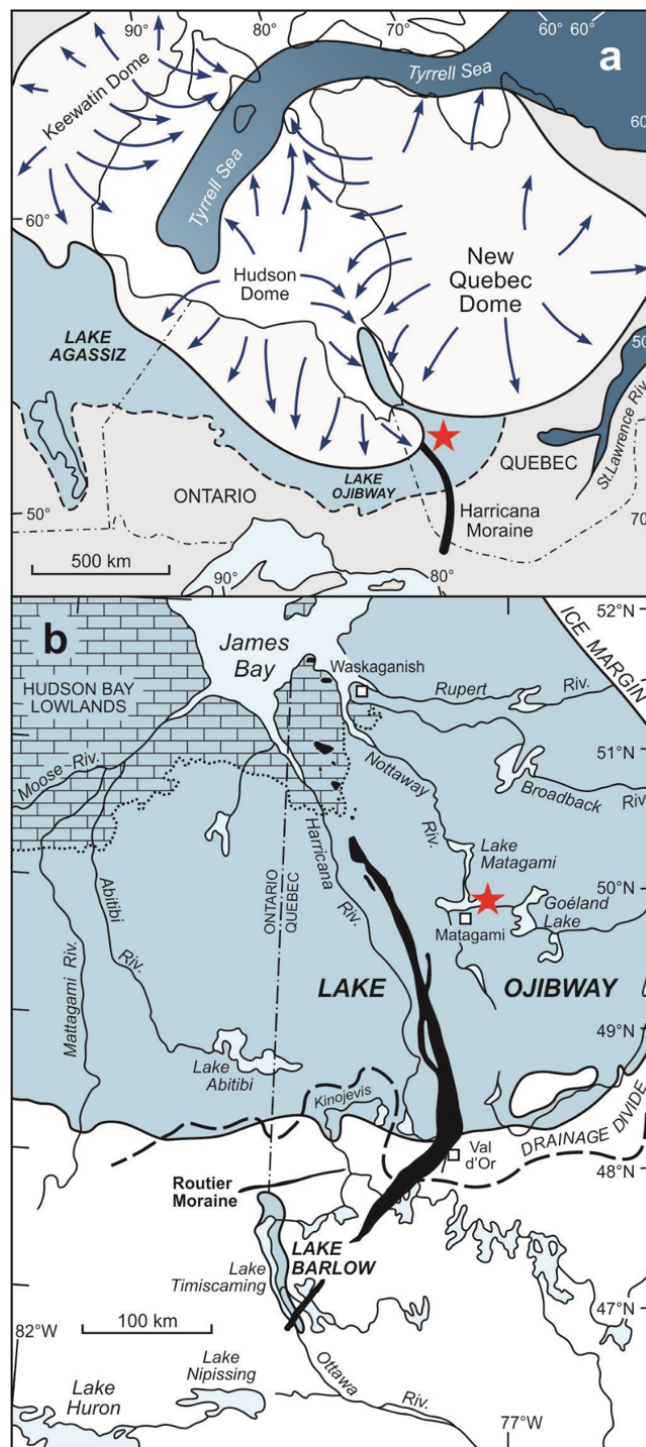


Figure 17: (a) Geographic locations of Lake Ojibway (b) and Lake Matagami during deglaciation ~8500 cal BP. Red stars indicate the site location. Blue arrows show glacial flow-lines associated with the residual ice domes. Modified from Roy et al. (2015).

Here, we selected a 3.6 m-thick sediment sequence composed of 256 varves from former proglacial Lake Ojibway (Hardy, 1976; Breckenridge et al., 2012). Given the annual periodicity of varves, the entire sequence does not exceed 250 years of geomagnetic history. It is therefore exempt of magnetic field variations by more than a few degrees in absence of any excursion or inversion.

## 2.4 ORIGIN OF SAMPLES AND GEOLOGICAL CONTEXT

Lake Ojibway (Figure 17a) formed during the last deglaciation through the accumulation of meltwater that was trapped between the decaying ice margin of the Laurentide Ice Sheet (LIS) to the north and the height of land forming the Hudson Bay/St. Lawrence River drainage divide to the south, where meltwater overflows were routed through the Ottawa River valley. This proglacial lake occupied vast portions of NE Ontario and NW Quebec (Canada) following the northward ice retreat and reached its greatest extent ~8.5 ka cal BP, when it presumably merged with Lake Agassiz to the west to form a very large meltwater reservoir (Elson, 1967; Dyke and Prest, 1987; Leverington et al., 2002; Teller et al., 2002; Dyke, 2004). Lake Ojibway disappeared shortly after ~8.5 cal BP, following the catastrophic subglacial drainage event(s) across the ice dam that was then resting in southern Hudson Bay (Shoemaker, 1992; Clarke et al., 2004; Lajeunesse and St-Onge, 2008; Roy et al., 2011; Brooks, 2018).

The high melting rate of the Laurentide Ice Sheet southern margin led to the deposition of varved sediments, which formed an important sedimentary archive that documents the deglacial ice dynamics and the lake paleohydrology during the early Holocene (e.g., Breckenridge et al., 2012). The existence of glaciolacustrine sediments in NE Ontario and NW Quebec has been known for a long time (Coleman, 1909; Antevs, 1925; 1928). In general, varves reflect the succession of summer-winter deposition. During summer, pronounced melting leads to the release of a large amount of detrital material to the basin with concomitantly high deposition rates, while the cold temperature in

wintertime considerably reduced the sediment inflow, with the attendant formation of ice cover over the lake favouring the settling of fine-grained sediments (Smith and Ashley, 1985).

We selected a 3.6 m-long sedimentary sequence containing 256 varves outcropping on the shore of Lake Matagami in Quebec ( $49^{\circ}56'43.494''$  N,  $77^{\circ}13'4.663''$  O) (Figure 17b). Paleogeographic considerations indicate that the sequence was deposited in  $\sim$ 150 m water depth (Veillette, 1994). This section was sampled twice within 61 cm-long gutters that stratigraphically overlap with each other. Every gutter was duplicated in order to obtain one sequence for sedimentary studies and a twin one for magnetic measurements. A small gap of some millimetres is possible between the sediment and magnetic gutter. Special attention was given to the G7 gutter, which contains the oldest sediments deposited well before the lake was drained. This interval also contains the thickest sedimentary varves with a  $2.01 \text{ cm a}^{-1}$  average sedimentation rate.

## 2.5 METHODS

### 2.5.1 Sedimentary analyses

Non-destructive measurements were performed at INRS-ETE. High-resolution tomograms (1 pixel =  $100 \times 600 \mu\text{m}$ ) of the varves were obtained by CT-Scan imaging with a Siemens SOMATOM Definition AS+ 128 (Boespflug et al., 1995; Crémer et al., 2002; St-Onge et al., 2007; Fortin et al., 2013). The resulting images are displayed in gray scale, darker and lighter zones representing lower and higher density, respectively.

X-Ray fluorescence, X-ray radiography and optical scans were obtained using an ITRAX core scanner from Cox Analytical Systems. Geochemical analyses performed with a  $500 \mu\text{m}$  resolution and 10 s counting time (Francus et al., 2002; Croudace et al., 2006; Rothwell et al., 2006; St-Onge et al., 2007) provided the downcore profiles of a wide range

of element contents at all stratigraphic levels. Grain size analyses were also carried out in each sedimentary layer, i.e. the centre of the summer and winter beds contained within the G7 gutter. Particle size was measured at UQAM using a Microtrac Bluewave/S3500-SDC laser diffraction particle size analyzer. Finally, organic matter content was determined by loss-on-ignition using a protocol adjusted for the clay content and composition of the Ojibway sediments that are rich in carbonates (i.e., 48 hours oven-dried at 60°C and heated for 4 hours at 450°C). To complete this study, a thin-section was sampled in the G7 gutter by following the method of Francus and Cosby (2001).

### 2.5.2 Magnetic measurements

The magnetic measurements were performed using 2 x 2 cm square section U-channels. However, U-channel measurements average the variations of remanent magnetization over several centimeters and therefore smoothed out detailed stratigraphic features that are inherent to the succession of fine laminations. In order to analyze individual varves, 1 cm<sup>3</sup> square plastic cubes were used to sample a fine sediment slice from each stratigraphic level. The resolution obtained by this technique remained evidently too low to resolve millimetric varves, but it was adequate for the individual thicker varves in the lower part of the core.

The natural remanent magnetization (NRM) was measured using a 2-G Enterprises Model 755.-1.65 DC cryogenic magnetometer at the Institut de Physique du Globe de Paris. The NRM of all samples was demagnetized along three orthogonal axes using alternating fields (a.f.) up to 140 mT in steps of 10 mT. An anhysteretic remanent magnetization (ARM) was then imparted in presence of 0.5 mT direct current field and 120 mT a.f. Additional magnetic measurements have been performed to characterize the magnetic mineralogy, magnetic grain size and magnetic anisotropy across winter and summer beds. The S-ratio defined as  $S = \frac{1}{2} [(-IRM_{0.3T}/SIRM_{1T}) + 1]$  (Bloemendal et al., 1992) represents the ratio between low and high coercivity minerals and was calculated after remagnetizing the samples in a 1T field (SIRM) and subsequently in a 0.3T (IRM) reversed field.

Measurements of magnetic susceptibility during heating up to 600°C at room temperature were performed using a KLY3 Kappabridge. Hysteresis loops were obtained with a Vibrating Sample Magnetometer (VSM). Lastly, anisotropy measurements of the ARM and magnetic susceptibility were carried out to determine preferential orientations of magnetic particles, if any.

All measurements were conducted on a large portion of the entire stratigraphic section. However, as mentioned above, the thickest varves sampled in the G7 gutter with 1 cm<sup>3</sup> plastic boxes provided the only opportunity to document each individual unit separately. This paper is primarily focusing on the results that were obtained from this gutter.

## 2.6 RESULTS

### 2.6.1 Lithological and chemical characteristics

A photograph of the G7 series is shown in Figure 18 along with CT-scan profiles showing the alternation of higher density summer (light) and lower density winter (dark) beds. The evolution of grain size within the G7 interval also shown as a function of depth in Figure 18 indicates a significant and systematic difference between the summer and winter beds. The winter beds have a mean grain size of  $0.7 \pm 0.1 \mu\text{m}$ , while the summer beds display four times larger values ( $2.8 \pm 0.8 \mu\text{m}$ ).

Similarly to previous analyses of varved sediments (Strüberger et al., 2011; Stoup et al., 2013) and ITRAX studies (Croudace et al., 2006; Rothwell et al., 2006), Ca/Fe ratio was used to define the exact limits of the beds that are different sedimentary units (Strüberger et al., 2011; Stoup et al., 2013). Like the previous study by Stoup et al. (2013), grain size and XRF data reveal that summer beds are richer (silty) in Ca and winter beds (clay) in Fe (Figure 18). Consequently, the Ca/Fe ratio of summer beds is characterized by larger values than winter beds, and was used to derive the bar code shown in Figure 18. The Ca/Fe ratio

of the winter beds is much lower than for the summer ones. The median value of this ratio defines the positions of the summer bed maxima and winter minima with a  $\pm 500 \mu\text{m}$  accuracy.

In parallel to the Ca/Fe profile, the downcore changes of magnetic susceptibility ( $k$ ) measured at room temperature largely exceed the values of paramagnetic minerals (Moskowitz, 1991) and therefore depict the downcore changes in concentration of iron oxides.

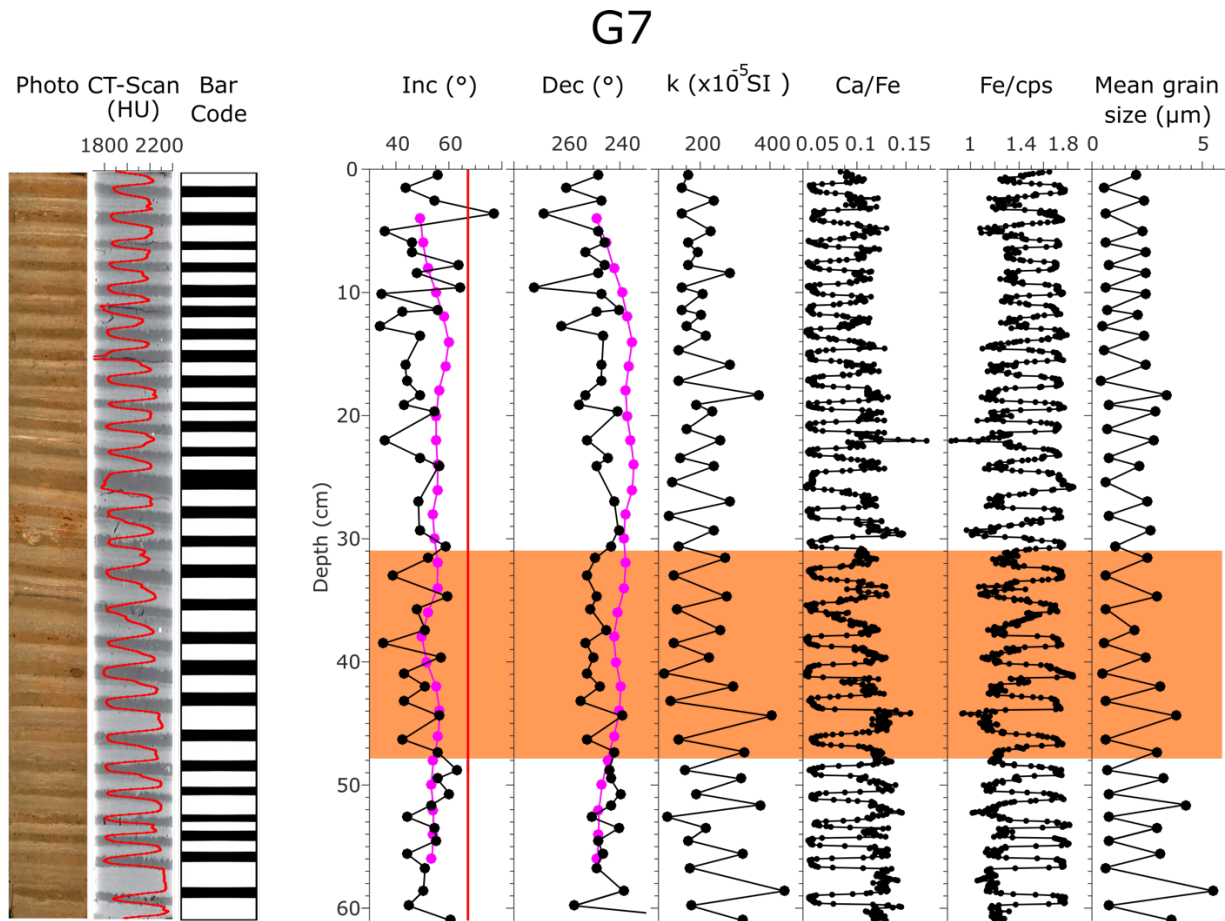


Figure 18: From left to right as a function of depth within the G7 core: core photograph, HU numbers related to sediment density derived from the CAT-Scan images and composite column that summarizes the succession of winter and summer beds. Downcore evolution of typical magnetic (inclination, declination, magnetic susceptibility) and sedimentary (Ca/Fe ratio, Fe/cps and grain size) parameters within the G7 core. Black (resp. pink dots) on

inclination and declination correspond to single samples (resp. U-channels). Red line in the inclination represents the GAD value. Fe profile in peak area is normalized by the counts per second (cps) at the corresponding depth.

A photography with normal light, one with polarized light and a bar code are shown on Figure 19. Summer beds and winter beds correspond respectively to white zones and black zones on the bar code (Figure 19). Summer beds present 3 different zones. At the bottom of the summer bed, load casts are observed. In the middle of summer bed, there are some laminations and at the top of summer bed there are coarse particles and calcite aggregates. The calcite aggregates are shown in gold on the polarized light photography. Winter beds are homogenous with more clay. These observations confirm the lithological difference between winter and summer beds.

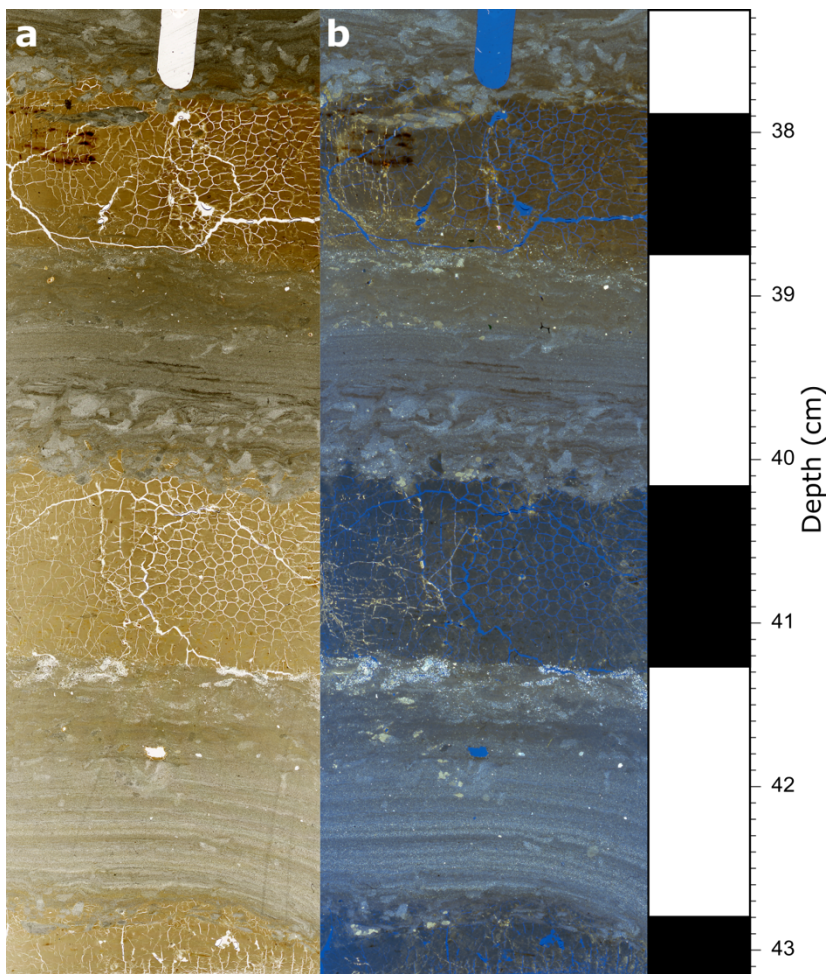


Figure 19 : Photography of a thin section from core G7 under normal light (a) and polarized light (b). A bar code is shown on the right, the white and black zones correspond respectively to summer and winter beds.

### 2.6.2 Magnetics properties

The thermomagnetic curves obtained for the summer and winter beds (Figure 20) are very similar. In both cases, there is a rapid decrease of magnetization from 560 °C to 610 °C that is consistent with the Curie temperature of magnetite (580 °C). No indication for higher Curie temperatures has ever been observed. The S-ratio values range from 99.3% to 100% and thus confirm the absence of high coercivity minerals like goethite or hematite.

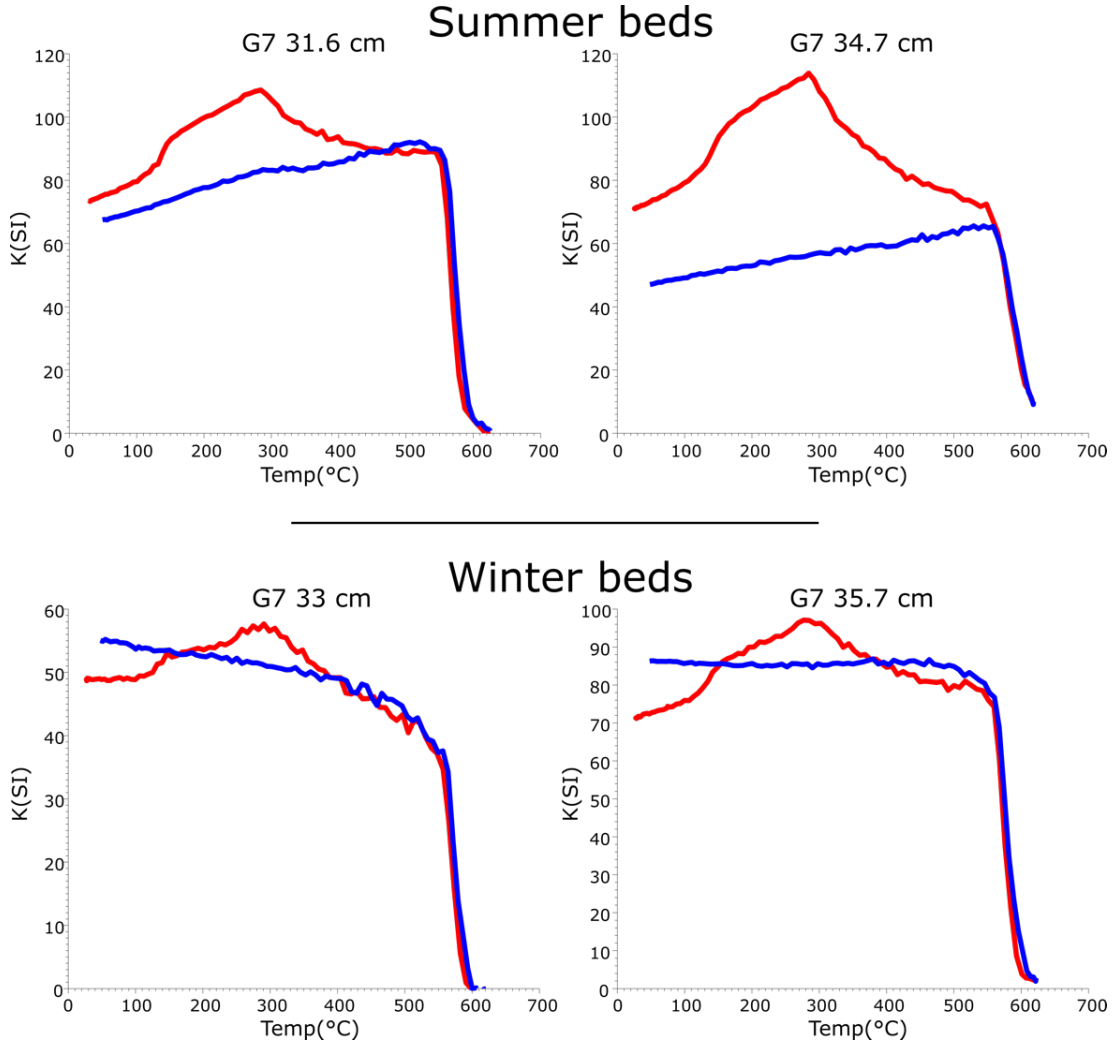


Figure 20: Thermomagnetic curves of low-field susceptibility versus temperature of two summer and two winter beds. Heating (resp. cooling) curves are shown in red (resp. in blue).

Typical demagnetization diagrams (Cogné, 2003) are shown in Figure 21 for two summer and two winter beds, respectively, while all others are displayed in supplementary material. No overprint, or viscous behaviour was detected. All samples are characterized by a univectorial component that was progressively demagnetized between the NRM and 140 mT. The large a.f. fields required to demagnetize these sediments are unusual, and likely reflect the presence of fine-grained magnetite. All characteristic directions were unambiguously defined by slightly curved lines that passes through the origin, with

maximum angular deviation (MAD) values generally lower than 1°. The stratigraphic evolution of declination and inclination are also plotted in Figure 18 for comparison with other parameters. Also, shown in pink color (Figure 18) are the directions derived from low-resolution U-channel measurements. As expected, the response curve of the magnetometer has considerably smoothed yearly variations that are resolved with discrete sample measurements.

The declinations of discrete samples oscillate between 240° and 265° and do not show any specific long-term trend. The amplitude of yearly variations can reach 30° within the upper 15 cm, while below this depth it does not exceed 10°. These 5 to 10° changes in declination can result from uncertainties such as those generated by sampling of very tiny specimens and/or whether they mainly reflect an influence of lithology and/or sediment matrix on the magnetic alignment. Declination was already successfully used to establish the chronostratigraphy of laminated glaciolacustrine sediments (Ridge et al. 1990) and, therefore, can be considered as reliable.

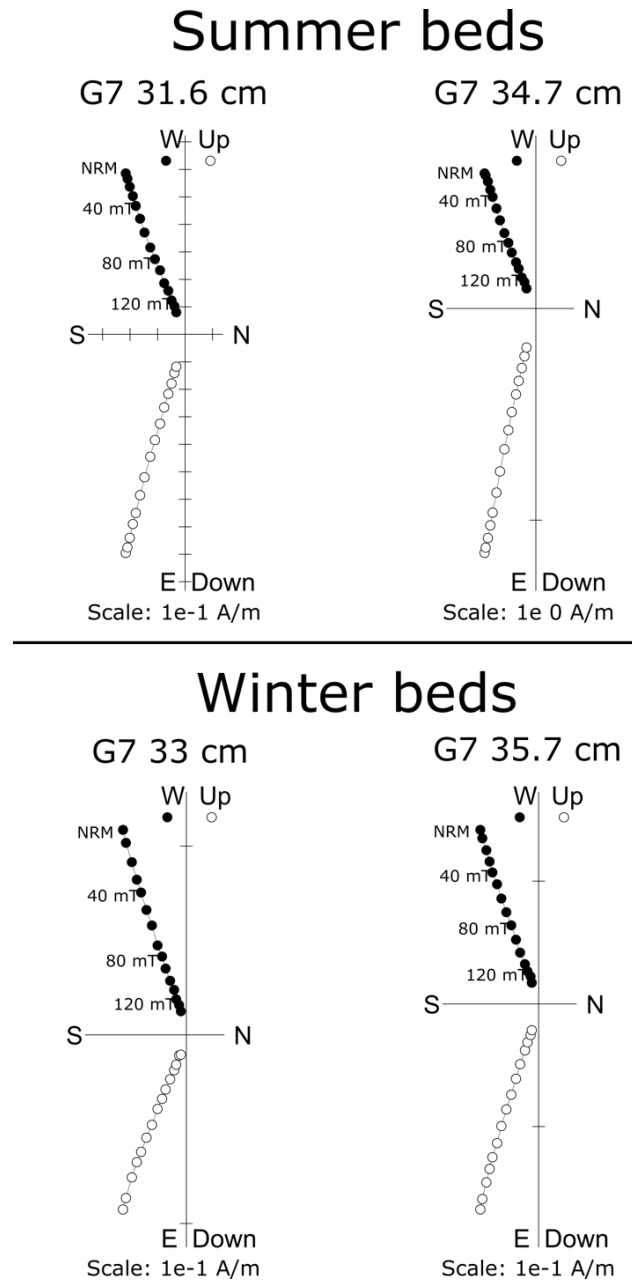


Figure 21: Demagnetization diagrams. Typical vector end-point diagrams for two summer and two winter beds. Solid symbols correspond to projections onto the horizontal plane, while open symbols represent projections onto the vertical plane.

Like declination, the amplitude of inclination variations reaches  $40^\circ$  in the upper part of the record, but is attenuated below 12-15 cm. Inclinations are significantly shallower than the  $67.2^\circ$  value predicted by the geocentric axial dipole (GAD) at this latitude

(Hospers, 1954). Given the short time interval (about 20 years) covered by the record, these variations cannot be representative of significant geomagnetic changes, although local non-dipole (ND) fields can generate some deviation. The ND present-day value could explain a deviation of about  $0.075^\circ \text{ a}^{-1}$  (Thébault et al., 2015), but non-dipole components can represent up to 20% of the dipole field and then yield deviations as high as  $15^\circ$ . These estimates are evidently amplified during periods of low dipole intensity. The current global determinations of paleointensity (Barletta et al., 2010) indicate that 8.5 ka cal BP ago (the age of these sediments), the dipole was about 10% weaker than present. This is not enough to account for  $30^\circ$  lower inclinations than the GAD inclination. Therefore, other factors, such as compaction, must be considered to explain the observed inclination shallowing.

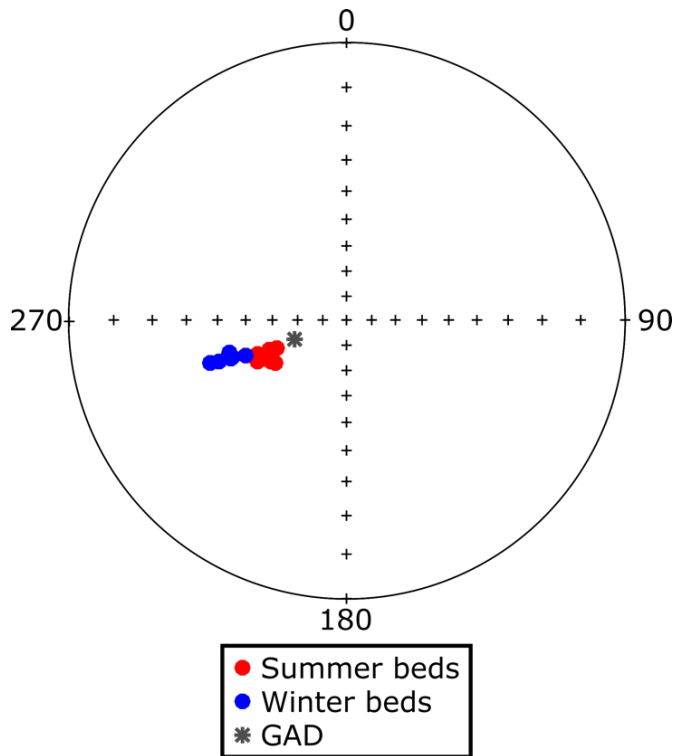


Figure 22: Stereoplot of the magnetic directions recorded by the 1-cm thick beds within the G7 interval. Red and blue dots indicate summer and winter beds, respectively. The present day-field direction is shown by an asterisk. The summer bed inclinations are closer to the geocentric axial dipole value at the site than the winter ones.

Given the millimetric size of the individual beds from the upper part of the sequence, we focused on the thickest layers interval between 48 cm and 31 cm which incorporates 7 summer beds and 6 winter beds (highlighted orange zone in Figure 18) and analysed each bed separately. The successive inclinations and declinations have been plotted as a function of depth in Figure 23 and have been combined in the stereographic projection of Figure 22. These detailed data reveal that the summer and winter beds display similar declinations (very low variation), but they also confirm that the winter inclinations ( $41.7^\circ \pm 4.3^\circ$ ) are  $13^\circ$  shallower than the summer ones ( $54.7^\circ \pm 3.3^\circ$ ). In addition, all values remain lower than the GAD inclination (Figure 23). But, if we take into consideration the geomagnetic field variability at the same latitude ( $50^\circ 10' N$ ) and at the same period (~9000 cal BP), the inclination is lower than the GAD and is approximately  $55^\circ$  (Stockhausen 1998, Barletta et al., 2010; Panovska et al. 2015). In reality, there is no inclination shallowing in the summer beds (Figure 23).

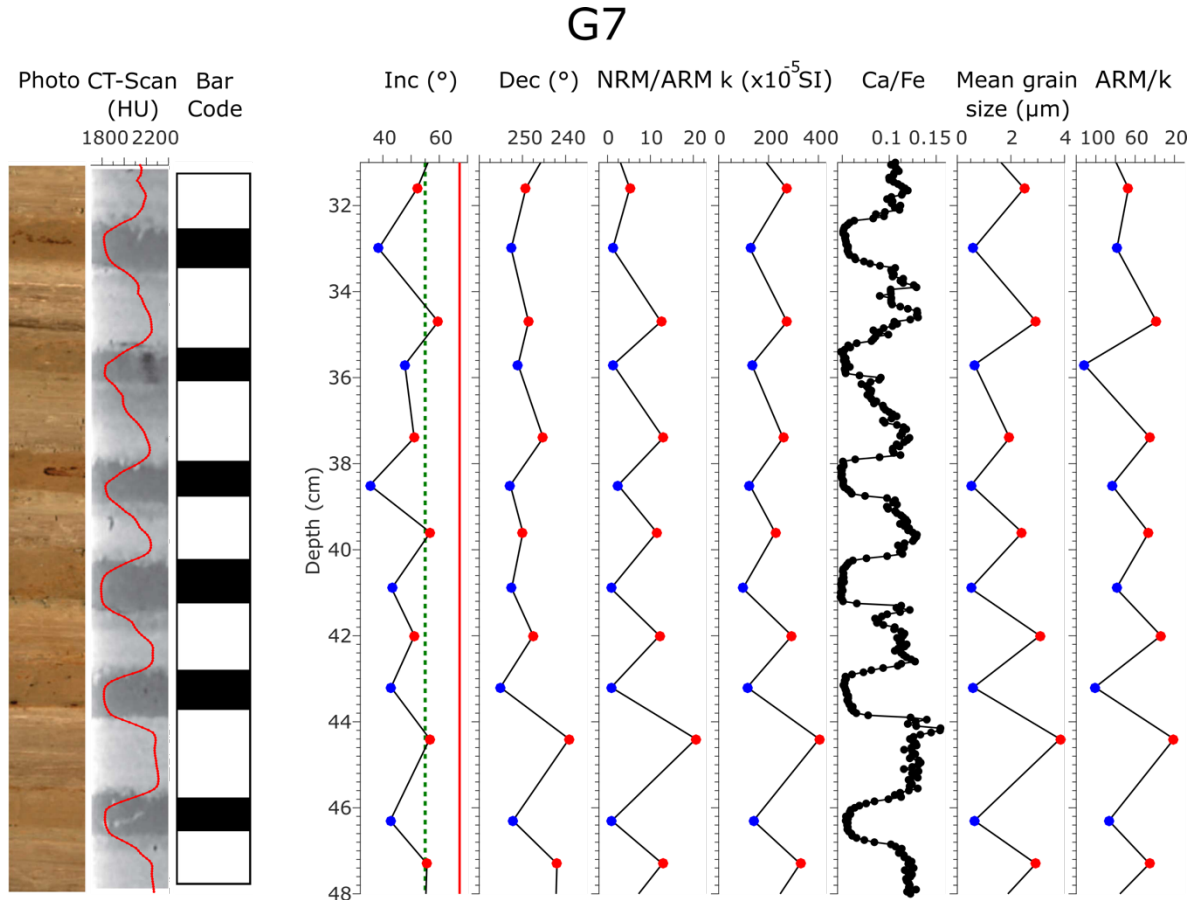


Figure 23: Magnetic and sedimentary properties for each individual 1-cm thick bed from the G7 core. Red and blue data points correspond to the summer and winter beds, respectively. Red line and green dashed line on inclination represent respectively the GAD value and the inclination value at the same latitude around 9000 cal BP.

The comparison between the downcore directional changes (Figure 23), the Ca/Fe ratios and the susceptibility variations confirm the observations drawn from the G7 sequence (Figure 18). The NRM/ARM ratio (ARM was induced in a 50  $\mu\text{T}$  DC field and a 60 mT AF peak field) complete the figure. Since no significant geomagnetic field intensity variation occurred during such a short period, this ratio tells us about changes of NRM acquisition efficiency. Lower values are systematically encountered for the winter beds. The NRM acquisition efficiency can be affected by the depositional environment (e.g. turbulence), the nature of the detrital material (and in particular the tendency to aggregate), and by the nature of the magnetic minerals (e.g. their magnetic moment). The latter

possibility has been investigated using the ratio between anhysteretic remanence (ARM) and low-field volume susceptibility ( $k$ ). This ratio has the advantage of being primarily sensitive to magnetite and thus avoids any bias that would be generated by subtle changes in magnetic mineralogy (Stoner and St-Onge, 2007). The ARM/ $k$  (Figure 23) ratio remarkably duplicates the pattern of the sedimentary grain size changes. The range of magnetic grain sizes was further constrained by Day plots (Day et al., 1977; Dunlop, 2002) (Figure 24). All samples are found within the pseudo-single domain (PSD) range (Dunlop, 2002), but the summer and winter beds define two separate clusters, which consistently with the ARM/ $k$  ratio, suggest magnetically finer winter beds.

To complete this observation and to have a better comprehension of the magnetic grains in winter and summer beds, first-order reversal curve (FORC) measurements (Roberts et al., 2000) of a summer bed at 39.6 cm and a winter bed at 40.9 cm were performed (Figure 25). The summer bed contains SD grains (Figure 25a) like the winter bed (Figure 25b), but contrary to the winter bed, the contribution of the central ridge (Figure 25c-e) is very small, with 2% of the remanent saturation against 10% for winter bed (Figure 25d-f). The distribution of coercivity in the summer beds is different, with a median destructive field of 20 mT and a maximum coercivity of 100 mT (Figure 25c), compared to the winter beds with a maximum destructive field of 0 mT and a maximum coercivity of 100 mT (Figure 25d). This result is typical for magnetic grains that are non-elongate with an irregular form for summer beds. This difference in coercivity can be explained by a variation of the mean magnetic grain size. Winter beds have a mean size under the lower limit of SD, i.e. that the majority of magnetic grains are superparamagnetic (SP) with a high coercivity (Figure 25b). This high coercivity can explain the position of the winter beds compared to summer beds in the day plot (Figure 24). To summaries, summer beds are coarser and composed by a mixture of SD and PSD with irregular forms, and winter beds are characterized by a mixture of superparamagnetic (SP) and single domain (SD) grains with a high coercivity.

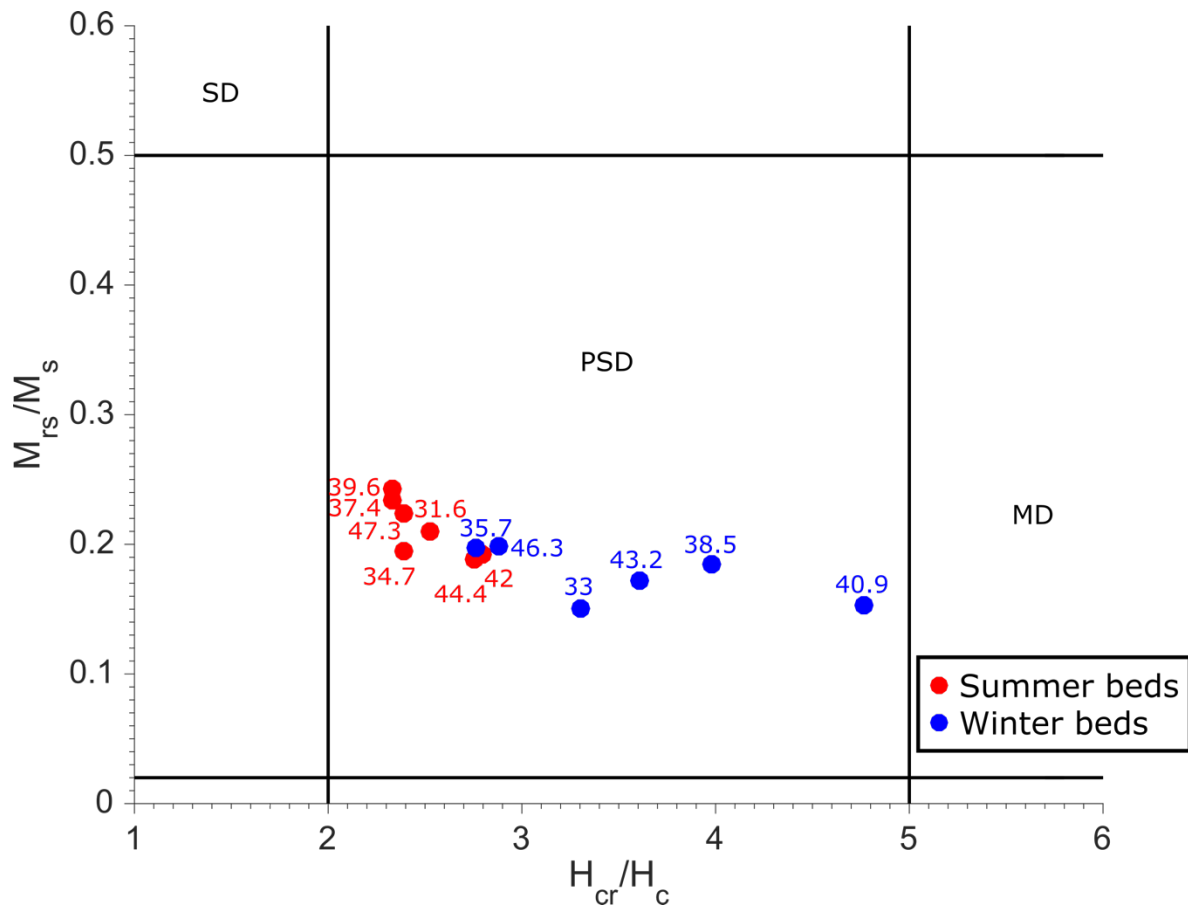


Figure 24: Day plot obtained for the 1-cm thick beds within the G7 core. Red (resp. blue) directions are for summer (resp. winter) beds. The orange star indicates the direction of the geocentric axial dipole at the site.

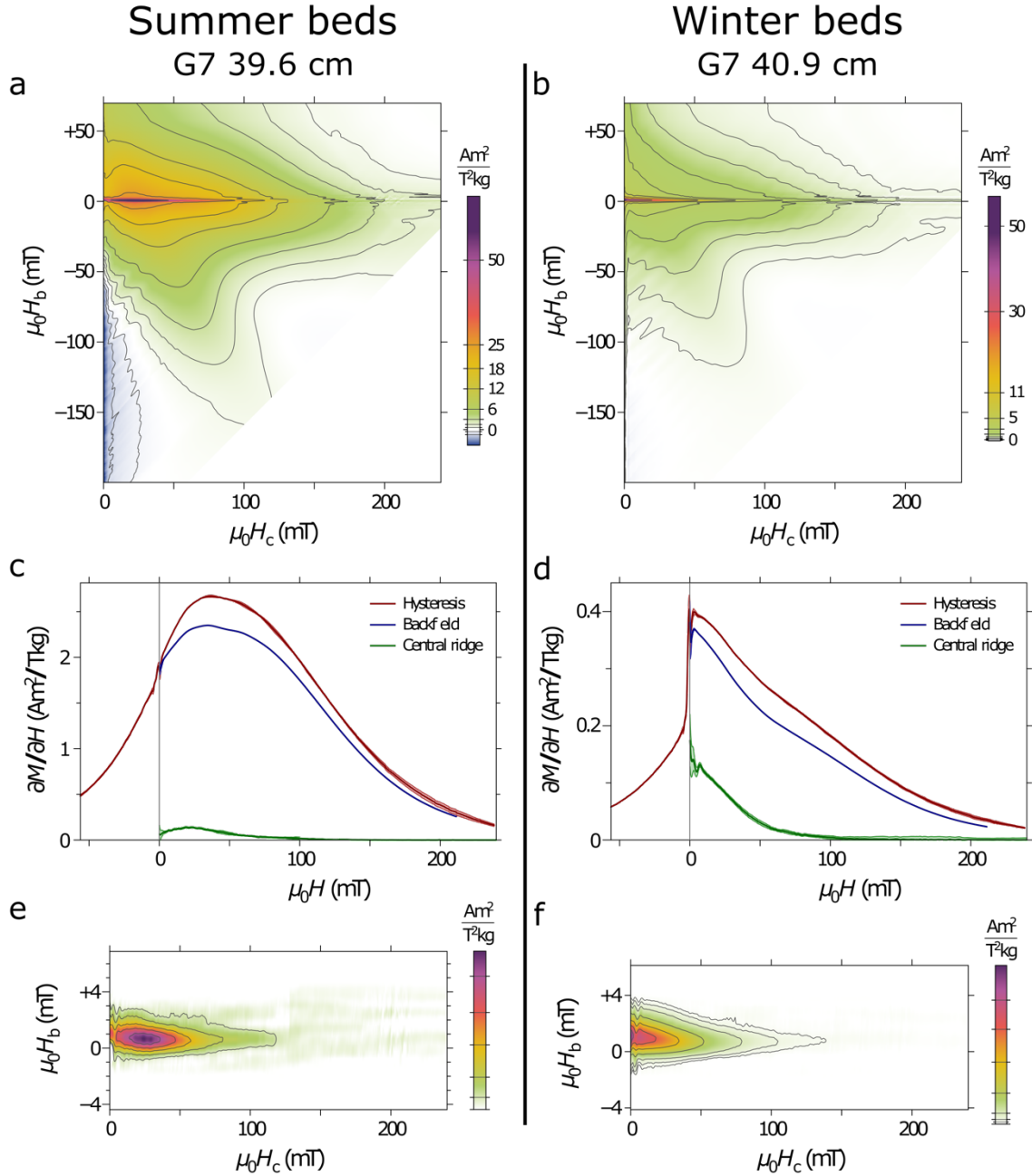


Figure 25: FORCs of the summer bed at 39.6 cm (a) and winter bed at 40.9 cm (b) in the G7 core. Backfield, hysteresis and central ridge coercivity distributions derived from the original FORC measurements for summer bed (c) and winter bed (d). FORC zoom of the central ridge isolate from the other contribution for summer bed (e) and winter bed (f). All diagrams have been generated using VARIFORC built-in functions (Egli, 2013).

The directions of the magnetic susceptibility ellipsoid axes are shown in Figure 26a, with  $k_1$  corresponding to  $k_{\max}$  and  $k_3$  to  $k_{\min}$ . The mean orientation of  $k_3$  is slightly more vertical in the winter beds than in the summer beds. The  $k_{\max}$  axes are nicely aligned along the north-south axis but are widely scattered in the winter beds. Two other plots are shown in Figure 26b and c to analyze the magnetic anisotropy. The Flinn diagram (Figure 26b) features lineation ( $k_1/k_2$ ) as a function of foliation ( $k_2/k_3$ ) (Jelinek, 1981, Cogné, 2003). The shape factor that provides information on the ellipsoid geometry is plotted in Figure 26c as a function of the corrected degree of anisotropy  $P'$  (Jelinek, 1981) which characterizes the deviation from a spherical shape. Both winter and summer beds are characterized by oblate anisotropy, with almost perfectly oblate summer beds and slightly more anisotropic winter beds. The elongated shape of the winter beds (Figure 26b-c) indicates additional compaction that may be related to their different lithology (Gravenor and Coyle, 1985) with lower carbonate (Figure 23) and therefore higher clay content.

To summarize, winter beds are thinner and finer (both physical and magnetic grain sizes) and characterized by a lower inclination, magnetic susceptibility, Ca/Fe ratio, and present a higher magnetic anisotropy than the summer beds.

## 2.7 DISCUSSION

Before discussing these results, it is useful to remind the processes involved in the formation of varved deposits. The large thickness of both summer and winter beds are related to the ice-proximal position of the Matagami varve sequence. High melting rates during summer resulted in an increased influx of coarse sediment particles rapidly reaching the bottom of the lake, while during winter reduced turbidity caused by the ice-cover yielded the deposition of the finer (clay) particles forming the winter beds (e.g. Smith and Ashley, 1985). Interestingly, magnetic granulometry behaves the same way with larger magnetic grains being observed within the summer beds.

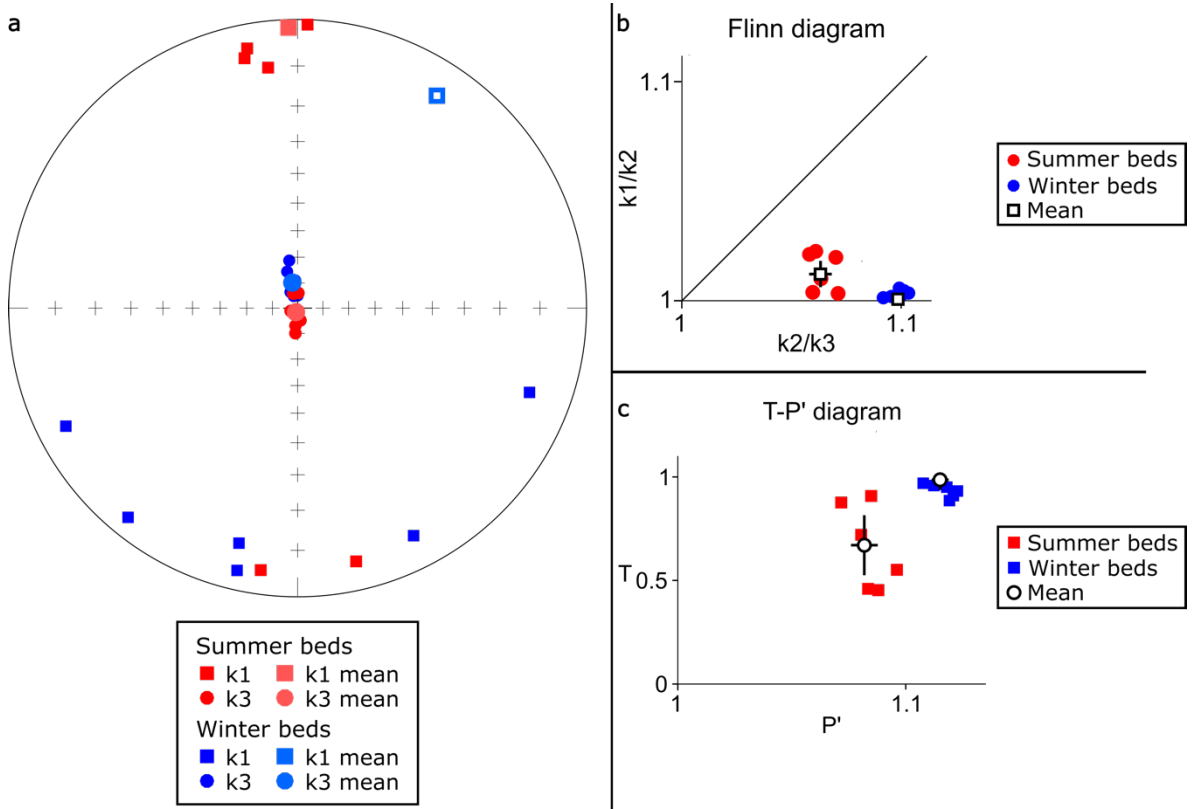


Figure 26: (a) Stereographic projection of the  $k_1$  and  $k_3$  axes of the magnetic susceptibility ellipsoid. (b) Flinn diagram,  $k_1/k_2$  represents the lineation and  $k_2/k_3$  the foliation. (c) T-P' diagram showing the shape factor  $T = (2\log k_2 - \log k_1 - \log k_3)/(\log k_1 - \log k_3)$  as a function of the corrected degree of anisotropy  $P' = \exp(\sqrt{2[\{\eta_1 - \eta\}^2 + \{\eta_2 - \eta\}^2 + \{\eta_3 - \eta\}^2]})$  with  $\eta_i = \ln(k_i)_{i=1,2,3}$  and  $\eta = (\eta_1 + \eta_2 + \eta_3)/3$  (Jelinek, 1981). Red and blue dots indicate summer and winter beds, respectively.

The aim of this study is to have a better comprehension of NRM acquisition mechanisms. Some parameters were previously identified to have an impact on NRM acquisition, and more particularly on orientation (Anson and Kodama, 1987; Arason and Levi, 1990; Tauxe, 1993; Katari and Bloxham, 2001; Tauxe et al., 2006; Shcherbakov and Sycheva, 2010; Roberts et al., 2013; Tanty et al., 2016). The first parameter, and the most important, is variations of the geomagnetic field. For example, an excursion or inversion can create an important variation. Similarly, paleomagnetic secular variations can create significant variations. The second parameter that can influence the NRM and the inclination is the magnetic mineral that is magnetized. The most important magnetic mineral for

paleomagnetic study is magnetite that is in the SD or PSD range (Dunlop, 2002), as these grains can record a strong and stable magnetization. One more possible parameter would be an important concentration of organic matter in the sediments as it can facilitate sulfate reduction diagenesis and affects the magnetic properties and create a chemical remanent magnetization (CRM) (e.g., Thompson and Oldfield, 1986). Then, the rapid deposition of sediments such as in turbidites can also create a shallowing, and this shallowing depends on the size of the event (Tanty et al., 2016), while bioturbation can resuspend and reflocculate sediments, also changing the initial magnetisation (Tauxe, 1993; Tauxe et al., 2006). Finally, substantial inclination shallowing in sediments can be caused by compaction (Anson and Kodama, 1987; Arason and Levi, 1990).

In this study, a  $13^\circ$  inclination shallowing is observed in winter beds, with no shallowing in summer beds. In addition, winter beds are associated with lower NRM/ARM ratios (Figure 23), which, given the absence of geomagnetic intensity changes during a year (varved sediments), reflects a poorer magnetic recording of the geomagnetic field than in summer beds. Moreover, the timescale of the varved sequence seen in Figure 23 (< 7 years) excludes any paleomagnetic significant secular variations. Variations in grain size exist between the winter and summer beds, but those variations are too small to explain the differences in inclination, while the absence of organic matter (less than 0.25% on average) does not favor diagenetic processes and suggests that no CRM has occurred. Moreover, diagenesis is not supported by the strong and stable NRM that is carried by SD to PSD magnetite grains. However, the Fe/k ratio is more important in winter beds ( $49.06 \pm 2.05$  Mcps) than in summer beds ( $10.77 \pm 1.83$  Mcps). Those values, above 40 Mcps, may suggest a possible influence of diagenesis on the acquisition of the NRM in winter beds (Hofmann et al., 2005; Hofmann and Fabian, 2009). According to Tanty et al. (2016), a turbidite of 47 cm is necessary to create a  $13^\circ$  inclination shallowing. However, the average thickness of the observed winter and summer beds in the G7 sample (Figure 23) are only  $1.76 \pm 0.21$  cm and  $0.9 \pm 0.1$  cm respectively and are not turbidites. Results of the magnetic anisotropy show a higher magnetic anisotropy of winter beds compared to summer beds. This difference of anisotropy can indicate that winter beds are more compacted than

summer beds (Figure 26, Sun and Kodama, 1992). However, FORC measurements indicate that summer beds are characterized by magnetic grains that do not present an elongated form, also contributing to the fact that summer beds show less magnetic anisotropy (Hrouda, 1982). The CT number variations (Figure 23) reflect the density (e.g., Boespflug et al. 1995; St-Onge et al. 2007) between the winter and summer beds. Summer beds are denser and thicker than winter beds. Those variations could lead to a differential compaction, where winter beds are composed of finer grains that are compacted by thicker and coarser summer beds. This is illustrated in Figure 27 where the thickness of the upper summer bed seems to have a direct effect on the inclination shallowing of the winter beds. Finally, the preservation of the varves and absence of traces of bioturbation in the photographs, CT scans and thin-section photographs exclude bioturbation as a possible cause of remagnetization

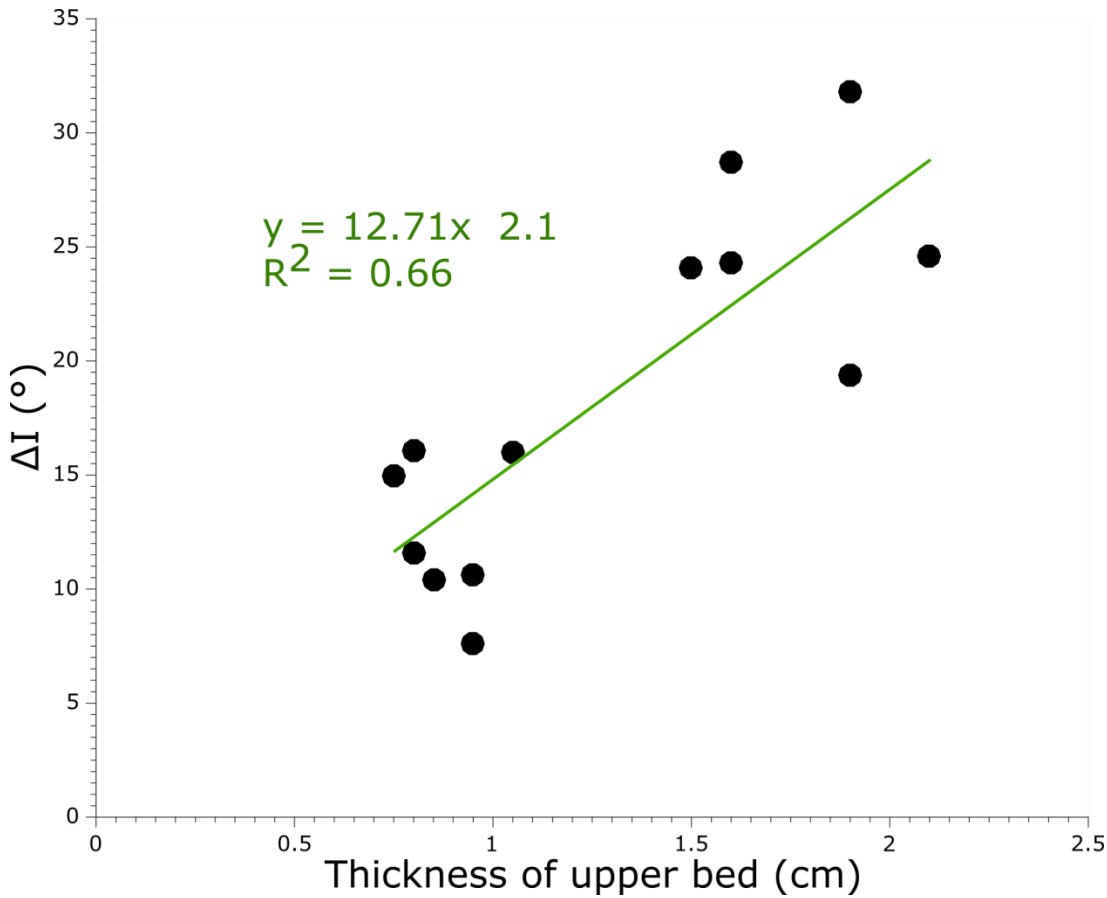


Figure 27: Inclination deviation relative to the GAD as a function of the thickness of upper bed. A linear regression is plotted in green.

This differential compaction cannot however explain the NRM/ARM variations observed (Figure 23). In this present study, the dominant magnetic carrier is a mixture of SD and PSD magnetite grains for summer beds and SP and SD grains for winter beds, which is optimal to record geomagnetic field changes. The SD and PSD grains of the summer beds are more stable ( $M_{rs}=0.32 \text{ Am}^2/\text{kg}$ ) compared to winter beds which are composed of fine SP and SD grains ( $M_{rs}=0.033 \text{ Am}^2/\text{kg}$ ). By looking at a simple model (Tauxe et al., 2006), we can see that those variations imply that summer beds are more saturated than winter beds, and that the direction of summer beds are relatively closer to the expected field than in the winter beds. This hypothesis is coherent with the variations observed in inclinations and NRM/ARM (Figure 23), with no shallowing and higher values

respectively for summer beds. In brief, there are important variations of inclination, NRM/ARM and much smaller variations of declination between summer and winter beds with no changes in terms of magnetic mineral (Figure 28). Those observations are the combination of two different mechanisms: compaction and magnetic grain composition.

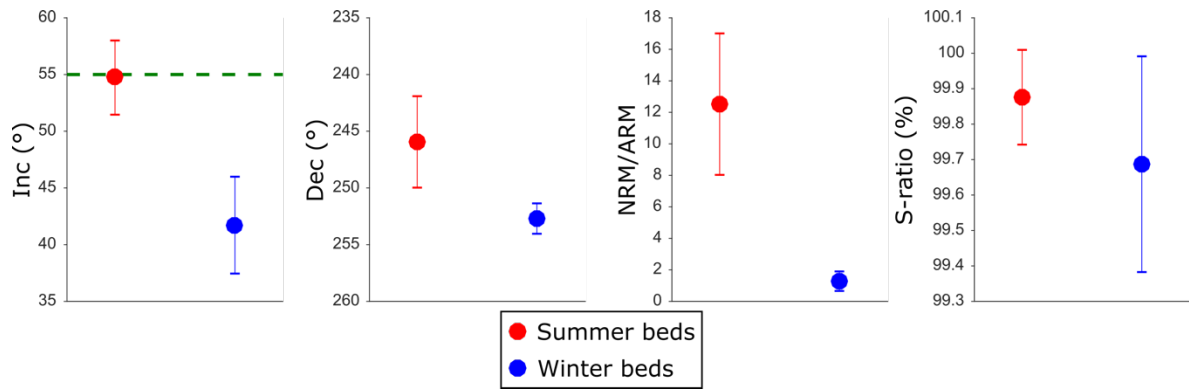


Figure 28: Mean of inclination, declination, NRM/ARM and S-ratio recorded by the 1-cm thick beds within the G7 interval. Red and blue dots indicate summer and winter beds, respectively. Green dashed line on inclination represents the inclination value at the same latitude around 9000 cal BP.

## 2.8 CONCLUSIONS

The varves of former glacial Lake Ojibway provide important information on the stable magnetic field associated with the deposition of detrital sediments in a large and natural depositional basin. Preservation of centimeter-thick varves allowed us to investigate the magnetic properties of winter and summer beds separately by using small  $1 \text{ cm}^3$  sample cubes for magnetic measurements. A dominant feature is that, despite the presence of finer grains, the inclinations in the winter beds are shallower. These changes were likely caused by the differential compaction and composition of magnetic grains between summer and winter beds, as well as diagenesis. This study points out the role of small variations of magnetic grain composition and lithological changes on the acquisition of paleomagnetic records.

## 2.9 ACKNOWLEDGMENTS

This research was funded by the Natural Sciences and Engineering Research Council of Canada (NSERC) Discovery grants to GSO and PF. Thanks to Fatoumata Camara at IPGP for her help for sampling and measurement. Many thanks to Laure Meynadier and France Lagroix at IPGP for their various advices. We also thank Geotop for its financial support through a scholarship to the first author.

## 2.10 REFERENCES

- Anson, G. L., & Kodama, K. P. (1987). Compaction-induced inclination shallowing of the post-depositional remanent magnetization in a synthetic sediment. *Geophysical Journal International*, 88(3), 673–692. <https://doi.org/10.1111/j.1365-246X.1987.tb01651.x>
- Antevs, E. (1925). Retreat of the Last Ice-Sheet from Eastern Canada. *Journal of Geology*, 34, 188–188.
- Antevs, E. (1928). The last glaciation: with special reference to the ice retreat in northeastern North America. *Geographical Society*, 17
- Arason, P., & Levi, S. (1990). Compaction and inclination shallowing in deep-sea sediments from the Pacific Ocean. *Journal of Geophysical Research: Solid Earth*, 95(B4), 4501–4510. <https://doi.org/10.1029/JB095iB04p04501>
- Barletta, F., St-Onge, G., Stoner, J. S., Lajeunesse, P., & Locat, J. (2010). A high-resolution Holocene paleomagnetic secular variation and relative paleointensity stack from eastern Canada. *Earth and Planetary Science Letters*, 298(1–2), 162–174. <https://doi.org/10.1016/j.epsl.2010.07.038>
- Bloemendal, J., King, J. W., Hall, F. R., & Doh, S.-J. (1992). Rock magnetism of Late Neogene and Pleistocene deep-sea sediments: Relationship to sediment source,

- diagenetic processes, and sediment lithology. *Journal of Geophysical Research: Solid Earth*, 97(B4), 4361–4375.
- Boespflug, X., Long, B. F. N., & Occhietti, S. (1995). CAT-scan in marine stratigraphy: a quantitative approach. *Marine Geology*, 122(4), 281–301.
- Breckenridge, A., Lowell, T. V., Stroup, J. S., & Evans, G. (2012). A review and analysis of varve thickness records from glacial Lake Ojibway (Ontario and Quebec, Canada). *Quaternary International*, 260, 43–54.
- Brooks, G. R. (2018). Thickness Records of Glacial Lake Ojibway Varves from Duparquet and Dufresnoy Lakes, Northwestern Quebec. Geological Survey of Canada.
- Clarke, G. K., Leverington, D. W., Teller, J. T., & Dyke, A. S. (2004). Paleohydraulics of the last outburst flood from glacial Lake Agassiz and the 8200BP cold event. *Quaternary Science Reviews*, 23(3), 389–407.
- Cogné, J. P. (2003). PaleoMac: a Macintosh™ application for treating paleomagnetic data and making plate reconstructions. *Geochemistry, Geophysics, Geosystems*, 4(1). <https://doi.org/10.1029/2001GC000227>
- Coleman, A. P. (1909). *Lake Ojibway, last of the great glacial lakes*. Bureau des mines.
- Crémer, J.-F., Long, B., Desrosiers, G., Montety, L. de, & Locat, J. (2002). Application de la scanographie à l'étude de la densité des sédiments et à la caractérisation des structures sédimentaires: exemple des sédiments déposés dans la rivière Saguenay (Québec, Canada) après la crue de juillet 1996. *Canadian Geotechnical Journal*, 39(2), 440–450.
- Croudace, I. W., Rindby, A., & Rothwell, R. G. (2006). ITRAX: description and evaluation of a new multi-function X-ray core scanner. *Geological Society, London, Special Publications*, 267(1), 51–63. <https://doi.org/10.1144/GSL.SP.2006.267.01.04>
- Day, R., Fuller, M., & Schmidt, V. A. (1977). Hysteresis properties of titanomagnetites: grain-size and compositional dependence. *Physics of the Earth and Planetary Interiors*, 13(4), 260–267.

- Dunlop, D. J. (2002). Theory and application of the Day plot (Mrs/Ms versus Hcr/Hc) 1. Theoretical curves and tests using titanomagnetite data. *Journal of Geophysical Research: Solid Earth*, 107(B3). <https://doi.org/10.1029/2001JB000486>
- Dyke, A., & Prest, V. (1987). Late Wisconsinan and Holocene History of the Laurentide Ice Sheet\*. *Géographie Physique et Quaternaire*, 41(2), 237–263. <https://doi.org/10.7202/032681ar>
- Dyke, A. S. (2004). An outline of North American deglaciation with emphasis on central and northern Canada. *Developments in Quaternary Sciences*, 2, 373–424. [https://doi.org/10.1016/S1571-0866\(04\)80209-4](https://doi.org/10.1016/S1571-0866(04)80209-4)
- Elson, J. A. (1967). Geology of glacial Lake Agassiz. *Life, Land and Water. University of Manitoba Press, Winnipeg*, 37–96.
- Egli, R. (2013). VARIFORC: An optimized protocol for calculating non-regular first-order reversal curve (FORC) diagrams. *Global and Planetary Change*, 110, 302–320. <https://doi.org/10.1016/j.gloplacha.2013.08.003>
- Fortin, D., Francus, P., Gebhardt, A. C., Hahn, A., Kliem, P., Lisé-Pronovost, A., et al. (2013). Destructive and non-destructive density determination: method comparison and evaluation from the Laguna Potrok Aike sedimentary record. *Quaternary Science Reviews*, 71, 147–153. <https://doi.org/10.1016/j.quascirev.2012.08.024>
- Francus, P., & Cosby, C. A. (2001). Sub-sampling unconsolidated sediments: A solution for the preparation of undisturbed thin-sections from clay-rich sediments. *Journal of Paleolimnology*, 26(3), 323–326. <https://doi.org/10.1023/A:1017572602692>
- Francus, P., Bradley, R. S., Abbott, M. B., Patridge, W., & Keimig, F. (2002). Paleoclimate studies of minerogenic sediments using annually resolved textural parameters. *Geophysical Research Letters*, 29(20), 1998. <https://doi.org/10.1029/2002GL015082>
- Gravenor, C. P., & Coyle, D. A. (1985). Origin and magnetic fabric of glacial varves, Nottawasaga River, Ontario, Canada. *Canadian Journal of Earth Sciences*, 22(2), 291–294. <https://doi.org/10.1139/e85-025>

- Hardy, L. (1976). Contribution à l'étude géomorphologique de la portion québécoise des basses terres de la baie de James, *thèse de doctorat non publiée*, Université McGill.
- Hofmann, D. I., & Fabian, K. (2009). Correcting relative paleointensity records for variations in sediment composition: Results from a South Atlantic stratigraphic network. *Earth and Planetary Science Letters*, 284(1), 34–43.  
<https://doi.org/10.1016/j.epsl.2009.03.043>
- Hofmann, D. I., Fabian, K., Schmieder, F., Donner, B., & Bleil, U. (2005). A stratigraphic network across the Subtropical Front in the central South Atlantic: Multi-parameter correlation of magnetic susceptibility, density, X-ray fluorescence and  $\delta^{18}\text{O}$  records. *Earth and Planetary Science Letters*, 240(3), 694–709.  
<https://doi.org/10.1016/j.epsl.2005.09.048>
- Hospers, J. (1954). Rock Magnetism and Polar Wandering. *Nature*, 173(4416), 1183–1184.  
<https://doi.org/10.1038/1731183a0>
- Hrouda, F. (1982). Magnetic anisotropy of rocks and its application in geology and geophysics. *Geophysical Surveys*, 5(1), 37–82. <https://doi.org/10.1007/BF01450244>
- Jelinek, V. (1981). Characterization of the magnetic fabric of rocks. *Tectonophysics*, 79(3), T63–T67. [https://doi.org/10.1016/0040-1951\(81\)90110-4](https://doi.org/10.1016/0040-1951(81)90110-4)
- Katari, K., Tauxe, L., & King, J. (2000). A reassessment of post-depositional remanent magnetism: preliminary experiments with natural sediments. *Earth and Planetary Science Letters*, 183(1), 147–160.
- Katari, K., Kaushik, S., & Bloxham, J. (2001). Effects of sediment aggregate size on DRM intensity: a new theory. *Earth and Planetary Science Letters*, 186(1), 113–122.
- Lajeunesse, P., & St-Onge, G. (2008). The subglacial origin of the Lake Agassiz-Ojibway final outburst flood. *Nature Geoscience*, 1(3), 184–188.  
<http://dx.doi.org/10.1038/ngeo130>
- Leverington, D. W., Mann, J. D., & Teller, J. T. (2002). Changes in the Bathymetry and Volume of Glacial Lake Agassiz between 9200 and 7700  $^{14}\text{C}$  yr BP. *Quaternary Research*, 57(2), 244–252. <https://doi.org/10.1006/qres.2001.2311>

- Mellström, A., Nilsson, A., Stanton, T., Muscheler, R., Snowball, I., & Suttie, N. (2015). Post-depositional remanent magnetization lock-in depth in precisely dated varved sediments assessed by archaeomagnetic field models. *Earth and Planetary Science Letters*, 410, 186–196. <https://doi.org/10.1016/j.epsl.2014.11.016>
- Moskowitz, B. M. (1991). Hitchhiker's guide to magnetism. In *Environmental Magnetism Workshop (IRM)* (Vol. 279, p. 48).
- Nagata, T. (1961). Rock Magnetism, 350 pp. *Maruzen, Tokyo*.
- Nilsson, A., Suttie, N., & Hill, M. J. (2018). Short-Term Magnetic Field Variations From the Post-depositional Remanence of Lake Sediments. *Frontiers in Earth Science*, 6. <https://doi.org/10.3389/feart.2018.00039>
- Panovska, S., Korte, M., Finlay, C. C., & Constable, C. G. (2015). Limitations in paleomagnetic data and modelling techniques and their impact on Holocene geomagnetic field models. *Geophysical Journal International*, 202(1), 402–418. <https://doi.org/10.1093/gji/ggv137>
- Ridge, J. C., Brennan, W. J., & Muller, E. H. (1990). The use of paleomagnetic declination to test correlations of late Wisconsinan glaciolacustrine sediments in central New York. *GSA Bulletin*, 102(1), 26–44. [https://doi.org/10.1130/0016-7606\(1990\)102<0026:TUOPDT>2.3.CO;2](https://doi.org/10.1130/0016-7606(1990)102<0026:TUOPDT>2.3.CO;2)
- Roberts, A. P., Pike, C. R., & Verosub, K. L. (2000). First-order reversal curve diagrams: A new tool for characterizing the magnetic properties of natural samples. *Journal of Geophysical Research: Solid Earth*, 105(B12), 28461–28475. <https://doi.org/10.1029/2000JB900326>
- Roberts, A. P., Tauxe, L., & Heslop, D. (2013). Magnetic paleointensity stratigraphy and high-resolution Quaternary geochronology: successes and future challenges. *Quaternary Science Reviews*, 61, 1–16.
- Rothwell, R. G., Hoogakker, B., Thomson, J., Croudace, I. W., & Frenz, M. (2006). Turbidite emplacement on the southern Balearic Abyssal Plain (western Mediterranean Sea) during Marine Isotope Stages 1–3: an application of ITRAX XRF scanning of sediment cores to lithostratigraphic analysis. *Geological Society,*

- London, Special Publications*, 267(1), 79–98.  
<https://doi.org/10.1144/GSL.SP.2006.267.01.06>
- Roy, M., Dell’Oste, F., Veillette, J. J., de Vernal, A., Hélie, J.-F., & Parent, M. (2011). Insights on the events surrounding the final drainage of Lake Ojibway based on James Bay stratigraphic sequences. *Quaternary Science Reviews*, 30(5), 682–692.
- Roy, Martin, Veillette, J. J., Daubois, V., & Ménard, M. (2015). Late-stage phases of glacial Lake Ojibway in the central Abitibi region, eastern Canada. *Geomorphology*, 248, 14–23.
- Shcherbakov, V., & Sycheva, N. (2010). On the mechanism of formation of depositional remanent magnetization. *Geochemistry, Geophysics, Geosystems*, 11(2). Q02Z13.  
<https://doi.org/10.1029/2009GC002830>
- Shoemaker, E. M. (1992). Water sheet outburst floods from the Laurentide Ice Sheet. *Canadian Journal of Earth Sciences*, 29(6), 1250–1264.  
<https://doi.org/10.1139/e92-100>
- Smith, N. D., & Ashley, G. (1985). Proglacial Lacustrine Environment. *Society of Economic Paleontologists and Mineralogists, Short Course* 16, 135 -216.
- Spassov, S., & Valet, J.-P. (2012). Detrital magnetizations from redeposition experiments of different natural sediments. *Earth and Planetary Science Letters*, 351, 147–157.
- Stockhausen, H. (1998). Geomagnetic palaeosecular variation (0–13 000 yr BP) as recorded in sediments from three maar lakes from the West Eifel (Germany). *Geophysical Journal International*, 135(3), 898–910. <https://doi.org/10.1046/j.1365-246X.1998.00664.x>
- Stoner, J. S., & St-Onge, G. (2007). Chapter Three Magnetic Stratigraphy in Paleoceanography: Reversals, Excursions, Paleointensity, and Secular Variation. In Hillaire-Marcel, C., De Vernal, A. (Eds.), *Developments in Marine Geology, Proxies in Late Cenozoic Paleoceanography* (Vol. 1, pp. 99–138). Elsevier.  
[https://doi.org/10.1016/S1572-5480\(07\)01008-1](https://doi.org/10.1016/S1572-5480(07)01008-1)

- Stroup, J. S., Lowell, T. V., & Breckenridge, A. (2013). A model for the demise of large, glacial Lake Ojibway, Ontario and Quebec. *Journal of Paleolimnology*, 50(1), 105–121. <https://doi.org/10.1007/s10933-013-9707-9>
- St-Onge, G., Mulder, T., Francus, P., & Long, B. (2007). Chapter Two Continuous Physical Properties of Cored Marine Sediments. In Hillaire-Marcel, C., De Vernal, A. (Eds.), *Developments in Marine Geology, Proxies in Late Cenozoic Paleoceanography* (Vol. 1, pp. 63–98). Elsevier. [https://doi.org/10.1016/S1572-5480\(07\)01007-X](https://doi.org/10.1016/S1572-5480(07)01007-X)
- Striberger, J., Björck, S., Ingólfsson, Ó., Kjær, K. H., Snowball, I., & Uvo, C. B. (2011). Climate variability and glacial processes in eastern Iceland during the past 700 years based on varved lake sediments. *Boreas*, 40(1), 28–45. <https://doi.org/10.1111/j.1502-3885.2010.00153.x>
- Sun, W. W., & Kodama, K. P. (1992). Magnetic anisotropy, scanning electron microscopy, and X ray pole figure goniometry study of inclination shallowing in a compacting clay-rich sediment. *Journal of Geophysical Research: Solid Earth*, 97(B13), 19599–19615. <https://doi.org/10.1029/92JB01589>
- Tanty, C., Valet, J.-P., Carlut, J., Bassinot, F., & Zaragosi, S. (2016). Acquisition of detrital magnetization in four turbidites. *Geochemistry, Geophysics, Geosystems*, 17(8), 3207–3223. <https://doi.org/10.1002/2016GC006378>
- Tauxe, L. (1993). Sedimentary records of relative paleointensity of the geomagnetic field: theory and practice. *Reviews of Geophysics*, 31(3), 319–354.
- Tauxe, L., Steindorf, J. L., & Harris, A. (2006). Depositional remanent magnetization: toward an improved theoretical and experimental foundation. *Earth and Planetary Science Letters*, 244(3), 515–529.
- Teller, J. T., Leverington, D. W., & Mann, J. D. (2002). Freshwater outbursts to the oceans from glacial Lake Agassiz and their role in climate change during the last deglaciation. *Quaternary Science Reviews*, 21(8–9), 879–887. [https://doi.org/10.1016/S0277-3791\(01\)00145-7](https://doi.org/10.1016/S0277-3791(01)00145-7)

- Thébault, E., Finlay, C.C., Beggan, C.D., Alken, P., Aubert, J., Barrois, O., Bertrand, F., Bondar, T., Boness, A., Brocco, L., Canet, E., Chambodut, A., Chulliat, A., Coïsson, P., Civet, F., Du, A., Fournier, A., Fratter, I., Gillet, N., Hamilton, B., Hamoudi, M., Hulot, G., Jager, T., Korte, M., Kuang, W., Lalanne, X., Langlais, B., Léger, J.-M., Lesur, V., Lowes, F.J., Macmillan, S., Mandea, M., Manoj, C., Maus, S., Olsen, N., Petrov, V., Ridley, V., Rother, M., Sabaka, T.J., Saturnino, D., Schachtschneider, R., Sirol, O., Tangborn, A., Thomson, A., Tøffner-Clausen, L., Vigneron, P., Wardinski, I., Zvereva, T. (2015). International Geomagnetic Reference Field: the 12th generation. *Earth, Planets and Space*, 67, 79. <https://doi.org/10.1186/s40623-015-0228-9>
- Thompson, R., & Oldfield, F. (1986). Chapter Four Environmental magnetism. *London: Allen and Unwin*, 21-38.
- Valet, J.-P., Tanty, C., & Carlut, J. (2017). Detrital magnetization of laboratory-redeposited sediments. *Geophysical Journal International*, 210(1), 34–41. <https://doi.org/10.1093/gji/ggx139>
- Veillette, J. J. (1994). Evolution and paleohydrology of glacial Lakes Barlow and Ojibway. *Quaternary Science Reviews*, 13(9), 945–971. [https://doi.org/10.1016/0277-3791\(94\)90010-8](https://doi.org/10.1016/0277-3791(94)90010-8)
- Yoshida, S., & Katsura, I. (1985). Characterization of fine magnetic grains in sediments by the suspension method. *Geophysical Journal International*, 82(2), 301–317. <https://doi.org/10.1111/j.1365-246X.1985.tb05139.x>



## CHAPITRE 3

# IMPACT DE LA TURBULENCE SUR L'ALIGNEMENT MAGNÉTIQUE DANS LES SÉDIMENTS

### 3.1 RÉSUMÉ EN FRANÇAIS DU TROISIÈME ARTICLE

Les couches de dépôts rapides (RDL) telles que les turbidites ou les hyperpycnites, sont principalement étudiées pour leurs propriétés sédimentaires, mais sont soigneusement évitées dans les études paléomagnétiques en raison des perturbations causées par une telle accumulation soudaine et rapide de sédiments. Par conséquent, ces couches peuvent également être considérées comme des indicateurs potentiels de paramètres sédimentaires susceptibles d'affecter l'alignement des grains magnétiques et, finalement, l'acquisition de l'aimantation rémanente naturelle (NRM). Nous avons compilé 13 RDL de l'Holocène à partir de la carotte MD99-2222 dans le fjord du Saguenay (St-Onge et al., 2004) avec des épaisseurs variables (de 7,1 cm à 1510 cm) et 4 turbidites du Quaternaire d'origines différentes afin de documenter l'influence des paramètres sédimentaires et magnétiques sur l'acquisition de la NRM. Nous avons trouvé une relation logarithmique entre l'amplitude des variations d'inclinaison, ainsi que l'amplitude des tailles de grains magnétiques et l'épaisseur des RDL. L'inclinaison et la taille des grains sont elles-mêmes corrélées les unes aux autres par une loi logarithmique. Comme il n'y a pas de relation entre l'écart d'inclinaison et la profondeur, la compaction ne peut expliquer à lui seul des écarts aussi importants. La flocculation varie probablement avec la taille des grains, mais encore une fois, l'amplitude des écarts d'inclinaison est difficile à expliquer. La turbulence inhérente au processus de dépôt de tels événements est probablement le facteur dominant. Cette interprétation est appuyée par des calculs visant à décrire l'impact des courants de fond.

Cet article, intitulé « *Impact of turbulence on magnetic alignment in sediments* », fut corédigé par moi-même ainsi que par mes deux directeurs Jean-Pierre Valet (IPGP) et Guillaume St-Onge (UQAR-ISMER). Ramon Egli, chercheur du *Central Institute for Meteorology and Geodynamics*, a aussi contribué à la rédaction de cet article notamment sur la partie modélisation. Le manuscrit sera soumis prochainement après la publication du modèle numérique, à la revue *Geochemistry, Geophysics, Geosystems*.

Une version abrégée de cet article a été présentée sous forme d'affiche au congrès des doctorants de l'IPGP qui s'est déroulé à Paris (France) en 2016 ainsi qu'au congrès de l'*European Geophysical Union* qui s'est déroulé à Vienne (Autriche) en 2016.

### **3.2 IMPACT OF TURBULENCE ON MAGNETIC ALIGNEMENT IN SEDIMENTS**

Rapid deposit layers (RDL) such as turbidites or hyperpycnites are mostly studied for their sedimentological properties, but are carefully avoided in paleomagnetic studies due to the disturbances caused by such sudden and rapid sediment accumulation. Therefore, these layers can also be seen as potential indicators of sediment parameters susceptible of affecting the alignment of magnetic grains and ultimately the acquisition of the natural remanent magnetization (NRM). We have compiled Holocene 13 RDL from core MD99-2222 in the Saguenay Fjord (St-Onge and al., 2004) with varying thicknesses (from 7.1 cm to 1510 cm) and 4 Quaternary turbidites of different origins in order to document the influence of sedimentary and magnetic parameters on NRM acquisition. We found a logarithmic relationship between the amplitude of inclination changes, as well as the amplitude of magnetic grain sizes and the RDL thickness. Inclination and grain sizes are themselves correlated to each other by a logarithmic law. As there is no relationship between the inclination deviation and depth, compaction cannot account for such significant deviations alone. Flocculation likely varies with grain size, but again the amplitude of the inclination deviations is difficult to explain. Turbulence inherent to the depositional process of such events is most likely the dominant factor. This interpretation is supported by calculations aimed at describing the impact of bottom currents.

### **3.3 INTRODUCTION**

Measurements of sediment natural remanent magnetisation (NRM) are useful to chronostratigraphic, paleomagnetic and paleoenvironmental studies (e.g., Meynadier et al., 1992; Valet and Meynadier, 1993; Roberts et al., 1997; Kissel et al., 1998; Stoner et al., 2000; Channell & Kleiven, 2000; Channell et al., 2000; Valet, 2003; Stoner and St-Onge, 2007; Lisé-Pronovost et al., 2009; Barletta et al., 2010; Macrì et al., 2010; Mazaud et al.,

2012; Deschamps et al., 2018). Despite considerable progress, the mechanisms that govern the detrital and post-detrital remanences remain relatively unconstrained (Tauxe et al., 2006) while they bear consequences regarding the interpretation of paleomagnetic records. Various processes controlling NRM acquisition have been proposed by analog and digital models (Nagata, 1961; Collinson, 1965; Stacey, 1972; Denham and Chave, 1982; Tauxe, 1993; Katari and Bloxham, 2001; Tauxe et al., 2006; Shcherbakov and Sycheva, 2010; Roberts et al., 2013). The first model of deposition proposed by Nagata (1961) focused on the rotation of magnetic grains within a fluid immersed in a magnetic field and predicted that all magnetic grains would be rapidly (< 1s) aligned by the field leading to saturation of the remanent magnetization. However, typical values of the natural remanence in sediments and in sediment redeposition experiments are two or three order of magnitudes below saturation (Tauxe, 1993; Tauxe et al., 2006; Spassov et Valet, 2012; Roberts et al., 2013). Collinson (1965) proposed that the absence of saturation could be linked to the Brownian motion, but this process mainly affects the fine particles and is not sufficient to reduce the alignment time (Stacey, 1972). Flocculation appears to be a more realistic parameter as it agglomerates sedimentary particles and therefore affects the alignment of the magnetic grains by the field (Shcherbakov and Shcherbakova, 1983; Tauxe, 1993; Katari and Bloxham, 2001; Tauxe et al., 2006). In fact, the timing of magnetization acquisition depends on various sedimentary and magnetic parameters that can also introduce a delay between sediment deposition and lock-in of the remanent magnetization (Verosub, 1977; Shcherbakov and Sycheva, 2010; Roberts et al., 2013).

Several experimental studies (Quidelleur et al., 1995; Katari et al., 2000; Carter-Stiglitz et al., 2006; Heslop et al., 2006; Tauxe et al., 2006; Spassov and Valet, 2012) attempted to evaluate the role played by specific parameters (e.g., water content, magnetic concentration, salinity, carbonate and clay content, flocculation, compaction) on the timing and alignment of magnetic grains within the sediment. However, the pertinence of laboratory redeposition experiment is limited by the size and short duration of the experiments compared to those in nature. Rapidly deposited layers (RDL) like turbidites can be seen as a natural analog to laboratory redeposition experiment. So far, RDLs have

been mostly studied for their sedimentological properties (e.g., Mulder and Alexander, 2001; Mulder et al., 2001) and only a few rock magnetic parameters have been investigated (e.g., St-Onge et al., 2004; Duboc et al., 2017).

A magnetic study of four distinct turbidites from the Bay of Bengal, Gulf of Corinth and Eastern China Sea was recently published by Tanty et al. (2016) (Figure 29). The sedimentary and magnetic grain sizes revealed a significant coarsening of both sediment particles and magnetic grains within the bottom layers. The most striking observation was the existence of decreasing shallowing of the magnetic inclinations between the bottom and upper layers that decreases with the size of the event and obeys a simple linear scaling law. These results have been however obtained from a low number of events. It is thus necessary to establish a more complete database that would incorporate RDLs of different sizes and nature and to assess whether common properties emerge that could pave the way to new developments about detrital remanent magnetization. In this paper, we will thus investigate 17 turbidites ranging from 7.1 cm to 15.1 m in order to determine NRM acquisition mechanisms during turbidites.

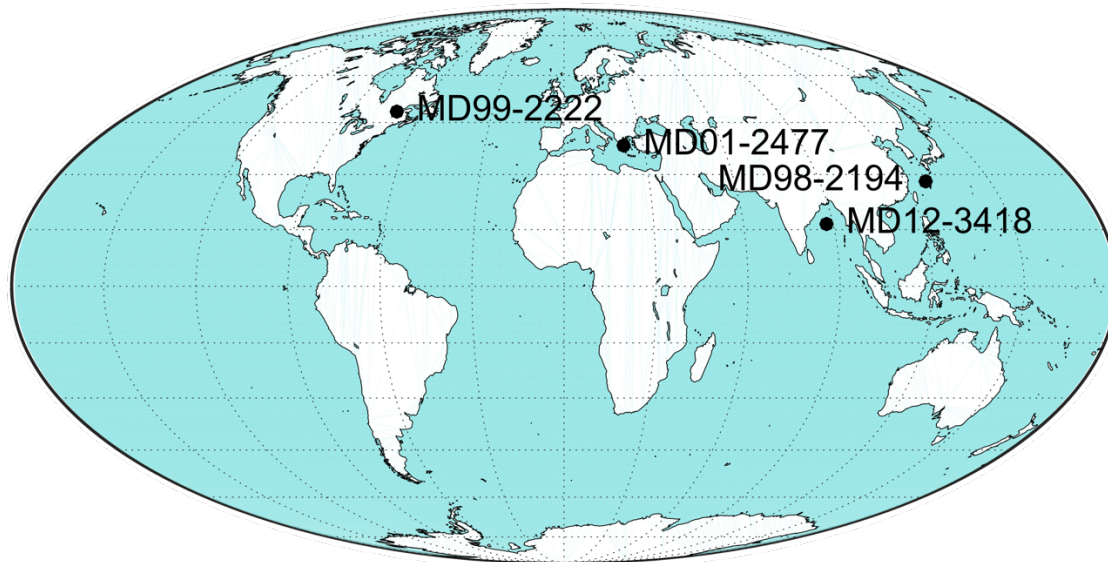


Figure 29: Location of the sampling sites of cores MD01-2477 (Gulf of Corinth), MD12-3418 (Bay of Bengal), MD98-2194 (China Sea) and MD99-2222 (Saguenay Fjord, Canada).

### 3.4 METHODOLOGY

#### 3.4.1 Core MD99-2222

All properties of core MD99-2222 have been studied by St-Onge et al. (2004). Core MD99-2222 was sampled in the from Saguenay Fjord in eastern Canada ( $48^{\circ}18.28' N$ ,  $70^{\circ}15.44' W$ , water depth 271 m, Figure 29). Low-field magnetic susceptibility ( $k$ ) was measured every 2 cm with a GEOTEK Multi Sensor Core Logger on board of the R/V Marion Dufresne II. Grain size analyses were conducted at the Université de Bordeaux with a Malvern Supersizer “S” laser grain size analyzer. The grain size data were analyzed using the Gradistat program (Blott and Pye, 2001). The cores were sampled using U-channels and sediment magnetization was measured every 1 cm interval at the University of California in Davis using a 2G Enterprises cryogenic magnetometer Model 755. The Natural Remanent Magnetization (NRM) was measured on U-channel samples and then demagnetized with an alternating field (AF) at 5 mT steps from 10 mT to 40 mT and then every 10 mT up to 80 mT. Inclination was calculated by principal component analysis (Kirschvink, 1980). An anhysteretic remanent magnetization (ARM) was produced using a 100 mT peak AF with a 50  $\mu T$  direct current (DC) biasing field. This ARM was subsequently demagnetized with an alternating field (AF) at 10 mT, steps from 10 mT to 20 mT every 5 mT to 40 mT and then every 10 mT up to 60 mT.

The  $k_{ARM}/k$  ratio was obtained by calculating the susceptibility of the ARM ( $k_{ARM}$ ) by normalizing the ARM by the strength of the biasing field. Because  $k$  is sensitive to the coarser fraction of magnetite, it is frequently associated with ARM that responds dominantly to small magnetic grains and is therefore often used as a magnetic grain size proxy (e.g., King et al., 1983; Stoner et al. 1996; Stoner and St-Onge, 2007). The ratio of the parameters depicts the evolution of magnetic grain size.

### **3.4.2 Cores from Tanty et al. (2016)**

The study of Tanty et al. (2016) focused on the detrital remanent magnetization of 4 turbidites found in cores MD12-3418, MD01-2477 and MD98-2194. Two turbidites were sampled and studied in core MD12-3418 from the Bay of Bengal ( $16^{\circ}30.27'N$ ,  $87^{\circ}47.92'E$ , water depth 2547 m) and one in core MD01-2477 from the Gulf of Corinth ( $38^{\circ}.133'N$ ,  $22^{\circ}.333'E$ , water depth 867 m) and one in core MD98-2194 from Eastern China Sea ( $28^{\circ}06'N$ ;  $127^{\circ}22'E$ , water depth 989 m, Figure 29). The turbidites of the first two cores were deposited during the Holocene, while the event identified in core MD98-2194 was dated to the Pleistocene (Tanty et al. 2016). The NRM of the discrete samples taken within each turbidite was measured at IPGP using a 2G Enterprises cryogenic magnetometer Model 755-R. All samples were demagnetized with an AF using an AGICO LDA-3 demagnetizer at 5 mT steps up to 30 mT and then by steps of 10 mT up to 80 mT.

## **3.5 COMPARISON OF RDL FROM CORE MD99-2222**

### **3.5.1 Magnetic characteristics**

Core MD99-2222 from the Saguenay Fjord (Figure 29) was previously studied by St-Onge et al. (2004). It includes 13 Holocene RDL with varying thicknesses from 7.1 cm to 1510 cm among which 6 turbidites, 6 hyperpycnites and one undefined event were identified (Figure 30). A hyperpycnite is different from a classic turbidite and can have recorded an inverse and then normal grading within the same event (e.g., Mulder et al., 1998; Mulder et al., 2003; Mulder and Chapron, 2011).

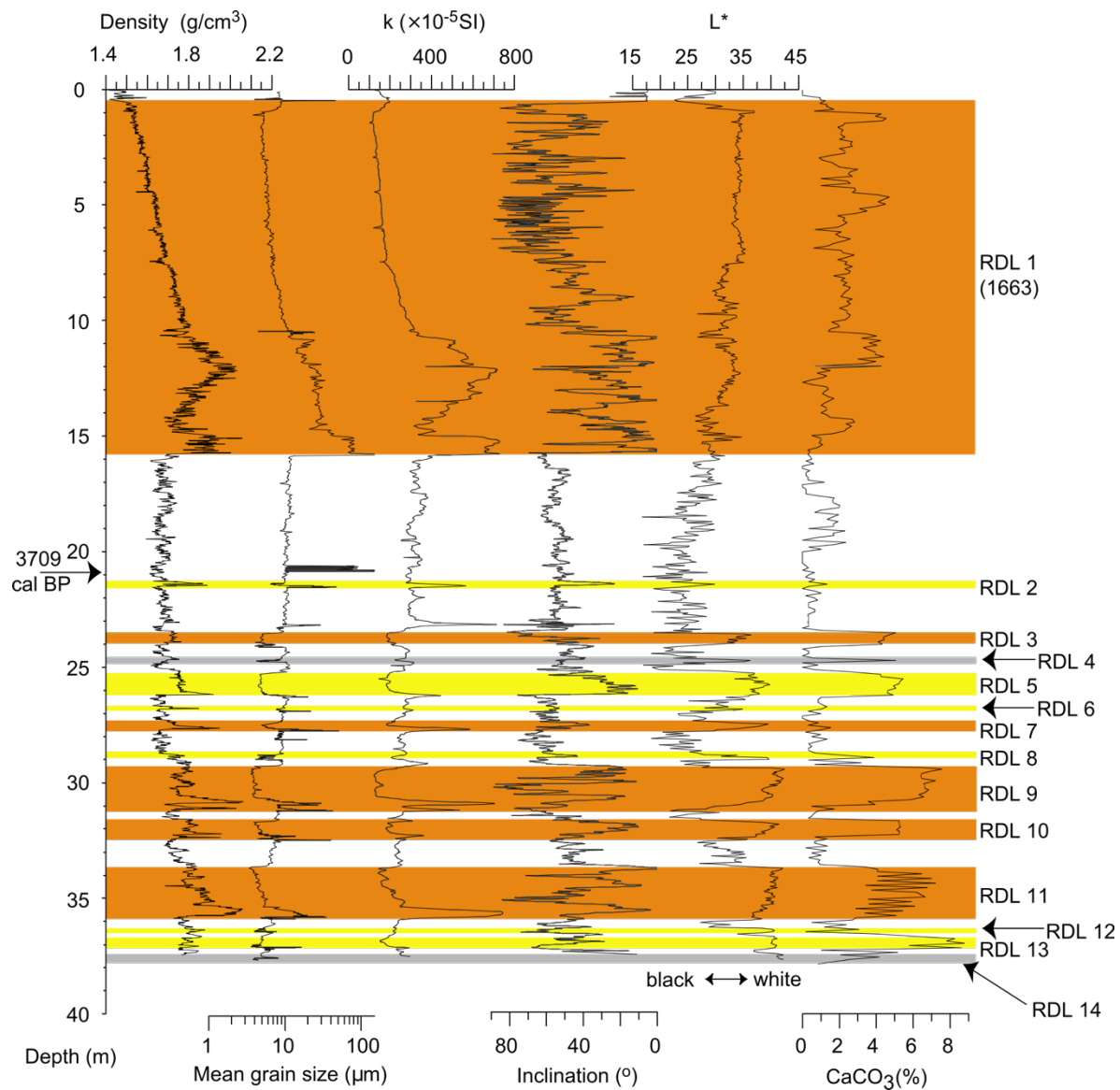


Figure 30: Sedimentological and physical properties of core MD99-2222 (St-Onge et al., 2004).

The sedimentological and physical properties of the material from core MD99-2222 have been previously reported by St-Onge et al. (2004) (Figure 30). Magnetic mineralogy was studied at 1.5 m intervals (St-Onge et al., 2004) and showed no change within the RDL. Magnetic granulometry indicates the presence of pseudo-single domain (PSD) and multidomain (MD) grains and these characteristics remain similar for each RDL. Overall,

these results indicate that the magnetic parameters do not vary significantly within each event. We infer that since the Earth's magnetic field remained constant during the very short period of a turbiditic process, any evolution in direction and/or intensity of the remanent magnetization can only result from changes in magnetization acquisition processes.

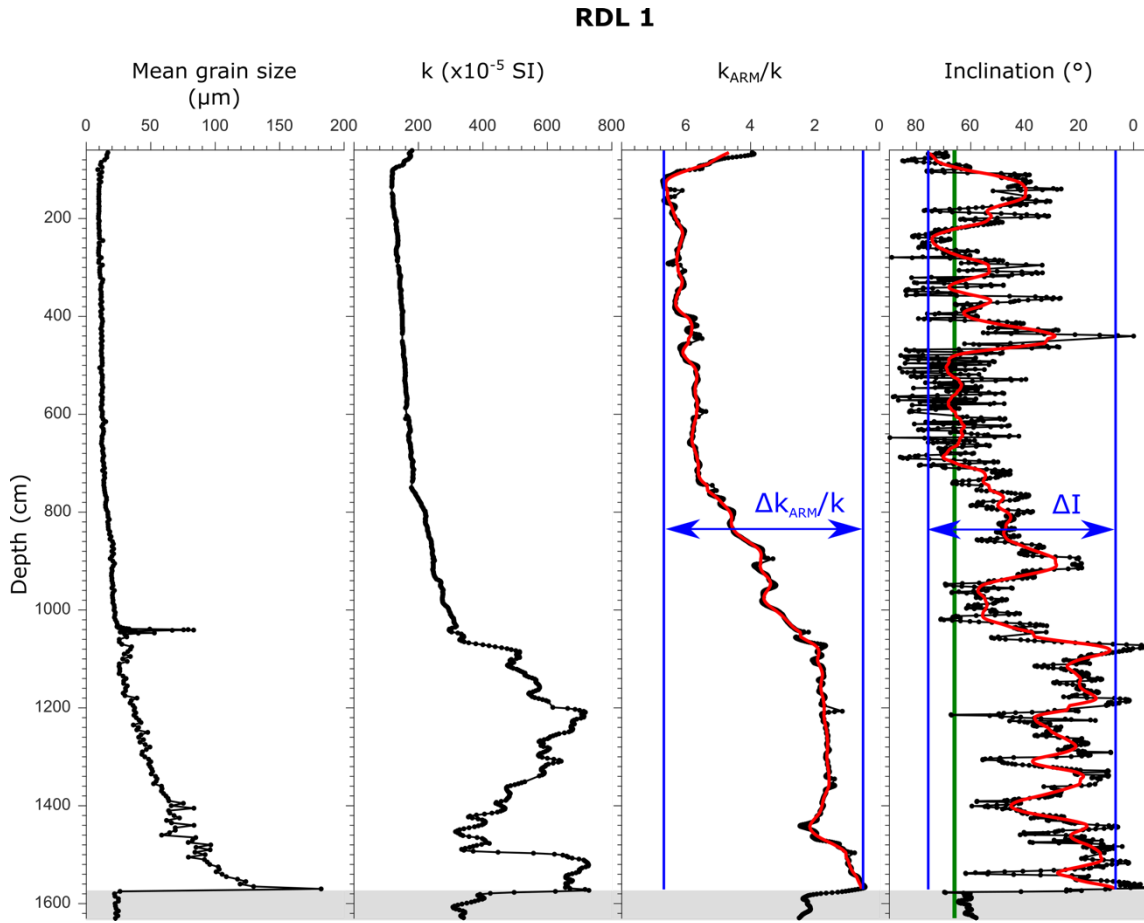


Figure 31: Sedimentological and physical properties of the RDL 1 event from core MD99-2222 (St-Onge et al., 2004). Red curves were obtained by singular spectrum analysis (SPA). The maximum amplitude changes in inclinations and grain sizes were calculated from the SPA results and are shown by blue arrows. Green line in the inclination represents the geocentric axial dipole (GAD) value. The grey zone represents a normal period of sedimentation before the RDL1 deposition.

Variations of sediment grain size, low-field magnetic susceptibility ( $k$ ), anhysteretic remanent magnetization/susceptibility ( $k_{ARM}/k$ ) ratio and inclination within the 1510-cm

thick hyperpycnite from core MD99-2222 are illustrated in Figure 31. The evolution of sediment grain size with depth is the most sensitive parameter to define the RDL boundaries. All four indicators follow a parallel evolution which confirms the characteristics reported by Tanty et al. (2016) from other turbidites. At the base of the event, there are coarser magnetic grains and sediment particles, while the inclination deviates significantly away from the inclination of the geomagnetic axial dipole (GAD) at the site.

### 3.5.2 Coherent features between RDL

Using this extended database, we can investigate further the relationship between magnetic parameters and RDL that was reported by Tanty et al. (2016). In Figure 31 are shown typical parallel evolutions of the inclinations and  $k_{ARM}/k$  ratios (Figure 31) within an RDL event. We selected RDL 1 due to its thickness (1510 cm), but we will see that similar features are valid for all events as seen in supplementary material. A singular spectrum analysis (Vautard and Ghil, 1989) has been applied to the inclinations and  $k_{ARM}/k$  ratios of all RDL events from core MD99-2222. The results are depicted in Figure 31 by the red lines which indicate a trend in the inclination variations (from 20° to 80°), as well as in the grain sizes with coarser grains at the bottom and smaller grains at the top. Superimposed to this global trend, the inclinations show higher frequency large amplitude changes, but those are not observed for grain sizes. They likely result from turbulent conditions that affected the alignment of the magnetic grains by the field while their size distribution remained controlled by similar segregation process after they have reached the bottom.

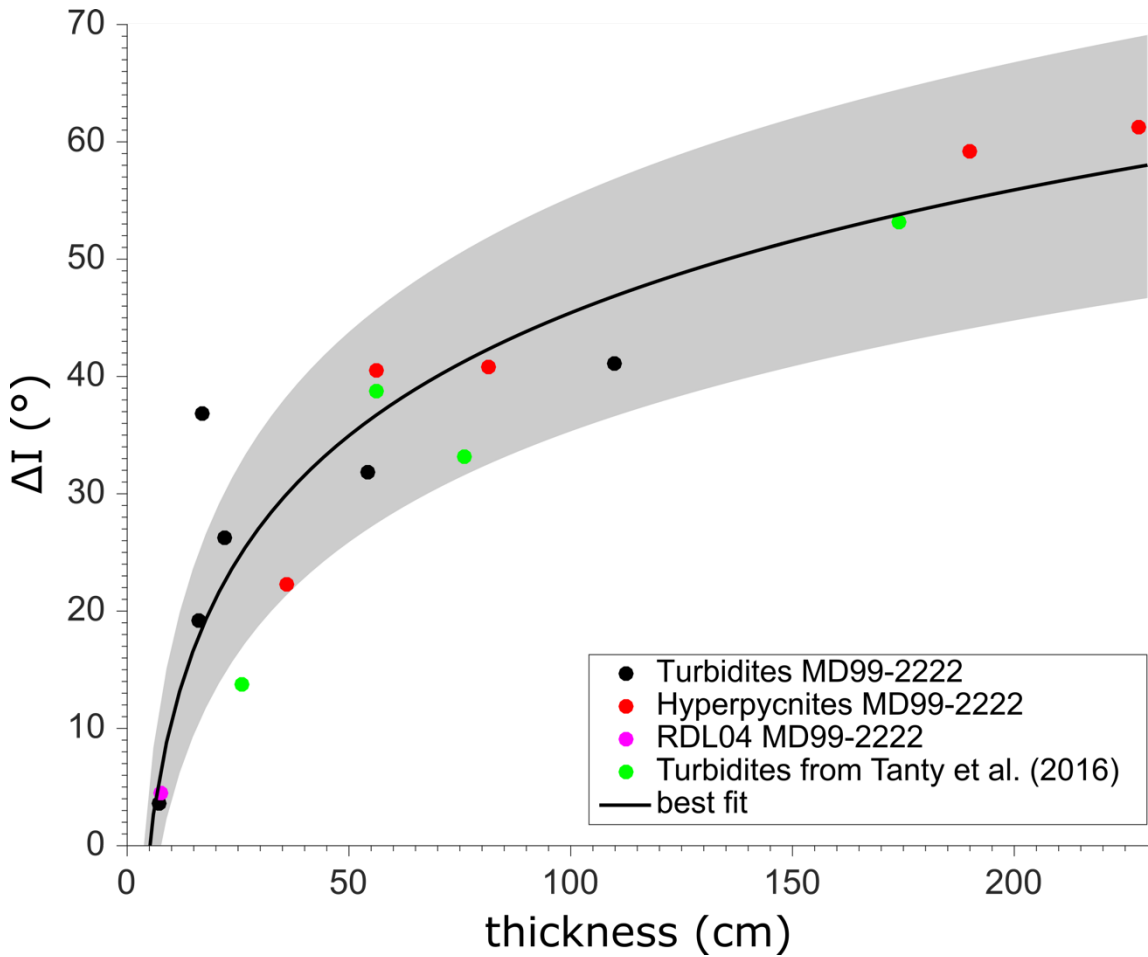


Figure 32: Amplitude of inclination changes within 16 RDLs as a function of their thickness. Black, red and pink closed circles are for turbidites, hyperpycnites and other RDLs from core MD99-2222, respectively. Green closed circles show the values of the four turbidites studied by Tanty et al. (2016).

We first scrutinized the inclination changes within each event and defined the inclination variability from the results of singular spectrum analysis by  $\Delta I = I_{\max} - I_{\min}$  (Figure 31). The amplitude of the inclination changes ( $\Delta I$ ) within each RDL sequence has been plotted in Figure 32 as a function of thickness including the turbidites that were studied by Tanty et al. (2016). Note that we did not include the 1510 cm thick turbidite which is much larger than all other events. The logarithmic curve shown as a black line (Figure 32) is the best fit between the two parameters and was calculated by using an estimator of parameters with a simulated annealing and bootstrap (Efron and Tibshirani,

1986). The correlation differs from the linear curve that was previously reported by Tanty et al (2016) and results from the refinement of the correlation induced by the larger number of data. The confidence interval is represented by the grey area (Figure 32). Except the smallest turbidite from Tanty et al. (2016) and one turbidite from MD9-2222, all other RDL lie within the confidence interval. We note that the turbiditic or hyperpycnic nature of the RDL does not seem to influence their distribution in the figure.

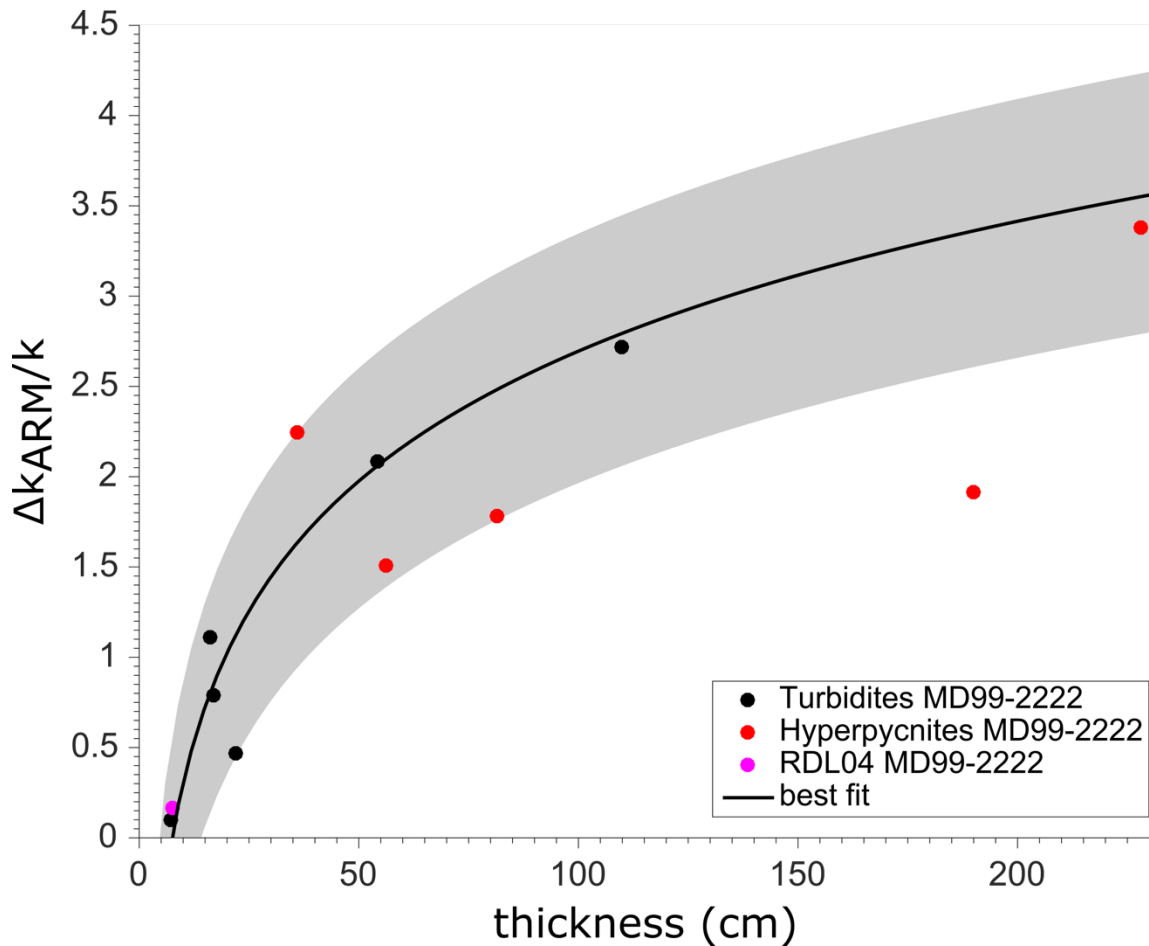


Figure 33: Amplitude of grain size changes within 12 RDLs as a function of their thickness. Black, red and pink closed circles are for turbidites, hyperpycnites and other RDLs from core MD99-2222, respectively.

Similarly, we investigated the relationship between the events thickness and the amplitude of the magnetic grain size variations depicted by  $\Delta(k_{ARM}/k)$ . In this case, we

were constrained to restrain the study to the 12 RDL events from core MD99-2222 because other field values were used by Tanty et al. (2016) to induce the ARMs. The results are shown as a function of the event thickness in Figure 33. Using the same bootstrap approach (Efron and Tibshirani, 1986), we found that the  $\Delta k_{\text{ARM}}/k$  ratios also follow a logarithmic curve (Figure 33). The data points lie in the confidence interval except for one hyperpycnite.

For layers thinner than 50 cm, the amplitude of the inclinations and magnetic grain sizes are almost linearly correlated with the thickness of the event. For layers thicker than 50 cm, the correlation slope weakens progressively. When plotted with respect to each other, the inclination and magnetic grain sizes amplitudes do not appear to be linearly correlated, but follow again a logarithmic dependence. One turbidite and one hyperpycnite do not lie within the confidence interval.

## 3.6 DISCUSSION

### 3.6.1 Compaction and flocculation

Magnetic and/or sedimentary material that feed the turbidites and the hyperpycnites in the Saguenay Fjord come from the same source (Mulder et al., 1998; St-Onge et al., 2004). The evolution of the magnetic and sediment grain sizes follows a similar pattern in all RDLs with significant decreasing grain size from the bottom to the top. The amplitude of the changes increases with the size of the event as shown by the data from core MD99-2222. Turbidites and hyperpycnites were produced in different water column thicknesses, and therefore the water column depth would have no significant impact on the grain sizes pattern within the sediment and also no influence on the magnetic alignment near or at the sea-floor. The high concentration of particles during a turbidity or an hyperpycnal current favoured clusters the formation of aggregates after segregation of

coarse magnetic and sedimentary grains, i.e. not during the primary stage of the discharge, but also no longer after they lie at the bottom because rapid accumulation of sediment reinforced the particle cohesion and impeded post-depositional reorientation (Tanty et al. 2016).

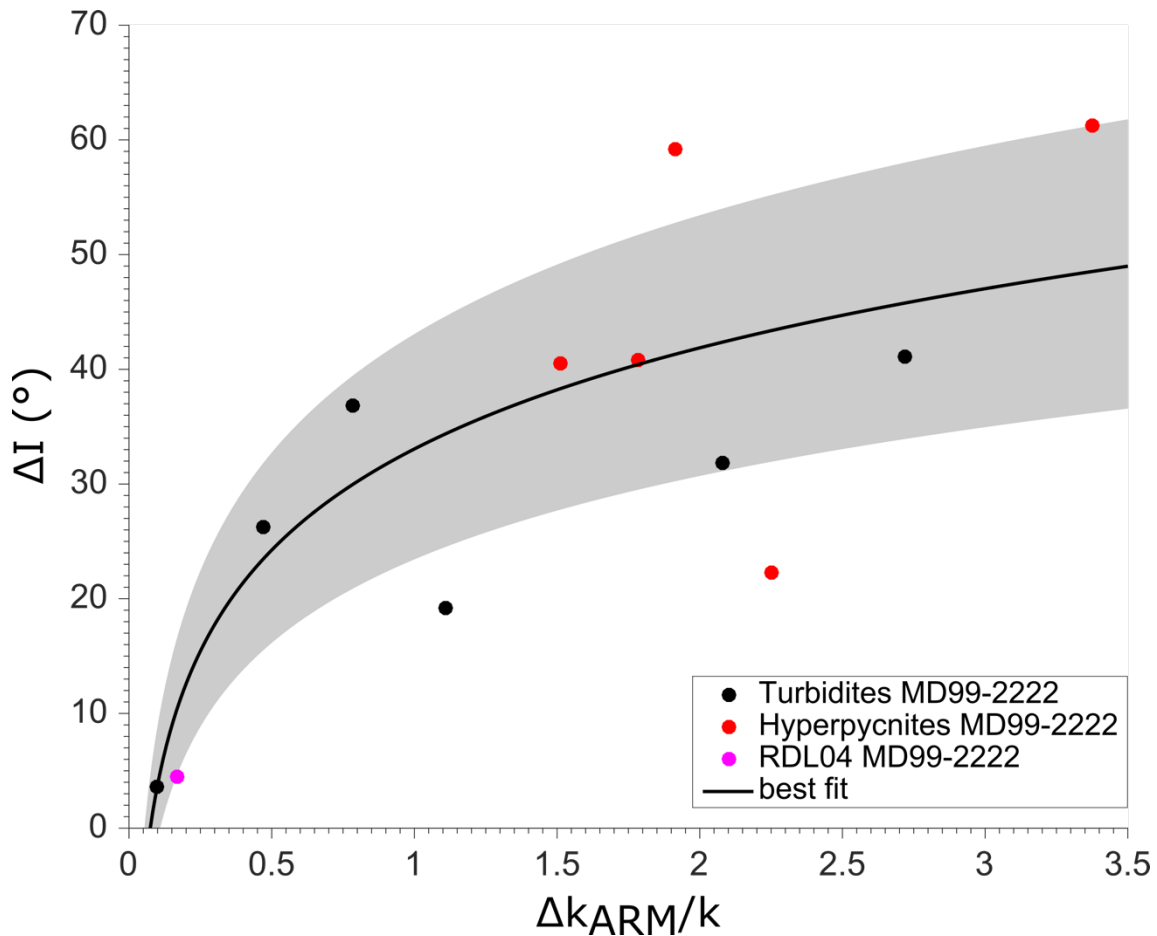


Figure 34: Amplitude of inclination changes as a function of grain sizes changes within 12 RDLs. Same symbols as in Figure 33.

As expected, the results in Figure 34 reveal that the large changes in magnetic grain size in the thick events correlate with large inclination changes. Inclination shallowing decreases within the event. The inclinations are near zero with some negative values at the base of the thickest turbidites like the 1510 cm thick hyperpycnite from core MD99-2222 (Figure 31). In this case, the inclination changes show a regular trend with a zone of chaotic

fluctuations below 1100 cm and a mean inclination  $\approx 25^\circ$ , then a transition from a mean Inc  $\approx 25^\circ$  to a mean Inc  $\approx 55^\circ$  between 1100 cm and 700 cm and an interval with a mean Inc  $\approx 55^\circ$  above 700 cm. For comparison, the modern field inclination at the site is  $71^\circ$ . The observed inclination trend correlates with the magnetic grain size coarsening recorded by the  $k_{\text{ARM}}/k$  variations.

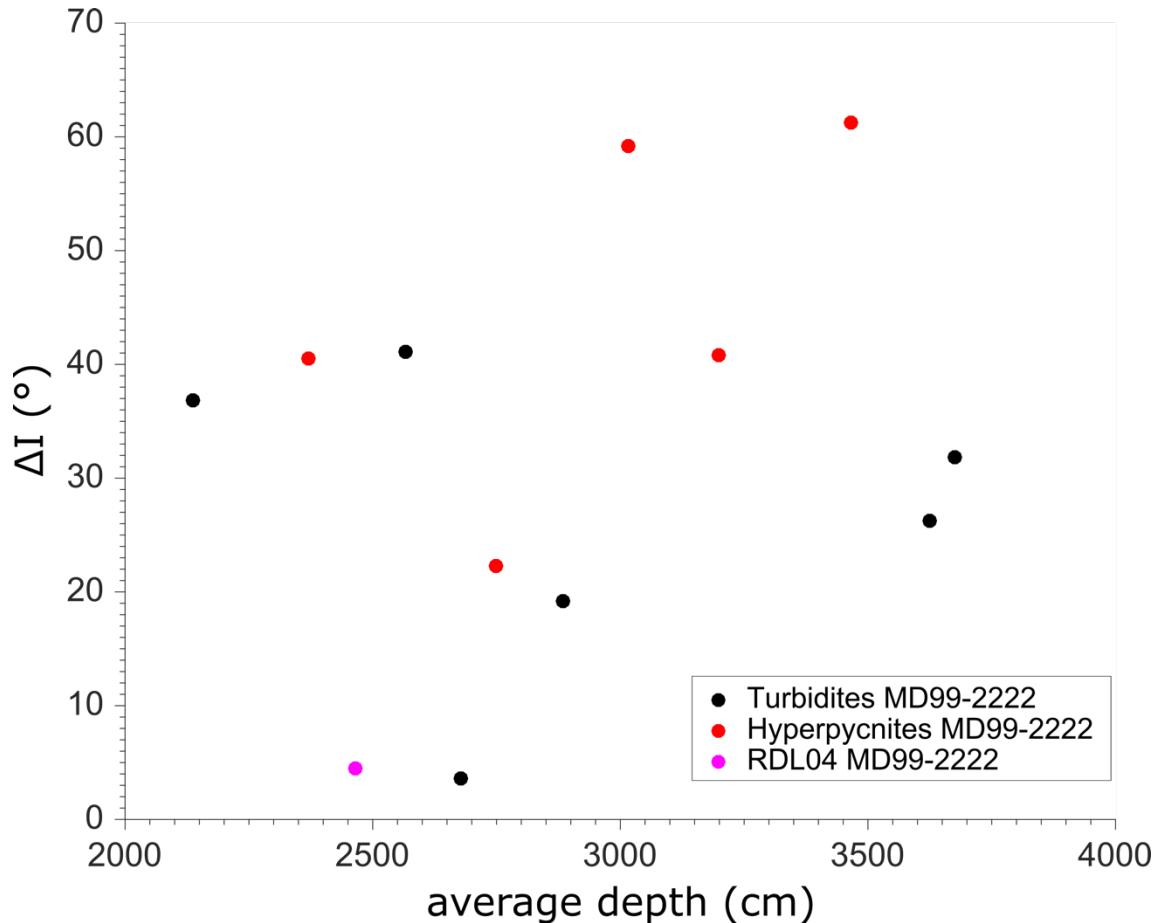


Figure 35: Amplitude of inclination changes within 12 RDLs as a function of their average depth in core MD99-2222. Black, red and pink closed circles are for turbidites, hyperpycnites and other RDLs from core MD99-2222, respectively.

Compaction is frequently considered to be responsible for inclination shallowing in sediments (Anson and Kodama, 1987; Arason and Levi, 1990). The logarithmic relationship between inclination and magnetic grain size may also support the role of compaction (Maier et al. 2013). However, compaction does not generate inclination

deviations as large as  $60^\circ$  (Anson and Kodama, 1987; Arason and Levi, 1990; Sun and Kodama, 1992) and becomes significant at much larger depths (below 100 m, Sun and Kodama, 1992). Therefore, this parameter seems difficult to reconcile with the present observations. The most conspicuous evidence is the absence of any relationship between the mean inclination of each RDL event and the core depth of the event. Assuming that compaction played a significant role, we would observe a direct effect of the sediment depth on the inclination shallowing. This is not the case (Figure 35). Therefore, we can reasonably exclude that compaction was dominantly responsible for the large inclination offsets and we now focus on other possible factors.

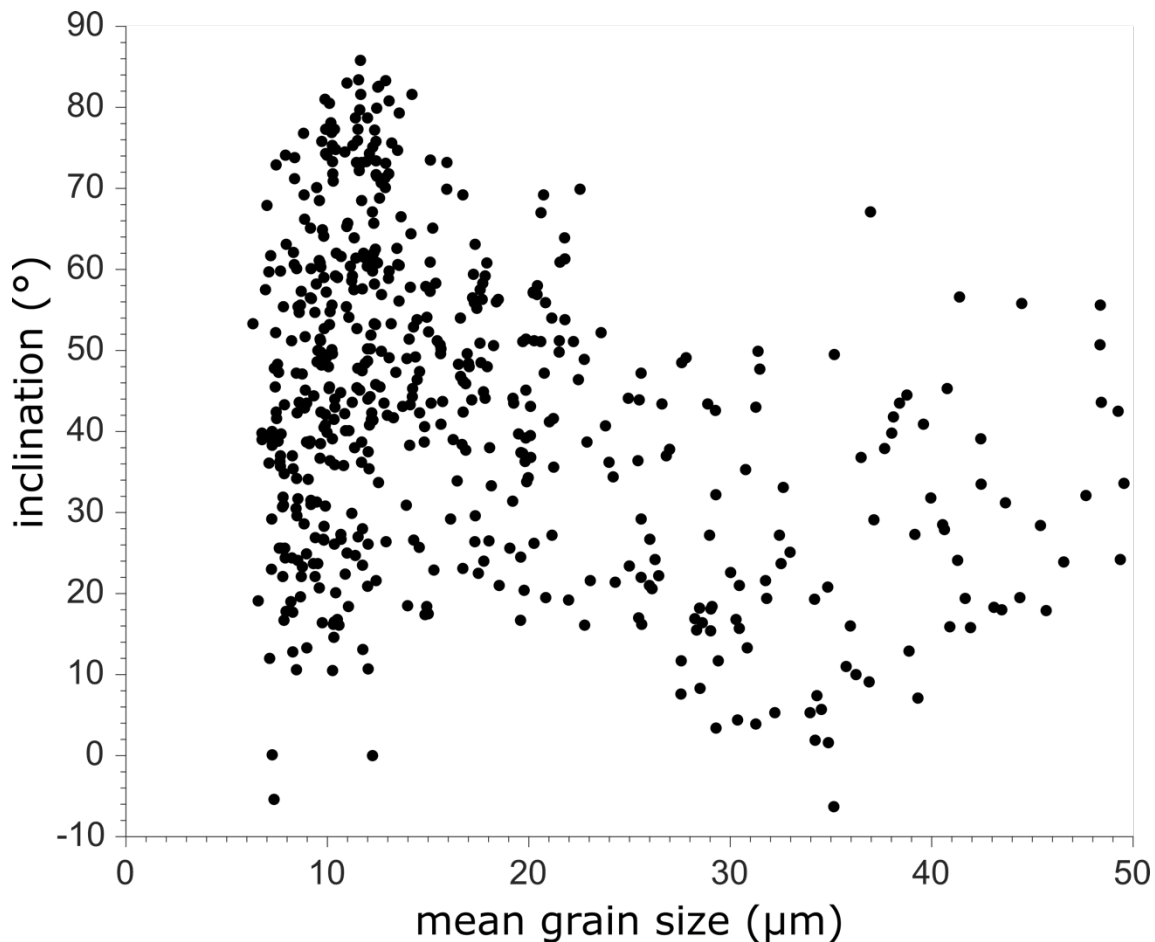


Figure 36: Inclination as a function of sediment mean grain size in 13 RDLs.

Turbulence and flocculation (Tauxe, 1993; Tanty et al., 2016) can both affect the orientation of the magnetic grains. Flocculation has been discussed in several models (Katari and Bloxham, 2001; Tauxe et al., 2006; Shcherbakov and Sycheva, 2010; Roberts et al., 2013). We cannot rule out that different grain sizes may be accompanied by different flocculation processes that in turn would affect the magnetic record. This assumption is testable through a plot of inclination as a function of sediment grain size and Figure 36 shows no evidence for a direct causality between the two parameters. We infer that flocculation might have only played a secondary role.

### 3.6.2 Effect of turbulence

The effect of turbulence on the acquisition of the magnetization in sediments has rather been neglected, the turbulence is more considered to have an impact on flocculation (Tauxe et al. 2006). It is often considered that sediment deposition occurs in calm environments while in fact significant bottom currents are frequently present. The effect of turbulence is evidently enhanced during turbidity and hyperpycnal currents (Mulder and Alexander, 2001; Alexander and Mulder, 2002; Cantero et al., 2012).

We have attempted to describe the effect of turbulence by numerically modeling the orientation of magnetic flocs settling through a horizontal, so-called wall flow above the sediment surface. Wall flows are characterized by universal scaling laws, with relevant characteristics, such as the flow velocity and the strength of the associated turbulence, depending on a single parameter, the so-called friction velocity (Chriss and Chaldwell, 1984). Typical friction velocities above pelagic marine sediments are of the order of 2 mm/s (Chriss and Chaldwell, 1984), while turbidites are characterized by one order of magnitude larger values (Xu, 2010).

Numerical DRM simulations have been performed in two main steps. First, a diffusion limited aggregation process for sediment particles in water has been simulated by letting a given number of particles perform a random walk that simulates the Brownian

motion in a natural environment. Every collision between individual particles or, in the later phase of the simulation, between particles and aggregates is assumed to be irreversible, yielding a larger aggregate. The process is performed until a single floc with the given number of initial particles (e.g. 100) is generated. The flocs produced in this manner have a fractal dimension of about 2, which is within the range (2-2.8) observed on natural flocs. Another set of denser flocs with higher fractal dimension (2.4) has been generated by adding a directed component to the random walk. These two groups of flocs, composed of a minimum of 2 and a maximum of 200 particles, are used to simulate natural flocs with a different degree of compactness and shape, whereby both parameters are controlled by the fractal dimension.

Next, the hydrodynamic properties of each floc are calculated in the form of a translational and a rotational viscous resistance tensor. These tensors represent the viscous resistance of the floc against translation (e.g. during settling), and reorientation. The latter is fundamental for modeling DRM acquisition. These tensors are used to calculate the forces and torques acting on a settling floc. The forces include (1) gravity, which is proportional to the net floc weight, applied to the floc center of mass, and (2) viscous resistance, which is determined by the product of the translational viscous resistance tensor and the velocity vector. Because gravity and viscous resistance apply to different points within the floc, a net torque is developed during the floc's fall, which is counteracted by the rotational viscous resistance. Finally, an additional torque results from the translation-rotation coupling tensor, which describes the conversion of translation motion into rotation motion (like in a falling maple seed), and vice-versa.

For DRM simulations in a resting water, the above mentioned torques are counteracted by the magnetic torque, resulting from the vector product between the floc's magnetic moment and the magnetic field. Each floc is given a different, randomly oriented magnetic moment in the range of  $fAm^2$ , which is representative for PSD magnetite. Each floc is then released from a great height above the sediment-water interface at a random orientation, and its motion is calculated using the forces and torques described above. The

DRM contribution of an individual floc is then given by the orientation of its magnetic moment at the moment it reaches the sediment-water interfaces. This orientation is almost random, but a small bias towards the applied magnetic field is obtained for a sufficiently large number of flocs (typically 106 different combinations of flocs, magnetic moments, and initial orientations). The DRM acquired in this manner suffers from a relatively large inclination shallowing, meaning that the DRM inclination is smaller than the field inclination. This is due to the fact that the randomizing torques, which result mainly from the difference between center of mass and viscous reaction, are predominantly horizontal. This means that all horizontal torque directions contribute to the randomization of the vertical magnetization component, while the horizontal magnetization component is affected mainly by that horizontal torque that are perpendicular to it.

More realistic DRM simulations must include the natural motion of the water column. Due to the boundary condition given by the sediment-water interface, the water flow in proximity to it is mainly horizontal. Furthermore, the viscous resistance of the interface creates a characteristic velocity profile, which is called the wall flow, where velocity increases logarithmically with increasing distance from the interface. The velocity gradient creates a shear flow and some turbulence, which exerts additional torques on suspended flocs. The effect of these torques depend on the flow azimuth with respect to the direction of the magnetic field, creating an additional modulation of DRM intensity, inclination, and declination.

The floc generation procedure, the calculation of its hydrodynamic properties, and numerical DRM simulations have been implemented in Mathematica. Due to its computational complexity, a DRM simulation with 106 flocs with a given combination of field and flow intensity and direction takes about 7 days on a personal computer with a 2 GHz four-core processor. Simulations in a resting water column have been performed for field inclinations of  $0^\circ$ ,  $15^\circ$ ,  $30^\circ$ ,  $60^\circ$ , and  $90^\circ$ , and field intensities ranging from 10% of the actual field to  $>1000\%$ , in order to check the saturation behavior. Wall flow simulations have been performed for a single field intensity, the same field inclinations, and flow

azimuths comprised between  $0^\circ$  and  $180^\circ$  in steps of  $15^\circ$ . A total of  $>500$  simulations has been obtained on 5 computers during 14 months. The complete description of numerical model will be presented in an upcoming publication.

The intensity, inclination and declination variations obtained for four different friction velocities (0, 2.5, 5 and 10 mm/s) are plotted in Figure 37 as a function of the deviation of the flow azimuth from the magnetic field. A  $30^\circ$  inclination shallowing occurs already in a resting water column with zero friction velocity. This effect is not directly related to the shape of flocs, since magnetic moments are oriented randomly. It is instead a statistical effect due to the preferential floc rotation about horizontal axes, which preferentially randomizes the vertical component of the magnetic moment vector. Horizontal flows add more rotation to the horizontal axis due to the flow shear near sediment, and the related turbulence. The shear flow is responsible for the strong azimuthal dependence of DRM inclination for friction velocities  $>2.5$  mm/s. Flow directed against the horizontal field component produces the opposite effect, i.e. inclination steepening. The net effect over all flow azimuths, however, is a strong additional shallowing that is compatible with the maximum values seen in core MD99-2222 below  $\sim 1100$  m. The transitional character of DRM inclination in MD99-2222 can be explained by the friction velocity threshold of  $\sim 2.5$  mm/s of the numerical model, above which the mean DRM inclination drops to zero. Chaotic deviations of the inclination from the mean trend by  $>50^\circ$ , on the other hand, can be explained by changes of the flow direction at friction velocities of 5 mm/s or more. The influence of current is proportional to the square of friction velocity. In Figure 37 we show the intensity and orientation of the DRM vector for increasing deviations of the flow azimuth away from the field direction. Each line corresponds to a different flow velocity. A 2.5 mm/s flow velocity has little influence on the magnetization direction, but above 5 mm/s it starts being significant with large inclination shallowing and significant dispersion in magnetization intensity that reaches almost 40% with a flow azimuth colinear with the field direction. The magnetization is not affected when the field and the flow are oriented along the same direction but increases progressively as the flow

deviates from the field orientation and reaches a maximum when it points  $180^\circ$  away from the field.

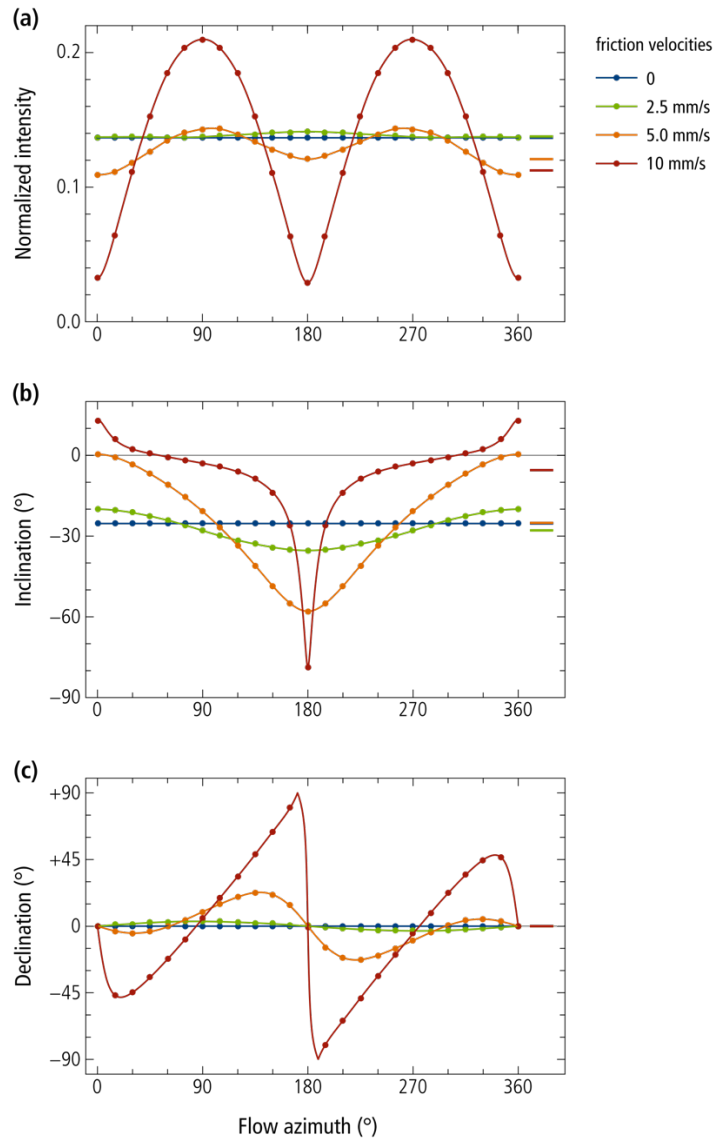


Figure 37: Numerical simulations of DRM acquired by flocs containing  $100 \times 2 \mu\text{m}$  diameter particles with a magnetic moment  $m = 5 \text{ fAm}^2$  in presence of a  $100 \mu\text{T}$  magnetic field with  $60^\circ$  inclination in an infinite water column for different friction velocities (a) Intensity profiles (after normalization) as a function of flow azimuth. (b) Inclination profiles as a function of flow azimuth. (c) Declination profiles as a function of flow azimuth.

### **3.7 CONCLUSION**

We have compared the magnetic characteristics of 17 RDL of different sizes and origins. The results confirmed most observations derived from a previous study of four turbidites regarding the alignment of magnetic grains in turbulent conditions. A first characteristic is that the variability of inclinations within the sequence increases with the importance of the events. The relationship between both parameters is well described by a logarithmic law. As a direct consequence, inclination variability appears to be linked to grain sizes variability. We have shown that inclination shallowing increases within thick RDL which are associated with coarser magnetic grains that are themselves imbedded within coarser particles. Using a simple model, we have shown that the present features can easily be generated by the turbulence generated by bottom currents. The difference with deposition in quiet environments points out the importance of post-depositional reorientation of the magnetic grains which does not occur at the bottom of the turbidites. These observations do not fully exclude a possible role played by flocculation and compaction, but in any case, turbulence should not be neglected to account for alignment deficit of magnetic grains by the geomagnetic field.

### **3.8 ACKNOWLEDGMENTS**

This research was funded by the Natural Sciences and Engineering Research Council of Canada (NSERC) Discovery grant to GSO and by the Fonds de Recherche du Québec Nature et Technologies (FRQNT). We also thank the captains, the crew and the scientific participants of the IMAGES IV, IMAGES V, MD124 Geosciences 2 and MD191 MONOPOL campaigns on board the Marion Dufresne II in 1998, 1999, 2001 and 2012, respectively. Many thanks to Cyrielle Tanty and Fernando Lopes at IPGP for various advices.

### 3.9 SUPPORTING INFORMATION

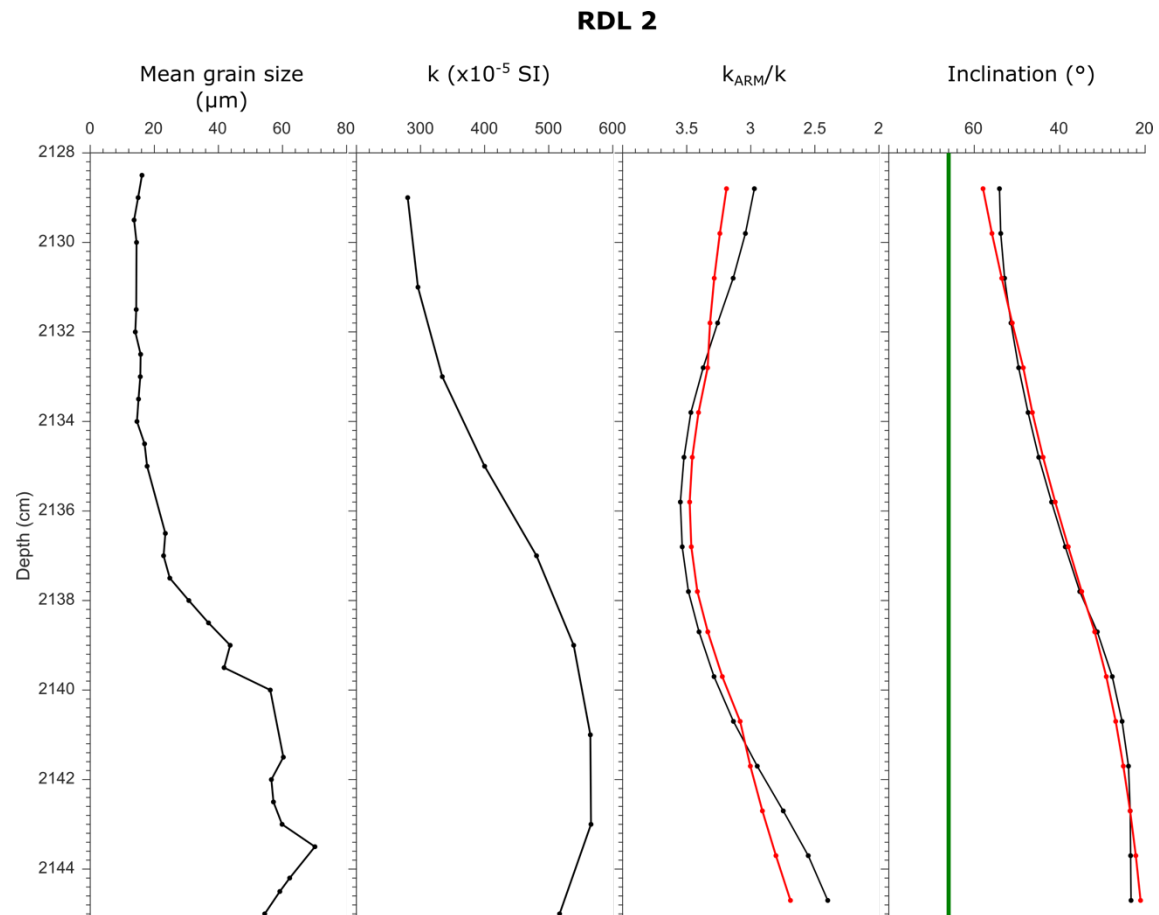


Figure 38: Sedimentological and physical properties of the RDL 2 event from core MD99-2222 (St-Onge et al., 2004). Red curves were obtained by singular spectrum analysis (SPA). Green line in the inclination represents the geocentric axial dipole (GAD) value.

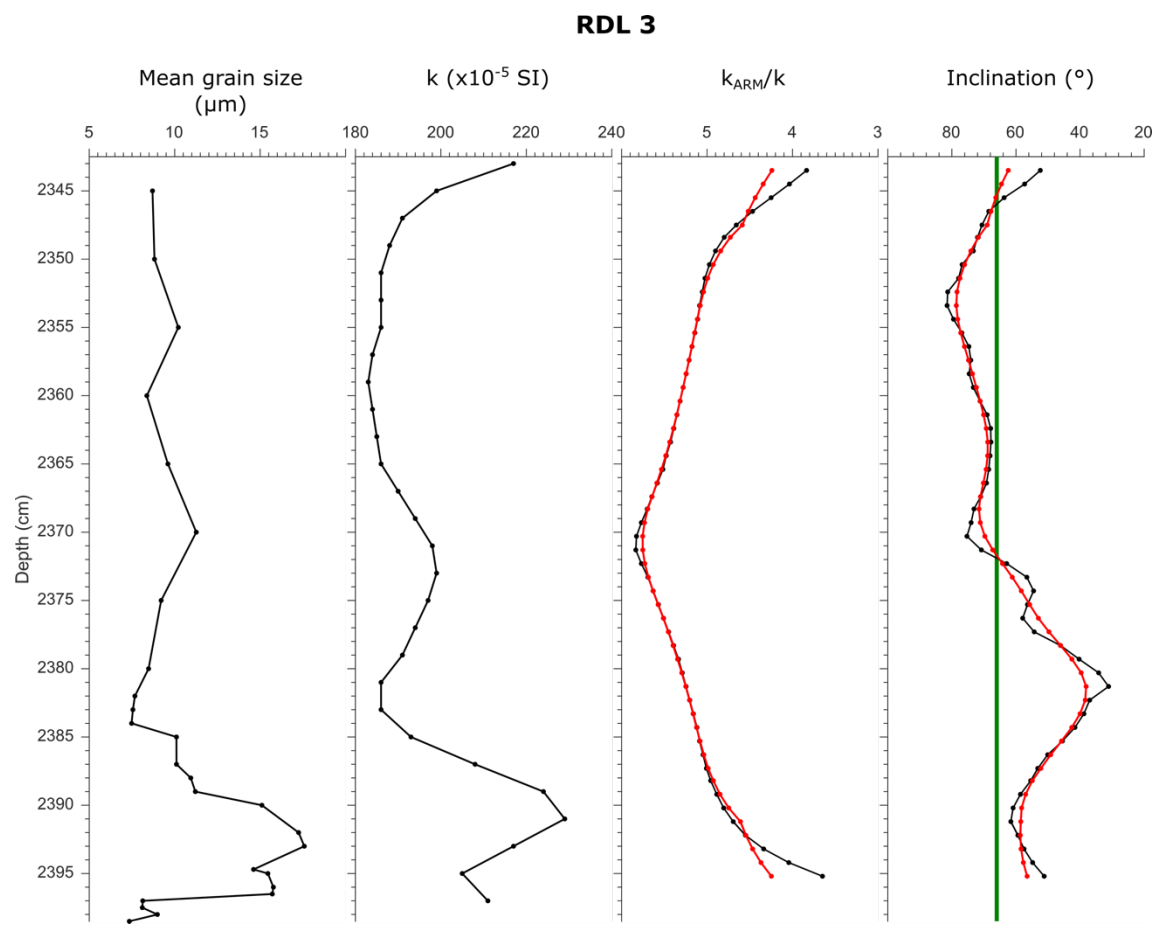


Figure 39: Same as Figure 38 for RDL 3 event.

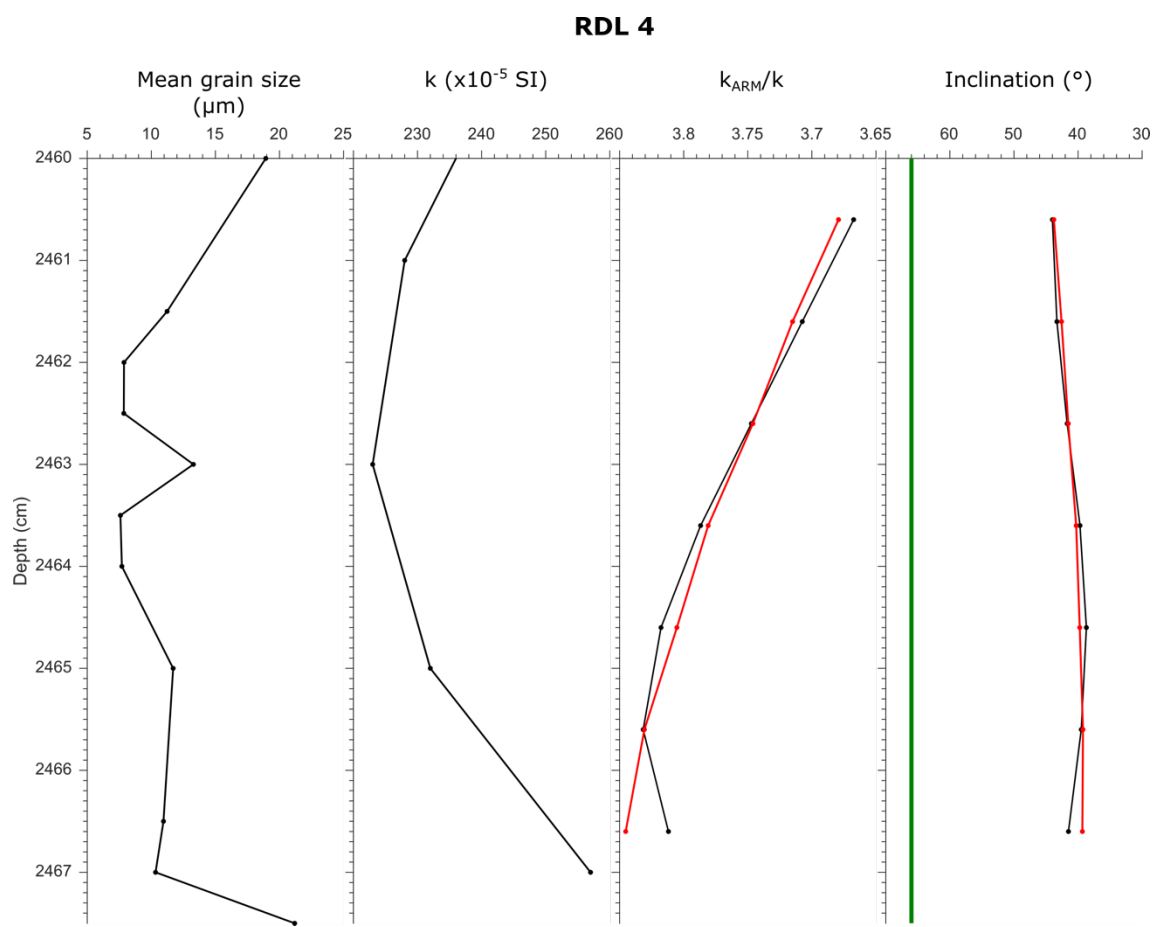


Figure 40: Same as Figure 38 for RDL 4 event.

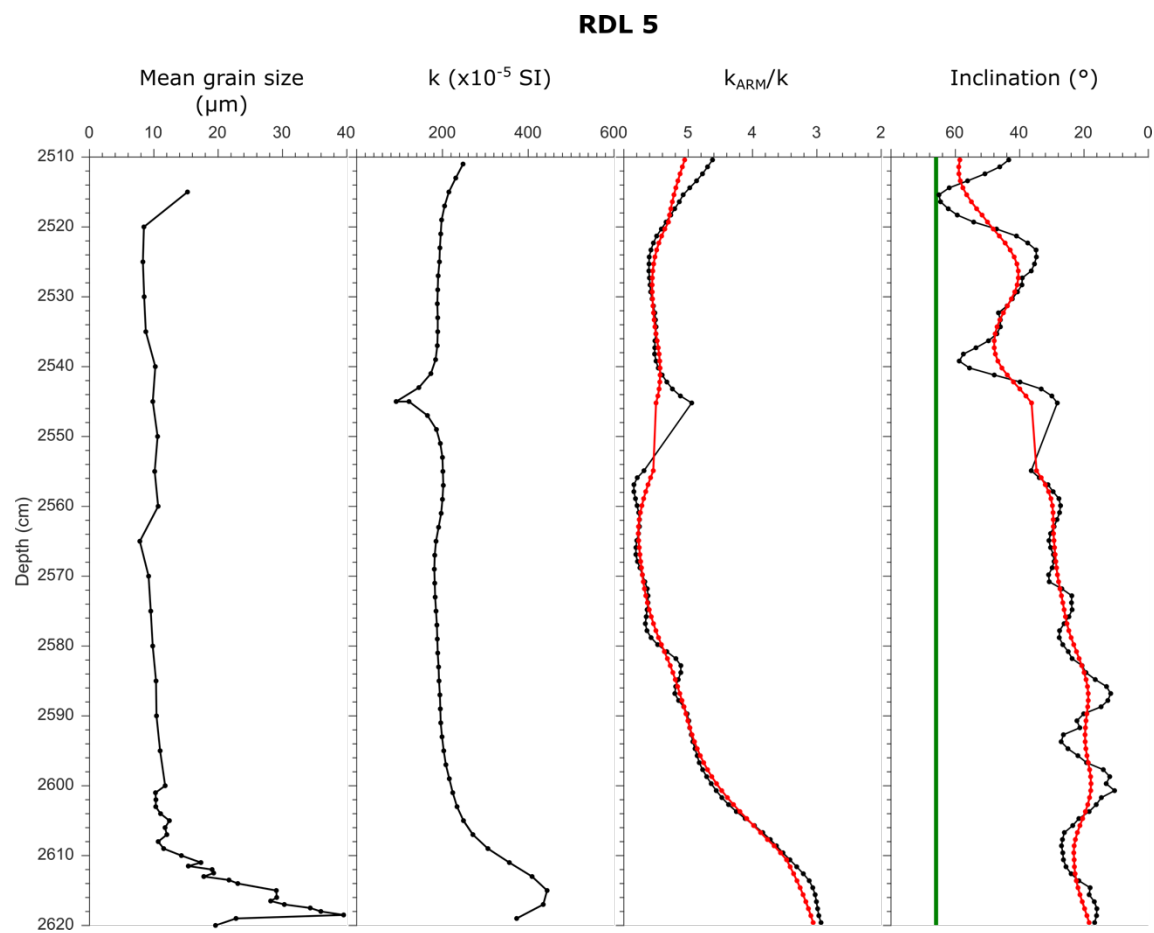


Figure 41: Same as Figure 38 for RDL 5 event.

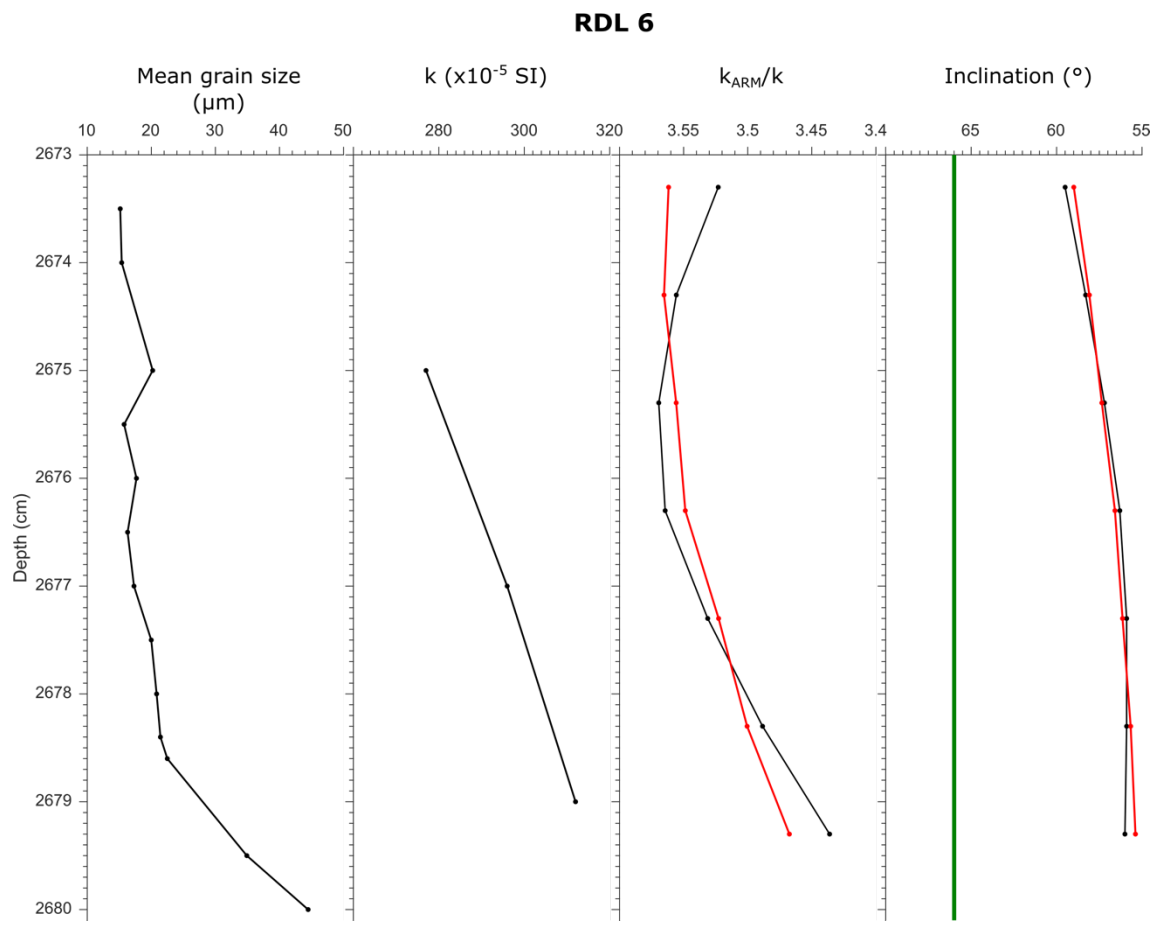


Figure 42: Same as Figure 38 for RDL 6 event.

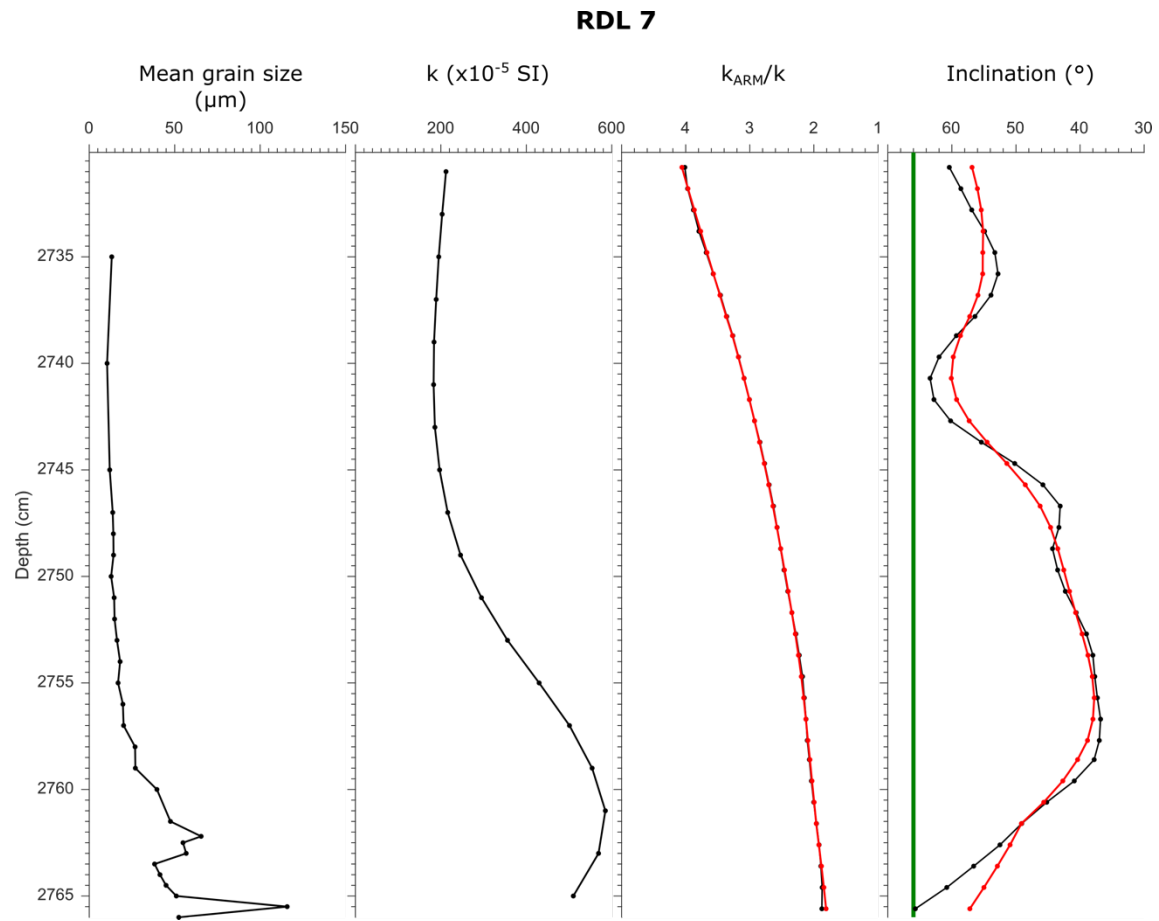


Figure 43: Same as Figure 38 for RDL 7 event.

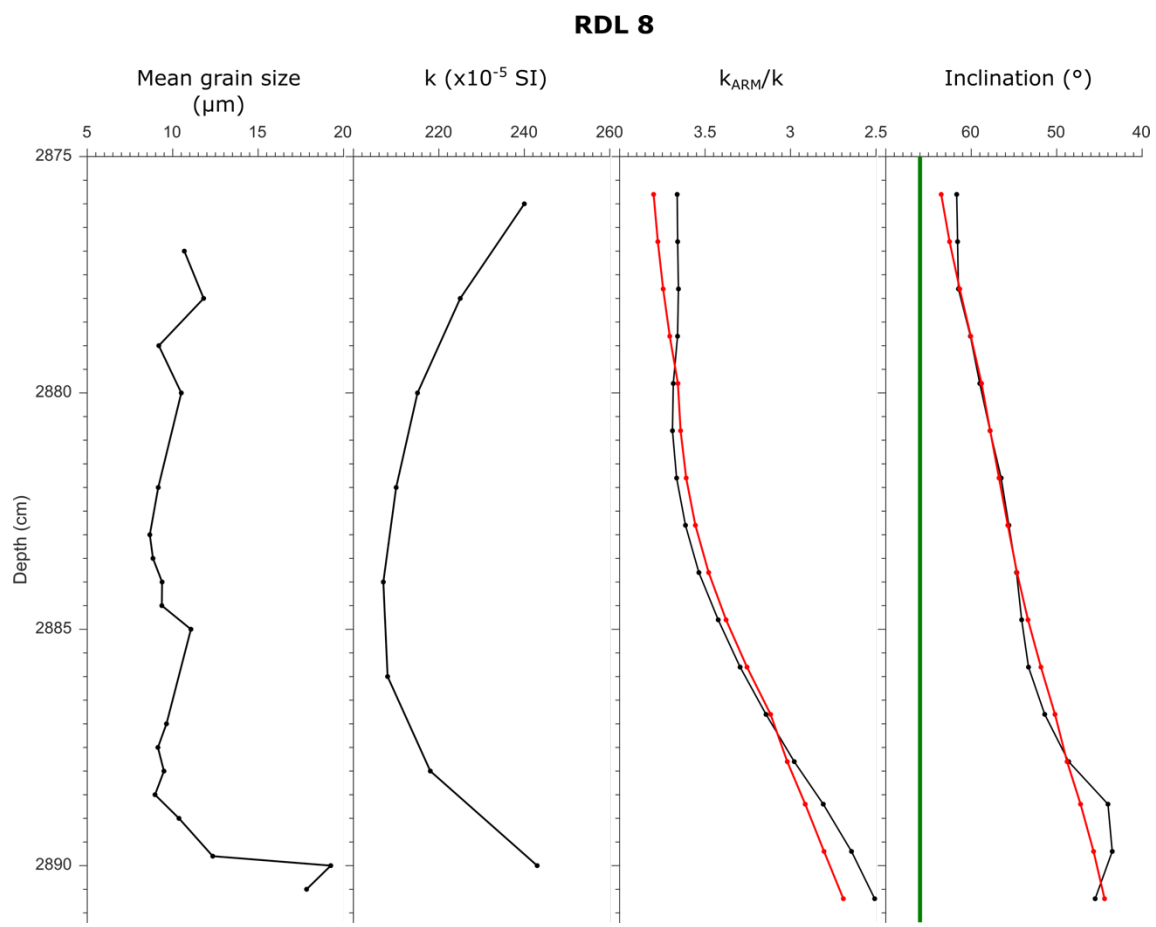


Figure 44: Same as Figure 38 for RDL 8 event.

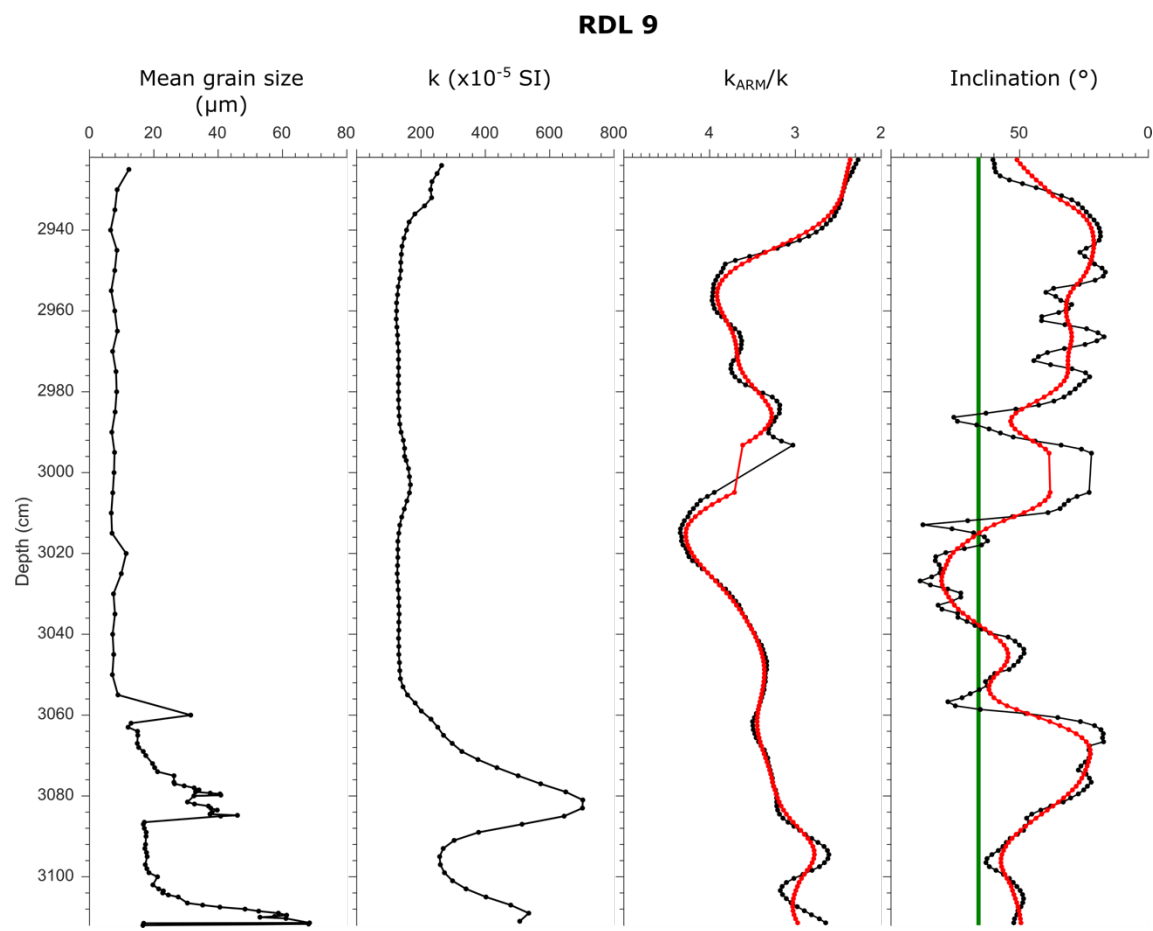


Figure 45: Same as Figure 38 for RDL 9 event.

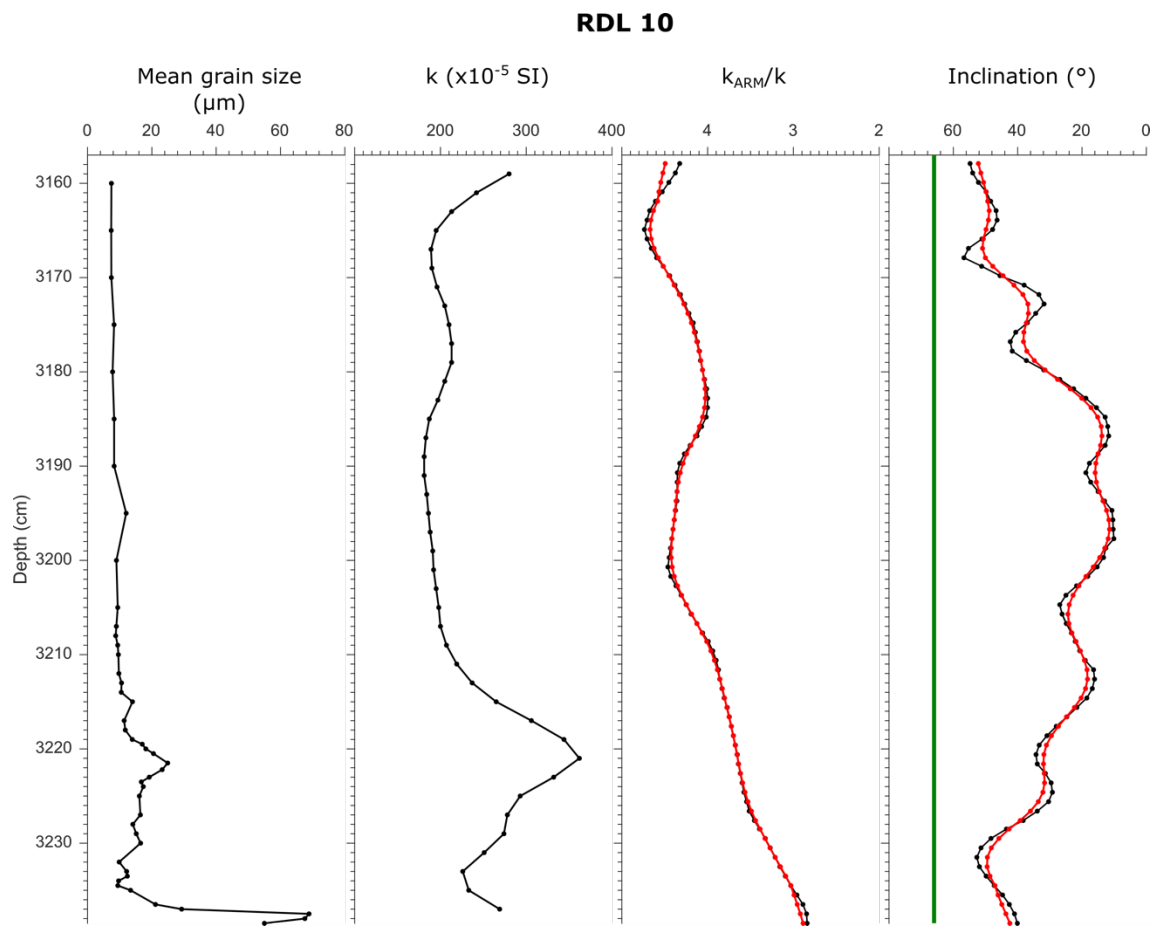


Figure 46: Same as Figure 38 for RDL 10 event.

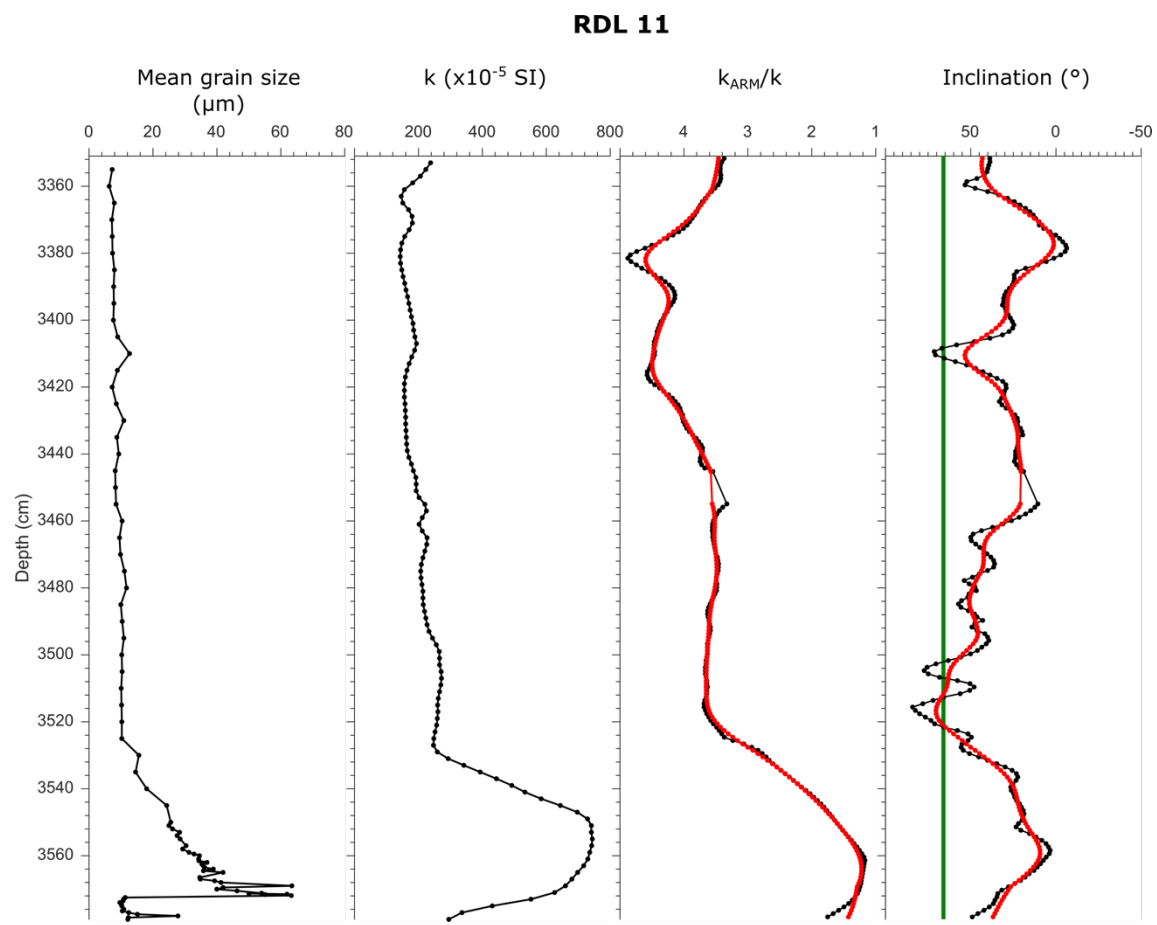


Figure 47: Same as Figure 38 for RDL 11 event.

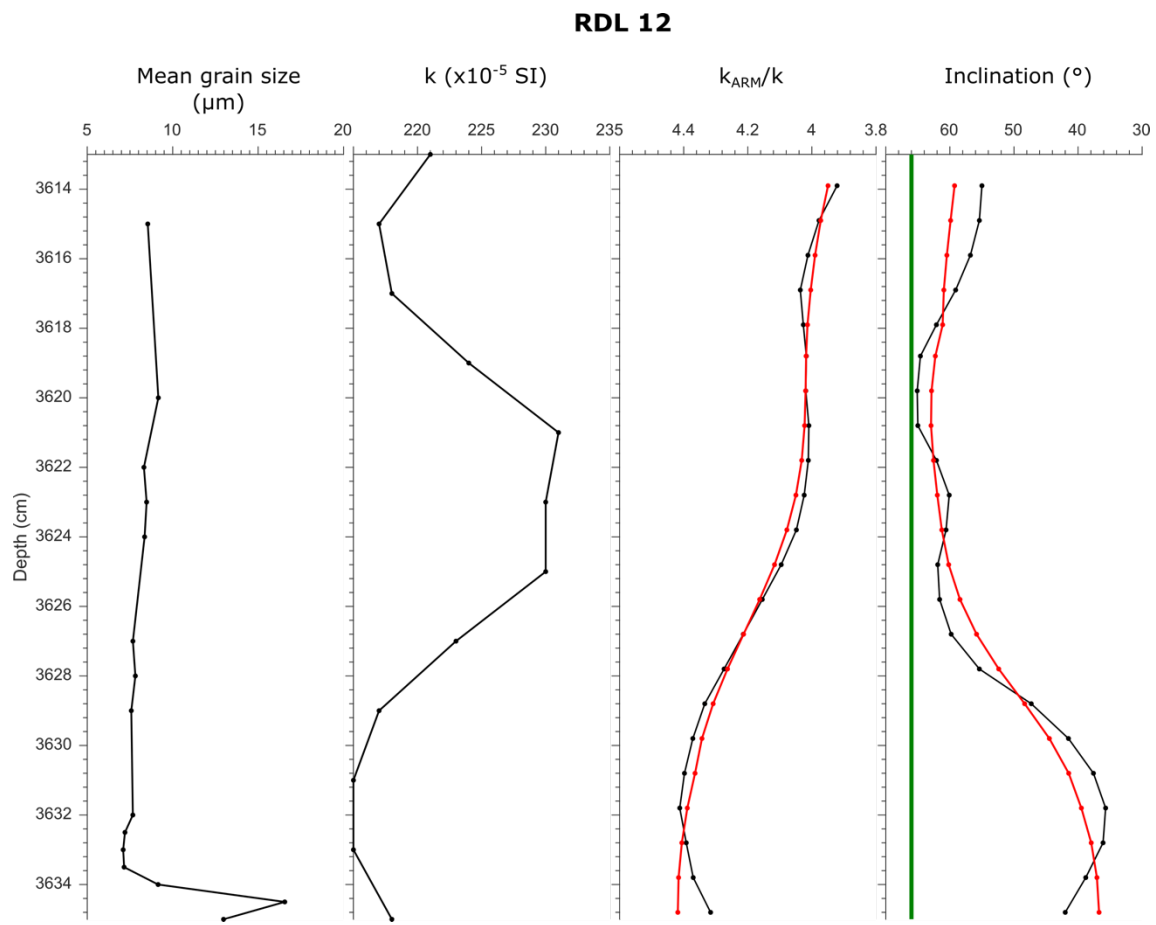


Figure 48: Same as Figure 38 for RDL 12 event.

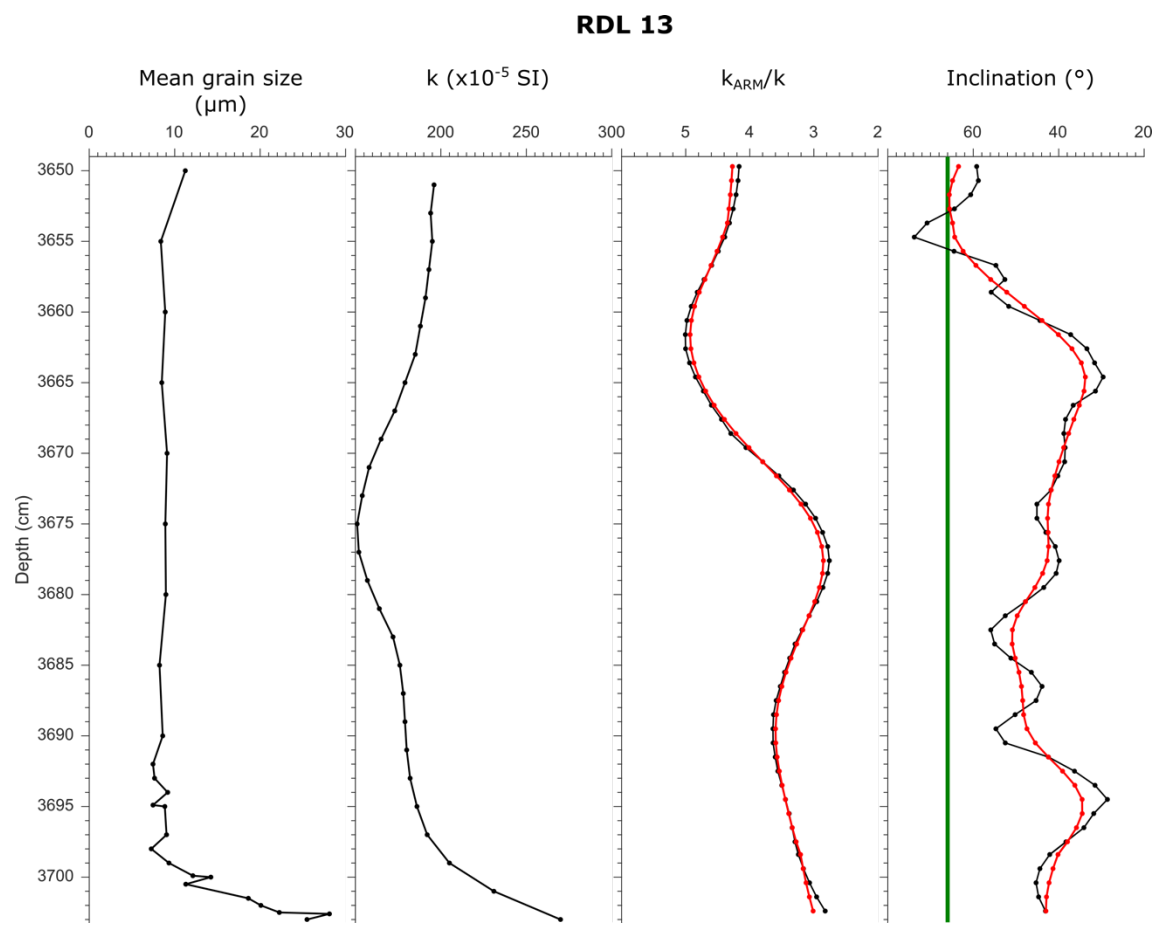


Figure 49: Same as Figure 38 for RDL 13 event.

### 3.10 REFERENCES

- Alexander, J., & Mulder, T. (2002). Experimental quasi-steady density currents. *Marine Geology*, 186(3), 195–210. [https://doi.org/10.1016/S0025-3227\(02\)00313-4](https://doi.org/10.1016/S0025-3227(02)00313-4)
- Anson, G. L., & Kodama, K. P. (1987). Compaction-induced inclination shallowing of the post-depositional remanent magnetization in a synthetic sediment. *Geophysical Journal International*, 88(3), 673–692. <https://doi.org/10.1111/j.1365-246X.1987.tb01651.x>
- Arason, P., & Levi, S. (1990). Compaction and inclination shallowing in deep-sea sediments from the Pacific Ocean. *Journal of Geophysical Research: Solid Earth*, 95(B4), 4501–4510. <https://doi.org/10.1029/JB095iB04p04501>
- Barletta, F., St-Onge, G., Stoner, J. S., Lajeunesse, P., & Locat, J. (2010). A high-resolution Holocene paleomagnetic secular variation and relative paleointensity stack from eastern Canada. *Earth and Planetary Science Letters*, 298(1–2), 162–174. <https://doi.org/10.1016/j.epsl.2010.07.038>
- Blott, S. J., & Pye, K. (2001). GRADISTAT: a grain size distribution and statistics package for the analysis of unconsolidated sediments. *Earth Surface Processes and Landforms*, 26(11), 1237–1248. <https://doi.org/10.1002/esp.261>
- Cantero, M. I., Cantelli, A., Pirmez, C., Balachandar, S., Mohrig, D., Hickson, T. A., Yeh, T., Naruse, H., Parker, G. (2012). Emplacement of massive turbidites linked to extinction of turbulence in turbidity currents. *Nature Geoscience*, 5(1), 42–45. <https://doi.org/10.1038/ngeo1320>
- Carter-Stiglitz, B., Valet, J.-P., & LeGoff, M. (2006). Constraints on the acquisition of remanent magnetization in fine-grained sediments imposed by redeposition experiments. *Earth and Planetary Science Letters*, 245(1), 427–437.
- Channell, J. E. T., & Kleiven, H. F. (2000). Geomagnetic palaeointensities and astrochronological ages for the Matuyama–Brunhes boundary and the boundaries of the Jaramillo Subchron: palaeomagnetic and oxygen isotope records from ODP Site 983. *Philosophical Transactions of the Royal Society of London A: Mathematical,*

- Physical and Engineering Sciences*, 358(1768), 1027–1047.  
<https://doi.org/10.1098/rsta.2000.0572>
- Channell, J. E. T., Stoner, J. S., Hodell, D. A., & Charles, C. D. (2000). Geomagnetic paleointensity for the last 100 kyr from the sub-antarctic South Atlantic: a tool for inter-hemispheric correlation. *Earth and Planetary Science Letters*, 175(1–2), 145–160. [https://doi.org/10.1016/S0012-821X\(99\)00285-X](https://doi.org/10.1016/S0012-821X(99)00285-X)
- Chriss, T. M., & Caldwell, D. R. (1984). Universal similarity and the thickness of the viscous sublayer at the ocean floor. *Journal of Geophysical Research: Oceans*, 89(C4), 6403–6414. <https://doi.org/10.1029/JC089iC04p06403>
- Collinson, D. W. (1965). Depositional remanent magnetization in sediments. *Journal of Geophysical Research*, 70(18), 4663–4668.
- Denham, C. R., & Chave, A. D. (1982). Detrital remanent magnetization: Viscosity theory of the lock-in zone. *Journal of Geophysical Research: Solid Earth*, 87(B8), 7126–7130.
- Deschamps, C.-E., St-Onge, G., Montero-Serrano, J.-C., & Polyak, L. (2018). Chronostratigraphy and spatial distribution of magnetic sediments in the Chukchi and Beaufort seas since the last deglaciation. *Boreas*, 47(2), 544–564. <https://doi.org/10.1111/bor.12296>
- Duboc, Q., St-Onge, G., & Lajeunesse, P. (2017). Sediment records of the influence of river damming on the dynamics of the Nelson and Churchill Rivers, western Hudson Bay, Canada, during the last centuries. *The Holocene*, 27(5), 712–725. <https://doi.org/10.1177/0959683616670465>
- Efron, B., & Tibshirani, R. (1986). Bootstrap Methods for Standard Errors, Confidence Intervals, and Other Measures of Statistical Accuracy. *Statistical Science*, 1(1), 54–75.
- Heslop, D., Witt, A., Kleiner, T., & Fabian, K. (2006). The role of magnetostatic interactions in sediment suspensions. *Geophysical Journal International*, 165(3), 775–785. <https://doi.org/10.1111/j.1365-246X.2006.02951.x>

- Katari, K., Tauxe, L., & King, J. (2000). A reassessment of post-depositional remanent magnetism: preliminary experiments with natural sediments. *Earth and Planetary Science Letters*, 183(1), 147–160.
- Katari, Kaushik, & Bloxham, J. (2001). Effects of sediment aggregate size on DRM intensity: a new theory. *Earth and Planetary Science Letters*, 186(1), 113–122.
- King, J. W., Banerjee, S. K., & Marvin, J. (1983). A new rock-magnetic approach to selecting sediments for geomagnetic paleointensity studies: Application to paleointensity for the last 4000 years. *Journal of Geophysical Research: Solid Earth*, 88(B7), 5911–5921.
- Kirschvink, J. L. (1980). The least-squares line and plane and the analysis of palaeomagnetic data. *Geophysical Journal International*, 62(3), 699–718.  
<https://doi.org/10.1111/j.1365-246X.1980.tb02601.x>
- Kissel, C., Laj, C., Mazaud, A., & Dokken, T. (1998). Magnetic anisotropy and environmental changes in two sedimentary cores from the Norwegian Sea and the North Atlantic. *Earth and Planetary Science Letters*, 164(3), 617–626.  
[https://doi.org/10.1016/S0040-1951\(98\)00223-6](https://doi.org/10.1016/S0040-1951(98)00223-6)
- Lisé-Pronovost, A., St-Onge, G., Brachfeld, S., Barletta, F., & Darby, D. (2009). Paleomagnetic constraints on the Holocene stratigraphy of the Arctic Alaskan margin. *Global and Planetary Change*, 68(1), 85–99.  
<https://doi.org/10.1016/j.gloplacha.2009.03.015>
- Macrì, P., Sagnotti, L., Dinarès-Turell, J., & Caburlotto, A. (2010). Relative geomagnetic paleointensity of the Brunhes Chron and the Matuyama–Brunhes precursor as recorded in sediment core from Wilkes Land Basin (Antarctica). *Physics of the Earth and Planetary Interiors*, 179(1), 72–86.  
<https://doi.org/10.1016/j.pepi.2009.12.002>
- Maier, D. B., Rydberg, J., Bigler, C., & Renberg, I. (2013). Compaction of recent varved lake sediments. *GFF*, 135(3–4), 231–236.  
<https://doi.org/10.1080/11035897.2013.788551>

- Mazaud, A., Channell, J. E. T., & Stoner, J. S. (2012). Relative paleointensity and environmental magnetism since 1.2 Ma at IODP site U1305 (Eirik Drift, NW Atlantic). *Earth and Planetary Science Letters*, 357–358, 137–144. <https://doi.org/10.1016/j.epsl.2012.09.037>
- Meynadier, L., Valet, J.-P., Weeks, R., Shackleton, N. J., & Hagee, V. L. (1992). Relative geomagnetic intensity of the field during the last 140 ka. *Earth and Planetary Science Letters*, 114(1), 39–57. [https://doi.org/10.1016/0012-821X\(92\)90150-T](https://doi.org/10.1016/0012-821X(92)90150-T)
- Mulder, T., Migeon, S., Savoye, B., & Jouanneau, J.-M. (2001). Twentieth century floods recorded in the deep Mediterranean sediments. *Geology*, 29(11), 1011–1014. [https://doi.org/10.1130/0091-7613\(2001\)029<1011:TCFRIT>2.0.CO;2](https://doi.org/10.1130/0091-7613(2001)029<1011:TCFRIT>2.0.CO;2)
- Mulder, Thierry, & Alexander, J. (2001). The physical character of subaqueous sedimentary density flows and their deposits. *Sedimentology*, 48(2), 269–299. <https://doi.org/10.1046/j.1365-3091.2001.00360.x>
- Mulder, Thierry, & Chapron, E. (2011). Flood deposits in continental and marine environments: character and significance. Retrieved from <http://archives.datapages.com/data/specpubs/study61/CHAPTER01/CHAPTER01.HTM>
- Mulder, Thierry, Syvitski, J. P. M., & Skene, K. I. (1998). Modeling of Erosion and Deposition by Turbidity Currents Generated at River Mouths. *Journal of Sedimentary Research*, 68(1). Retrieved from <http://archives.datapages.com/data/sepm/journals/v66-67/data/068/068001/0124.HTM>
- Mulder, Thierry, Syvitski, J. P. M., Migeon, S., Faugères, J.-C., & Savoye, B. (2003). Marine hyperpycnal flows: initiation, behavior and related deposits. A review. *Marine and Petroleum Geology*, 20(6–8), 861–882. <https://doi.org/10.1016/j.marpetgeo.2003.01.003>
- Nagata, T. (1961). Rock Magnetism, 350 pp. Maruzen, Tokyo.

- Quidelleur, X., Valet, J.-P., LeGoff, M., & Boudoire, X. (1995). Field dependence on magnetization of laboratory-redeposited deep-sea sediments: First results. *Earth and Planetary Science Letters*, 133(3), 311–325.
- Roberts, A. P., Lehman, B., Weeks, R. J., Verosub, K. L., & Laj, C. (1997). Relative paleointensity of the geomagnetic field over the last 200,000 years from ODP Sites 883 and 884, North Pacific Ocean. *Earth and Planetary Science Letters*, 152(1), 11–23. [https://doi.org/10.1016/S0012-821X\(97\)00132-5](https://doi.org/10.1016/S0012-821X(97)00132-5)
- Roberts, A. P., Tauxe, L., & Heslop, D. (2013). Magnetic paleointensity stratigraphy and high-resolution Quaternary geochronology: successes and future challenges. *Quaternary Science Reviews*, 61, 1–16.
- Shcherbakov, V., & Sycheva, N. (2010). On the mechanism of formation of depositional remanent magnetization. *Geochemistry, Geophysics, Geosystems*, 11(2). Retrieved from <http://onlinelibrary.wiley.com/doi/10.1029/2009GC002830/full>
- Shcherbakov, V. P., & Shcherbakova, V. V. (1983). On the theory of depositional remanent magnetization in sedimentary rocks. *Geophysical Surveys*, 5(4), 369–380. <https://doi.org/10.1007/BF01453987>
- Spassov, S., & Valet, J.-P. (2012). Detrital magnetizations from redeposition experiments of different natural sediments. *Earth and Planetary Science Letters*, 351, 147–157.
- Stacey, F. D. (1972). On the role of Brownian motion in the control of detrital remanent magnetization of sediments. *Pure and Applied Geophysics*, 98(1), 139–145.
- Stoner, J., & St-Onge, G. (2007). Chapter Three Magnetic Stratigraphy in Paleoceanography: Reversals, Excursions, Paleointensity, and Secular Variation. *Developments in Marine Geology*, 1. [https://doi.org/10.1016/S1572-5480\(07\)01008-1](https://doi.org/10.1016/S1572-5480(07)01008-1)
- Stoner, J. S., Channell, J. E. T., Hillaire-Marcel, C., & Kissel, C. (2000). Geomagnetic paleointensity and environmental record from Labrador Sea core MD95-2024: global marine sediment and ice core chronostratigraphy for the last 110 kyr. *Earth and Planetary Science Letters*, 183(1–2), 161–177. [https://doi.org/10.1016/S0012-821X\(00\)00272-7](https://doi.org/10.1016/S0012-821X(00)00272-7)

- Stoner, Joseph S., Channell, J. E. T., & Hillaire-Marcel, C. (1996). The magnetic signature of rapidly deposited detrital layers from the Deep Labrador Sea: Relationship to North Atlantic Heinrich layers. *Paleoceanography*, 11(3), 309–325. <https://doi.org/10.1029/96PA00583>
- St-Onge, G., Mulder, T., Piper, D. J. W., Hillaire-Marcel, C., & Stoner, J. S. (2004). Earthquake and flood-induced turbidites in the Saguenay Fjord (Québec): a Holocene paleoseismicity record. *Quaternary Science Reviews*, 23(3–4), 283–294. <https://doi.org/10.1016/j.quascirev.2003.03.001>
- Sun, W. W., & Kodama, K. P. (1992). Magnetic anisotropy, scanning electron microscopy, and X ray pole figure goniometry study of inclination shallowing in a compacting clay-rich sediment. *Journal of Geophysical Research: Solid Earth*, 97(B13), 19599–19615. <https://doi.org/10.1029/92JB01589>
- Tanty, C., Valet, J.-P., Carlut, J., Bassinot, F., & Zaragosi, S. (2016). Acquisition of detrital magnetization in four turbidites. *Geochemistry, Geophysics, Geosystems*, 17(8), 3207–3223. <https://doi.org/10.1002/2016GC006378>
- Tauxe, L. (1993). Sedimentary records of relative paleointensity of the geomagnetic field: theory and practice. *Reviews of Geophysics*, 31(3), 319–354.
- Tauxe, L., Steindorf, J. L., & Harris, A. (2006). Depositional remanent magnetization: toward an improved theoretical and experimental foundation. *Earth and Planetary Science Letters*, 244(3), 515–529.
- Valet, J.-P. (2003). Time variations in geomagnetic intensity. *Reviews of Geophysics*, 41(1), 1004. <https://doi.org/10.1029/2001RG000104>
- Valet, J.-P., & Meynadier, L. (1993). Geomagnetic field intensity and reversals during the past four million years. *Nature*, 366(6452), 234–238.
- Vautard, R., & Ghil, M. (1989). Singular spectrum analysis in nonlinear dynamics, with applications to paleoclimatic time series. *Physica D: Nonlinear Phenomena*, 35(3), 395–424. [https://doi.org/10.1016/0167-2789\(89\)90077-8](https://doi.org/10.1016/0167-2789(89)90077-8)

- Verosub, K. L. (1977). Depositional and postdepositional processes in the magnetization of sediments. *Reviews of Geophysics*, 15(2), 129–143. <https://doi.org/10.1029/RG015i002p00129>
- Xu, J. P. (2010). Normalized velocity profiles of field-measured turbidity currents. *Geology*, 38(6), 563–566. <https://doi.org/10.1130/G30582.1>



## **CONCLUSION GÉNÉRALE**

À l'origine, le but premier de ce doctorat était d'ordre très pratique. Il avait pour objectif d'améliorer les connaissances sur les mécanismes d'enregistrement du champ magnétique terrestre dans les sédiments. Pour ce faire, cette thèse s'est concentrée sur deux cas d'étude intéressants: les varves et les turbidites. En effet, ces dernières présentent une variation lithologique importante avec un champ magnétique quasi constant durant le dépôt sédimentaire, ce qui en fait d'excellents cas d'étude. Toutefois, il était important, dans un premier temps, de définir la limite de l'utilisation des U-channels. Il nous fallait savoir s'il était préférable de faire des mesures continues, ou bien des mesures ponctuelles, pour reconstituer les variations d'aimantation enregistrées dans le sédiment. C'est pour cela que le premier chapitre pose les limites de l'utilisation des U-channels. Le deuxième chapitre, quant à lui, s'est concentré sur l'impact d'une variation lithologique sur l'enregistrement magnétique à travers l'étude de varves centimétriques du lac Ojibway. Enfin, le dernier chapitre se focalise sur l'étude de l'enregistrement de différentes couches sédimentaires déposées rapidement afin de déterminer les mécanismes d'acquisition durant ce type de dépôt. Ces trois chapitres ont donc permis d'atteindre l'objectif général de cette thèse, qui était d'améliorer les connaissances actuelles sur l'acquisition de l'aimantation par les sédiments.

**Objectif 1: Définir la limite d'utilisation des U-channels pour l'étude de la variation du champ magnétique terrestre, notamment dans le cas des excursions et des inversions.**

Dans ce chapitre, nous avons défini les limites de l'utilisation des U-channels pour reconstituer les variations d'aimantation enregistrées dans le sédiment, notamment dans le cas d'excursions et d'inversions. Pour ce faire, une approche directe a été menée en procédant successivement à des mesures d'échantillons ponctuels synthétiques et en les comparant à la mesure du U-channel synthétique équivalent. Ces mesures ont été effectuées avec le magnétomètre cryogénique de *2G-Enterprises* à l'IPGP. Ce dernier est caractérisé par une fonction de réponse de 7 cm. Par ailleurs, une comparaison a été faite avec d'autres magnétomètres cryogéniques ayant des fonctions de réponse différentes.

Suite à la création d'excursions de différentes épaisseurs, il a été mis en avant que les excursions inférieures à 7,5 cm n'étaient pas détectables par des mesures U-channels. De plus, même quand les plus épaisses sont détectées, le signal mesuré est considérablement lissé. Pour pouvoir détecter une polarité opposée, il est nécessaire d'avoir un événement d'au moins 20 cm, soit une vitesse de sédimentation d'au moins 10 cm/ka. Cependant, l'intensité de l'aimantation est plus sensible que les directions. Elle peut donc être utilisée pour indiquer la présence d'une excursion, ce qui pourra être vérifié par la suite via une étude ponctuelle.

Quant aux inversions, les mesures sur des U-channels ne permettent pas de reproduire le pôle géomagnétique virtuel original, même dans le cas de longues transitions de 30 cm. Le signal du U-channel est lissé et génère des directions artificielles. Le résultat de ces mesures correspond à une simple convolution d'un train d'échantillons ponctuels par la fonction de réponse du magnétomètre de l'IPGP. À l'aide de convolutions numériques, nous avons pu tester l'impact d'un changement de la fonction de réponse en utilisant celle de différents magnétomètres. Il a été constaté que les directions de transition, et par conséquent, le modèle de transition, sont sensibles aux largeurs des fonctions de réponse pour des différences aussi petites que 1 cm.

En conclusion, les mesures réalisées sur des U-channels n'arrivent pas à reproduire parfaitement les changements rapides du champ magnétique terrestre, notamment dans le cas des excursions et des inversions. La mesure obtenue dépend du magnétomètre cryogénique utilisé. Malgré cela, le U-channel reste un outil utile pour les études à grande échelle sur de nombreuses carottes ou pour établir la chronostratigraphie des carottes.

Cette étude remet donc en cause de nombreuses études passées, faites à l'aide de U-channels, sur les variations du champ durant des excursions et des inversions. Il est donc important de se remémorer, en fonction de l'objectif de l'étude, qu'il est parfois intéressant de faire des mesures ponctuelles même si cela nécessite un temps de mesure beaucoup plus long.

## **Objectif 2. Déterminer l'influence d'un changement lithologique important sur l'enregistrement magnétique.**

Dans ce second chapitre, des sédiments varvés du lac proglaciaire Ojibway ont été étudiés. Ces varves possèdent un enregistrement magnétique stable associé à une variation lithologique importante. Les varves centimétriques ont permis d'examiner les propriétés magnétiques en échantillonnant de manière dissociée les lits d'hiver et les lits d'été à l'aide de petits cubes de 1 cm<sup>3</sup>. En parallèle de quoi, un échantillonnage par U-channel a été effectué. Les premiers résultats des mesures magnétiques ont mis en avant les résultats du chapitre 1. Ce qui nous a conforté dans l'idée qu'il était donc nécessaire de faire un échantillonnage ponctuel pour pouvoir étudier l'évolution de l'aimantation dans les varves.

Malgré une minéralogie magnétique inchangée, de fortes variations d'inclinaison et d'intensité, ainsi qu'une petite variation de déclinaison, ont été observées entre les lits d'été et les lits d'hiver. La variation d'inclinaison observée présente un aplatissement des grains de 13° en moyenne pour les lits d'été et de 26° en moyenne pour les lits d'hiver. Des analyses sédimentaires et magnétiques ont été effectuées pour tenter de mettre en lumière les mécanismes pouvant être à l'origine de ces variations. Les mesures magnétiques

classiques nous avaient laissé penser que le seul paramètre qui aurait pu être mis en cause était la compaction. Mais une étude magnétique beaucoup plus approfondie, via des mesures *First Order Reversal Curve* (FORC) à très haute résolution, a permis de constater qu'il y avait un léger changement de composition des grains magnétiques entre ces deux lits. Ainsi, nos résultats illustrent que les variations observées sont principalement dues à l'intervention de deux mécanismes: la compaction et la variation de la composition des grains magnétiques entre les lits d'été et les lits d'hiver. Malheureusement, nos résultats n'ont pas permis de différencier l'impact de ces deux paramètres de manière indépendante.

Cette étude montre l'importance qu'une petite variation de la composition des grains magnétiques peut avoir. Elle montre également l'utilité des varves pour l'étude de l'impact de la variation lithologique sur l'enregistrement magnétique. De plus, elle met en avant la nécessité de faire des analyses FORC à très haute résolution pour mieux comprendre l'impact de la variation lithologique sur l'enregistrement magnétique.

### **Objectif 3. Déterminer l'impact d'une sédimentation rapide sur l'enregistrement magnétique.**

Dans ce dernier chapitre, une comparaison statistique des caractéristiques magnétiques de 17 couches sédimentaires déposées rapidement allant de 7,1 cm à 1510 cm a été réalisée. Les mesures magnétiques proviennent de deux anciennes études (St-Onge et al., 2014; Tanty et al., 2016).

Nous avons constaté que la variation d'inclinaison dans le dépôt augmente en fonction de l'épaisseur de ce dernier. Cela avait déjà été observé via une relation linéaire par Tanty et al. (2016). Cependant, grâce à l'augmentation du nombre d'événements de différentes tailles, nous avons pu observer que cette relation est en réalité logarithmique, avec un effet de saturation pour les grands événements. De plus, la variation d'inclinaison est aussi reliée à la variation de la taille des grains magnétiques. Ainsi, les plus gros événements sont les événements turbulents et ils présentent un fort aplatissement de

l'inclinaison associé à de gros grains magnétiques et sédimentaires. Trois mécanismes ont été proposés pour expliquer ces observations: la compaction, la floculation et la turbulence. La compaction est probablement minimale alors que la floculation ne semble pas ressortir.

À l'aide d'un modèle numérique, il a été prouvé que les effets d'aplanissement de l'inclinaison observés peuvent être générés par des courants de fonds. Ce résultat n'exclut pas la floculation et la compaction, mais montre que la turbulence ne doit pas être négligée comme mécanisme impactant l'enregistrement du champ magnétique, notamment pour l'inclinaison.

Comme dans le chapitre précédent, il n'a malheureusement pas été possible de distinguer l'impact de ces deux paramètres de manière indépendante. Cependant, la turbulence est à prendre en compte comme mécanisme d'acquisition de l'aimantation. De plus, cette étude montre l'intérêt d'étudier l'aimantation des turbidites et des hyperpicnites pour mieux comprendre l'acquisition de l'aimantation par les sédiments.

## **Portés et perspectives de l'étude**

### *Instrumentation*

L'instrumentation est à la base de toute étude paléomagnétique. L'avenir du paléomagnétisme passera par une meilleure analyse magnétique, que ce soit à travers l'amélioration des mesures ou l'amélioration du traitement des données obtenues par ces mesures.

Pour améliorer les mesures d'aimantation magnétique, il faut améliorer le magnétomètre utilisé, notamment en réduisant la taille de la fonction de réponse pour limiter le lissage. Le microscope SQUID (*Superconducting QUantum Interference Device*) est un exemple d'évolution. Ce dernier permet de faire des mesures beaucoup plus précises spatialement permettant par exemple d'étudier des laminations millimétriques. La durée de la mesure, par contre, est beaucoup plus longue. Il est encore nécessaire d'améliorer les

appareils pour pouvoir mesurer le plus rapidement possible tout en augmentant la résolution de la mesure.

Dans le cas de l'utilisation des U-channels, la déconvolution proposée récemment par Xuan & Oda (2015) permet de réduire l'effet de lissage dû à la mesure des U-channels. Mais il reste encore du travail à faire sur la déconvolution pour réussir à parfaitement retrouver le signal d'origine, surtout dans le cas de faibles taux de sédimentation.

### *Sédiments varvés*

Les sédiments varvés sont de parfaits cas d'étude en ce qui a trait à l'acquisition de l'aimantation par les sédiments. C'est pour cela qu'il faut continuer de les étudier pour améliorer nos connaissances sur l'aimantation. La limite de leur étude est surtout liée à l'épaisseur des couches, empêchant l'échantillonnage ponctuel pour les mesures magnétiques. Il faut donc développer l'instrumentation afin de mesurer des varves beaucoup plus fines et donc avoir accès à une plus grande quantité d'échantillons. L'utilisation du microscope SQUID sur des lames minces serait envisageable.

### *Turbidites et hyperpicnites*

Comme pour les varves, les turbidites et les hyperpicnites sont aussi de parfaits cas d'étude concernant l'acquisition de l'aimantation par les sédiments. L'étude statistique a été menée sur une base de 17 événements, dont un a dû être écarté de la statistique à cause de sa trop grande taille. Il est nécessaire d'ajouter à notre base de données différents événements de différentes tailles et d'origines différentes, pour améliorer la statistique. Il nous faudrait notamment plusieurs événements de petite taille ( $<20$  cm), étudiés ponctuellement, pour mieux caractériser le comportement magnétique, ainsi que des événements de grande taille ( $>2$  m) pour mieux caractériser l'effet de saturation. Cela permettrait aussi d'affiner la courbe obtenue.

## Mot de la fin

Cette thèse répond à l'ensemble des questions scientifiques posées durant le doctorat. L'objectif principal avait pour but de mieux comprendre l'acquisition du champ magnétique terrestre par les sédiments. Dans un premier temps, le chapitre 1 a mis en avant la limite de l'utilisation des U-channels, ainsi que l'importance des mesures ponctuelles, pour l'étude de l'acquisition du champ magnétique terrestre par les sédiments. Par la suite, à travers les chapitres 2 et 3, plusieurs mécanismes ont été mis en avant: la compaction, la flocculation, la turbulence, et une légère variation de la composition des grains magnétiques. Au travers de ces recherches, la bioturbation ne faisait pas partie des mécanismes observés, mais elle ne doit pas être négligée car elle peut remettre en suspension les grains magnétiques créant une remise à zéro de l'ensemble des autres mécanismes observés. Pour synthétiser ceci, sur la Figure 50 sont représentés l'ensemble des mécanismes jouant un rôle important dans l'acquisition de l'aimantation. De plus, une inclinaison fictive est représentée sur la gauche de la Figure 50, variant en fonction des mécanismes impactant l'inclinaison. La compaction et la flocculation sont des mécanismes bien connus pour jouer un rôle dans l'acquisition de l'aimantation. Les deux paramètres, que sont la turbulence et le fort impact d'une faible variation de la composition des grains magnétiques, sont de nouveaux mécanismes à prendre en compte. Cependant, il n'a pas encore été possible de séparer l'impact de chaque mécanisme. Il faut donc continuer ce type d'études pour améliorer la compréhension de l'acquisition du champ magnétique terrestre par les sédiments et mieux quantifier l'impact de chaque mécanisme.

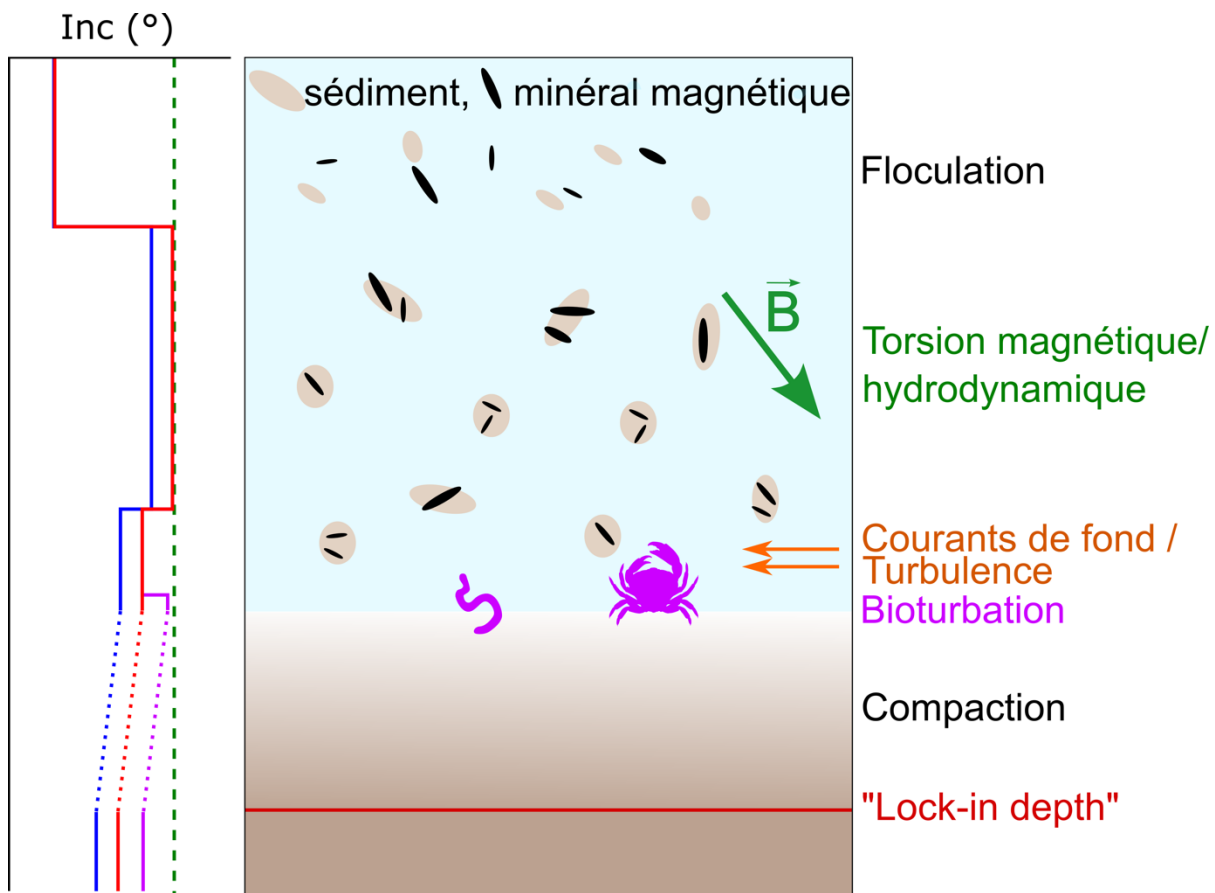


Figure 50: Processus d'acquisition de l'aimantation par les sédiments mis en avant dans cette étude. Les courbes rouge et bleue représentent la variation de l'inclinaison hypothétique pour deux compositions de grains magnétiques différentes soumises à un champ magnétique avec une inclinaison représentée en vert. La variation de l'inclinaison durant la compaction est en pointillé car son comportement n'est pas encore bien connu (Roberts et Winklhofer, 2004). La courbe en violet représente un cas particulier où la bioturbation jouerait un rôle important de remise en suspension des grains.

## Références

- Roberts, A. P., & Winklhofer, M. (2004). Why are geomagnetic excursions not always recorded in sediments? Constraints from post-depositional remanent magnetization lock-in modelling. *Earth and Planetary Science Letters*, 227(3), 345–359. <https://doi.org/10.1016/j.epsl.2004.07.040>
- St-Onge, G., Mulder, T., Piper, D. J. W., Hillaire-Marcel, C., & Stoner, J. S. (2004). Earthquake and flood-induced turbidites in the Saguenay Fjord (Québec): a Holocene paleoseismicity record. *Quaternary Science Reviews*, 23(3–4), 283–294. <https://doi.org/10.1016/j.quascirev.2003.03.001>
- Tanty, C., Valet, J.-P., Carlut, J., Bassinot, F., & Zaragosi, S. (2016). Acquisition of detrital magnetization in four turbidites. *Geochemistry, Geophysics, Geosystems*, 17(8), 3207–3223. <https://doi.org/10.1002/2016GC006378>
- Xuan, C., & Oda, H. (2015). UDECON: deconvolution optimization software for restoring high-resolution records from pass-through paleomagnetic measurements. *Earth, Planets and Space*, 67, 183. <https://doi.org/10.1186/s40623-015-0332-x>